UNIVERSITY OF SOUTHAMPTON

Faculty of Natural and Environmental Sciences

School of Chemistry

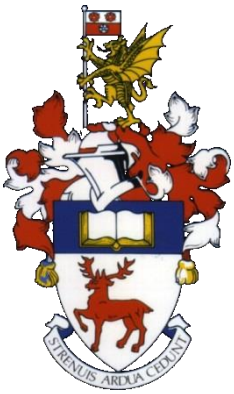

Chemically tagged DNA probes for sensing of DNA biomarkers using Lab-on-a-chip technology

by

Joanna Patricia Pursey

Thesis for the degree of Doctor of Philosophy

November 2017

UNIVERSITY OF SOUTHAMPTON

ABSTRACT

FACULTY OF NATURAL AND ENVIRONMENTAL SCIENCES

School of Chemistry

Thesis for the degree of Doctor of Philosophy

CHEMICALLY TAGGED DNA PROBES FOR SENSING OF DNA BIOMARKERS USING LAB-ON-A-CHIP TECHNOLOGY

By Joanna Patricia Pursey

DNA methylation is a common epigenetic abnormality found in cancer. Although a high content of DNA methylation is found in cancer patients, the amount is still very low and multiple round of amplification is necessary. In addition, multiple genes are methylated in cancer patients. Therefore a high sensitivity and multiplexed sensor is desired for methylated DNA detection. This work develops a single sensor device and a multi sensor device multiplex work. To show the capability of these devices, bladder cancer biomarkers are selected for demonstration. In bladder cancer, three genes (DAPK, E. Cadherin and RARβ) are found to be methylated in the promoter region. A hairpin probe was designed with a redox active chemical tag incorporated into the design. Anthraquinone and porphyrin modified DNA probes were synthesised and compared with the commercially available methylene blue. Simultaneous detection of these three genes is essential for bladder cancer diagnosis. This work shows that with the multi sensor device, all three biomarkers can be detected in single run using only 20 minutes operational time, with a limit of detection of 250 fM.

Alongside detection of DNA methylation, an additional biomarker found in bladder cancer patients, microRNA, was investigated. Hairpin and linear probe designs were compared. The miRNA was detected in spiked Surine (urine negative control) to demonstrate the feasibility of the system with detection in human samples.

Table of Contents

List of Figures

List of Tables

List of Schemes

DECLARATION OF AUTHORSHIP

I, Joanna Patricia Pursey, declare that this thesis and the work presented in it are my own and has been generated by me as the result of my own original research.

Thesis entitled: CHEMICALLY TAGGED DNA PROBES FOR SENSING OF DNA BIOMARKERS USING LAB-ON-A-CHIP TECHNOLOGY

I confirm that:

1. This work was done wholly or mainly while in candidature for a research degree at this University;
2. Where any part of this thesis has previously been submitted for a degree or any other qualification at this University or any other institution, this has been clearly stated;
3. Where I have consulted the published work of others, this is always clearly attributed;
4. Where I have quoted from the work of others, the source is always given. With the exception of such quotations, this thesis is entirely my own work;
5. I have acknowledged all main sources of help;
6. Where the thesis is based on work done by myself jointly with others, I have made clear exactly what was done by others and what I have contributed myself;
7. Parts of this work have been published as:

    - P. Kongsuphol, H. H. Ng, **J. P. Pursey**, S. K. Arya, C. C. Wong, E. Stulz and M. K. Park, *Biosens Bioelectron*, 2014, **61**, 274-279
    - M. Balaz, I. Mames, **J. P. Pursey**, L. L. Sargisson, E. Stulz, K. Varga, Handbook of Porphyrin Science, Ed. K. M. Kadish, K. M. Smith, R. Guilard, 2016, **44**, World Scientific
    - **J. P. Pursey**, Y. Chen, M. K. Park, P. Kongsuphol, E. Stulz, *Sens Actuator B-Chem*, 2017, **251**, 34-39

Signed: .....

Date: .....

Acknowledgements

I would first like to give a huge thanks to Dr Eugen Stulz for all of the help and support over the last four years. I am very grateful for the opportunity that he gave to me.

Thank you to Dr Mi Kyoung Park and Dr Patthara Kongsuphol for their support and guidance during my two years in Singapore. I would also like to thank A*STAR, Institute of Microelectronics for the funding to carry out my research in Singapore. While the time presented a number of challenges I am happy that I was able to overcome them.

Thank you to Dr Iwona Mames and Christina Xyrafaki for the synthesis and purification of DNA probes for me while I was in Singapore. Also to Dr. Maja Choma, Dr Daniel Singleton and Ceilidh Armer for proof reading different sections for me.

Thank you to everyone from Lab 5003 in Southampton and the TEA-BUGS in Singapore for your support and friendship during the last four years. In particular I would like to mention the endless support from Lauren Sargisson – I couldn't have done this without you!

Lastly I would like to thank my parents. I would not have got this far without you. Your continued support means so much to me, especially with everything that has happened during these four years. I will always remember $CaCO_3$, even if I have not used a Bunsen burner throughout this work…

Definitions and Abbreviations

Å	Angstrom
δ	Chemical shift in ppm
λ	Wavelength
λ_{ex}	Excitation wavelength
λ_{em}	Emission wavelength
µ	Micro
A	Adenine
aq	Aqueous
C	Cytosine
CEP-Cl	2-cyanoethyl *N*,*N*-diisopropylchlorophosphoramidite
CoP	Cobalt Porphyrin
CPG	Controlled pore glass
CV	Cyclic Voltammetry
CVD	Chemical vapour deposition
d	Doublet
DAPK	Death associated protein kinase
DCM	Dichloromethane
DDQ	2, 3-dichloro-5, 6-dicyano-*p*-benzoquinone
DIC	*N*, *N*'-diisopropylcarbodiimide
DIPEA	*N*, *N*-diisopropylethylamine
DMAP	4-dimethylaminopyridine
DMF	Dimethylformamide
DMT	4, 4'- Dimethoxytrityl
DMT-Cl	4, 4'- Dimethoxytrityl chloride
DNA	2'-deoxyribonucleic acid
DPV	Differential pulse voltammetry
DTT	Dithiothreitol
DUV	Deep Ultra-Violet (lithography)
E. Cad	Epithelial cadherin
EDC	1-Ethyl-3-(3-dimethylaminopropyl)carbodiimide
EIS	Electrical Impedance Spectroscopy

EOT	Extraordinary Optical Transmission
Equiv	Equivalents
f	Femto
FB-P	Free Base Porphyrin
G	Guanine
HCl	Hydrochloric acid
HEG	18-*O*-Dimethoxytritylhexaethylene glycol, 1-((2-cyanoethyl)-(*N*,*N*-diisopropyl)) phosphoramidite
Hz	Hertz
H_2O	Water
H_2O_2	Hydrogen Peroxide
H_2SO_4	Sulphuric acid
HFIP	1,1,1,3,3,3-Hexafluoro-2-propanol
HOBt	Hydroxybenzotriazole
HPLC	High performance liquid chromatography
HPLC-MS	High performance liquid chromatography - Mass spectrometry
IME	Institute of Microelectronics (Singapore)
J	Coupling constant
k	Kilo
KOH	Potassium hydroxide
LOC	Lab-on-a-chip
m	Multiplet
M	Molar – mol dm^{-3}
MB	Methylene Blue
MCH	6-Mercapto-1-hexanol
MeOH	Methanol
Min	Minute
miRNA	MicroRNA
Mmol	Milimoles
MMT	4-Methoxytriphenylmethyl
MSP	Methylation Specific PCR
n	Nano
N_2	Nitrogen

NaCl	Sodium Chloride
NaOH	Sodium Hydroxide
NH_4Cl	Ammonium chloride
$(NH_4)_2MoO_4$	Ammonium molybdate
NHS	N-Hydroxysuccinimide
NMR	Nuclear magnetic resonance
Oligo	oligonucleotide
p	Pico
PAGE	Polyacrylamide gel electrophoresis
PAH	Polyallyamine hydrochloride
PBS	Phosphate Buffered Saline
PCR	Polymerase chain reaction
Pd(PPh3)4	Tetrakis palladium triphenyl phosphine
PECVD	Plasma enhanced chemical vapour deposition
POC	Point of care
PSS	Polysodium styrene sulfonate
PVD	Physical vapour deposition
QY	Quantum yield
RARβ	Retinoic acid receptor beta
R_{ct}	Charge transfer resistance
RIE	Reactive ion etching
RNA	Ribonucleic acid
rpm	Rotations per minute
RT	Room temperature
s	Singlet
SDS	Sodium dodecyl sulfate
SEM	Scanning Electron Microscope
SNP	Single-nucleotide polymorphism
SPS	Solid phase synthesis
T	Thymine
TCA	Trichloroacetic acid
TCEP	Tris(2-carboxyethyl)phosphine
TEA	Triethylamine

TEAA	Triethylammonium acetate
TEMED	Tetramethylethlenediamine
TFA	Trifluoroacetic acid
THF	Tetrahydrofuran
TLC	Thin layer chromatography
TNF	Tumour necrosis factor
TPP	5, 10, 15, 20-tetraphenyl porphyrin
UV-Vis	Ultra violet - visible
$Zn(OAc)_2$	Zinc acetate

1. Introduction

1.1 Deoxyribonucleic Acid

In 1953 J. Watson and F. Crick with R. Franklin and M. Wilkins deciphered the accepted structure of 2'deoxyribonucleic acid (DNA) [1-3]. DNA consists of two antiparallel strands, which form a double helix. The main building blocks of DNA are the four nucleobases: adenine (A), cytosine (C), guanine (G) and thymine (T), which are shown in Figure 1-1(A). Adenine and guanine are based on purines while thymine and cytosine are based on pyrimidines. These nucleobases are connected to a sugar ring (2'-deoxyribose) to form a nucleoside. Nucleosides are joined together via a phosphodiester backbone to form a nucleotide. An example dinucleotide is shown in Figure 1-1(B).

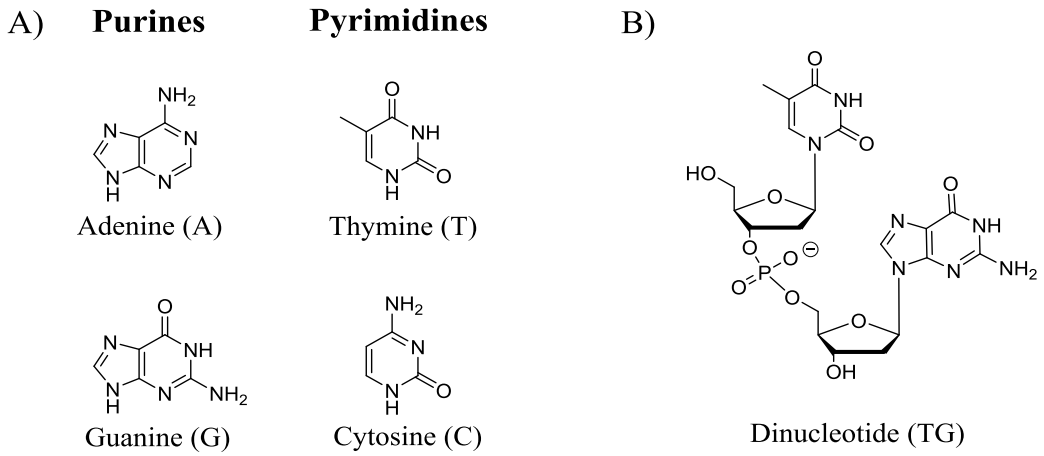

Figure 1-1: A) Structure of the four nucleobases, B) An example dinucleotide, showing the phosphate diester linkage between the deoxyribonucleotides.

Two single strands of DNA run antiparallel to each other and hydrogen bonds form between base pairs A-T and C-G to from a double helix. The Watson-Crick base pairings are shown in Figure 1-2 where A-T has two hydrogen bonds and C-G has three hydrogen bonds.

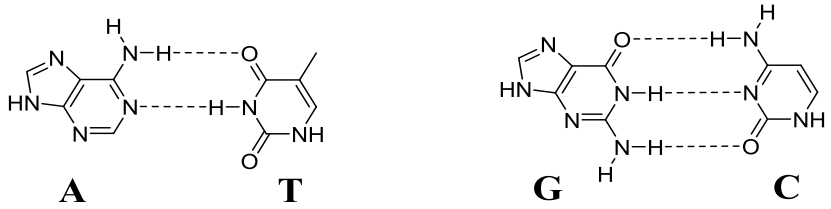

Figure 1-2: Watson-Crick base pairings A-T and C-G.

The binding strength and stability of the duplex is increased via the hydrophobic effect inside the duplex, π-stacking of heterocyclic bases, dipole-dipole interactions, and the negative charge of the backbone [4].

There are three main forms of DNA as shown in Figure 1-3. These are A-form, B-form and Z-form. B-form is the most common form found in DNA-DNA duplexes. Both the A-form and the B-form are right-handed helices while Z-form is a left-handed helix. The A-form is found in RNA-RNA and RNA-DNA duplexes while the Z-form appears when there is a high GCGC frequency in a solution of high salt concentration. However, there is no definitive biological significance of the Z-form of DNA.

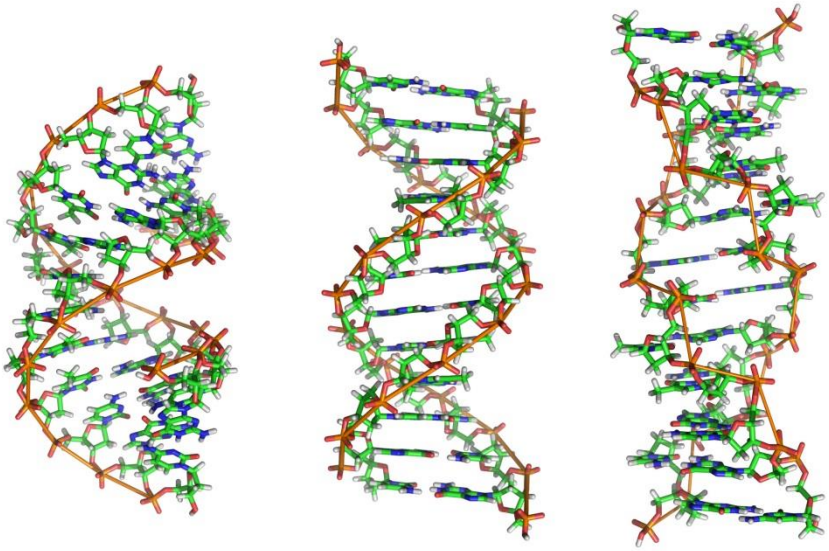

Figure 1-3: Three main forms of DNA duplexes – A-form (left), B-form (middle) and Z-form (right) [5].

The nucleobases have two different conformations which they can form. These are labelled as *syn* and *anti* in relation to the ribose ring and shown in Figure 1-4. Due to steric clashes the *anti* conformation, relative to the ribose ring, is preferred. However, in Z-form there is a mixture of *syn* and *anti* conformation whereby guanine adopts the *anti* while cytosine adopts the *syn* conformation.

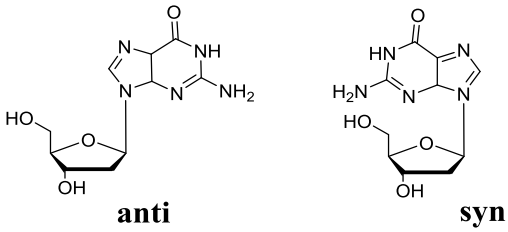

Figure 1-4: Two different conformations of nucleobases, *anti* and *syn*, shown with guanine as an example.

The ribose sugar ring can adopt two different conformations as shown in Figure 1-5. The 3'-endo conformation is more commonly found within ribonucleic acid (RNA) duplexes while the 2'-endo conformation is found in DNA.

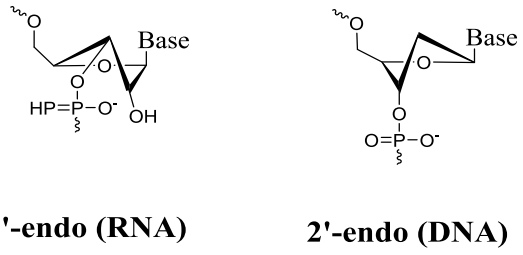

Figure 1-5: Conformations of the ribose sugar ring, 3'-endo and 2'-endo.

Ribonucleic acid (RNA) is commonly found as a single strand that can fold back on itself. It has a ribose sugar ring in comparison to DNA, which contains a deoxyribose ring. The additional 2' hydroxyl group present in RNA causes the A-form to be taken. The A-form consists of a major groove, which is narrow and deep, and the minor groove which is wide and shallow. Strands of RNA, which contain in the region of 22 nucleotides are called microRNA (miRNA). The miRNA are non-coding and have roles in RNA silencing and also play a part in the regulation of gene expression. Several bodily fluids (blood, urine, tears, breastmilk) have been found to contain miRNA, corresponding to different forms of cancer [6]. Previous work for the detection of miRNA often involved amplification or complex procedures [7-9]. A review from Tian *et al* compared recent methods listing their advantages and disadvantages [10]. While methods such as isothermal exponential amplification require no PCR amplification, the probe design is complex and multiple enzymes are used [11]. Other methods require specialised equipment and are unsuitable for multiplexing work. A highly sensitive simple method would be required to overcome this. This is investigated in section 6.2.

1.2 Oligonucleotide Synthesis

Oligonucleotides can nowadays be synthesised rapidly in any sequence up to about 100 bases, though specialised laboratories will synthesise up to 500 bases in exceptional cases. Synthesis is generally carried out using solid-phase synthesis (SPS) on CPG (controlled pore glass) beads within a column. Solid-phase synthesis has several advantages over solution-based methods, such as the solid support being fully contained within filters. Purification is not needed after each step as any impurities and reagents that are left are washed away through the column. Synthesis can be achieved and controlled with the use of computers. The solid supports are comprised of insoluble particles, which range in size from between 50 and 200 μm. The CPG beads contain deep pores in which the DNA synthesis occurs. Short chains, containing 40 bases and less, are synthesised using a pore size of 500 Å. However, if a longer chain is desired it is recommended that a bigger pore size is used, otherwise the yield of the synthesis will be reduced. The larger the pore size the more fragile the solid support is. The decrease in yield from using a pore size which is too small, however, warrants the use of larger pores. For example, a chain up to 100 bases in length can be synthesised using pore size 1000 Å while longer chains may need to use a pore size of 2000 Å.

An alternative to using CPGs is the use of polystyrene beads. Due to steric hindrance, polystyrene beads are usually only used for small scale synthesis. This is due to adjacent DNA strands causing large scale synthesis to be less efficient. However, for short strands this method can be used to produce large quantities of DNA.

The favoured method for DNA synthesis is the phosphoramidite method. This method was first introduced in 1983 by McBride and Caruthers [12]. It is crucial to use anhydrous solvents due to the phosphoramidite reaction being very sensitive to any moisture that might be present. During this method the strand is synthesised 3’-5’ with one additional base added in each cycle. This cycle has 4 main steps: detritylation, activation and

coupling, capping and finally oxidation. These steps are explained in detail in the following sections.

1.2.1 Step 1: Detritylation

The first step of the phosphoramidite method is to deprotect the DMT-protected 5' position. The first nucleoside, which is preloaded onto the column, is deprotected by the addition of an acid (3% TCA in DCM). This process is shown in Scheme 1-1. Note that the 'ball' that is attached to the end of the oligonucleotide represents the resin solid support of the CPG column. This holds for all the following figures.

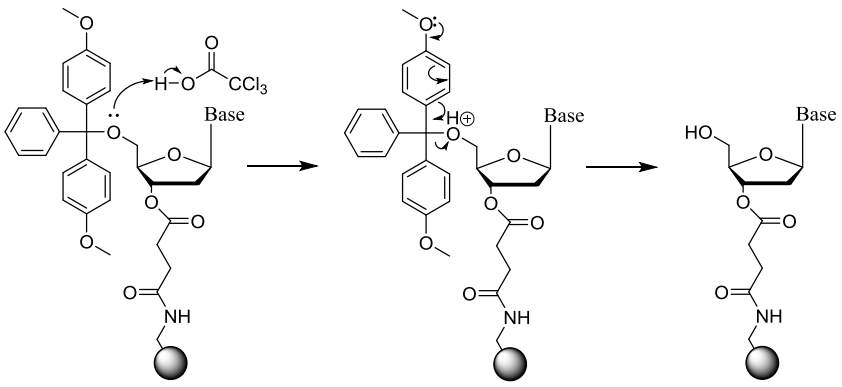

Scheme 1-1: Mechanism of step 1 of oligonucleotide synthesis: detritylation.

During this step an orange colour is observed. This is due to the release of the DMT cation. This orange coloured can be monitored in real time throughout the synthesis to confirm coupling yields qualitatively. If no orange colour is observed, then it is likely that the synthesis has failed or that only a very small yield will be obtained. Once the 5'-position has been deprotected the oligonucleotide synthesis cycle can continue.

1.2.2 Step 2: Activation and Coupling

The second step of the phosphoramidite method is the activation and coupling stage in which the next base of the sequence is added. This is done by adding the monomer in a large excess together with tetrazole, which acts as an activator. The main solvent used is acetonitrile, which is known to work well in oligonucleotide synthesis. Scheme 1-2 shows the mechanism of this second step.

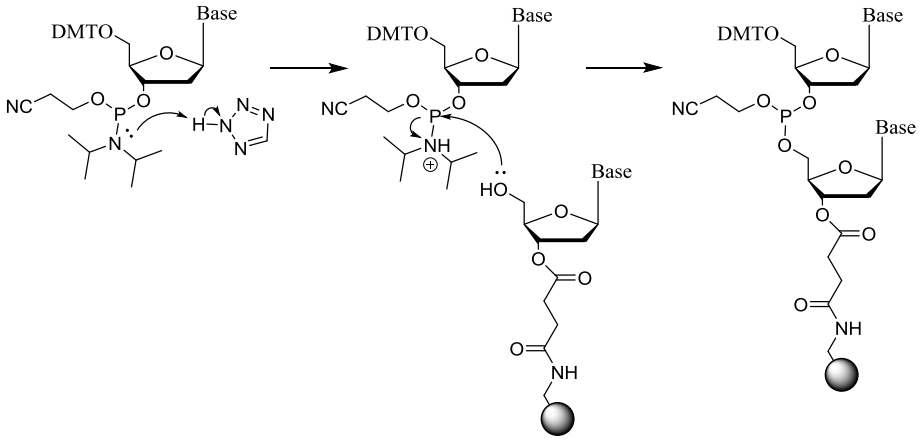

Scheme 1-2: Mechanism of step 2 of oligonucleotide synthesis: activation and coupling.

1.2.3 Step 3: Capping

The third step of the phosphoramidite method for oligonucleotide synthesis is capping. This is to cap any unreacted 5' hydroxyl groups. While a yield of 99.5% can be achieved the capping step is still required. Any unreacted 5'-hydroxyl groups can potentially react with further monomers that are added, which create shorter chains from being synthesised with missing bases, which are not the desired sequence. These chains would be increasingly difficult to remove from longer sequences and therefore further experiments with the oligonucleotides would not be accurate.

Two different solutions are used for the capping step. One is acetic anhydride:pyridine:THF (1:1:8) while the other is 17.6% w/v *N*-methyl imidazole in acetonitrile. The pyridine is used to maintain basic pH. The basic conditions ensure that detritylation of the nucleoside will not occur. Scheme 1-3 shows the mechanism for this step.

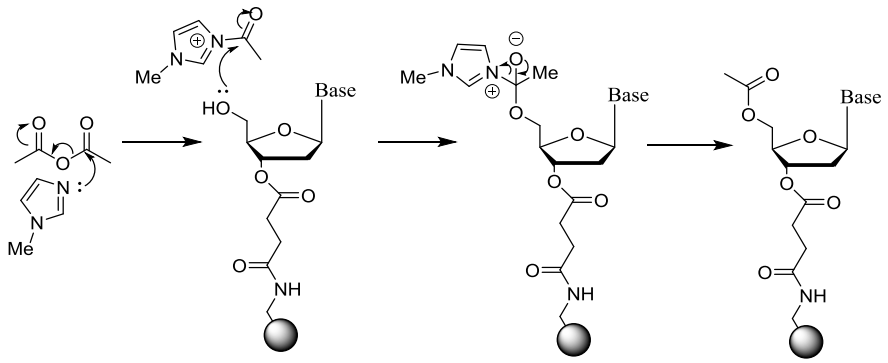

Scheme 1-3: Mechanism of step 3 of oligonucleotide synthesis capping mechanism.

The capping step makes the failed sequences inactive and unable to react further which can then be removed easily during the purification stage.

1.2.4 Step 4: Oxidation

The final step in the oligonucleotide synthesis is the oxidation step. After the coupling step the P(III) centre is unstable in the acidic conditions that will be required for further cycles. Therefore, the P(III) is oxidised to P(V). This is achieved by using a solution containing 0.015 M iodine in water:pyridine:THF (2:20:78). The mechanism for this step is shown in Scheme 1-4.

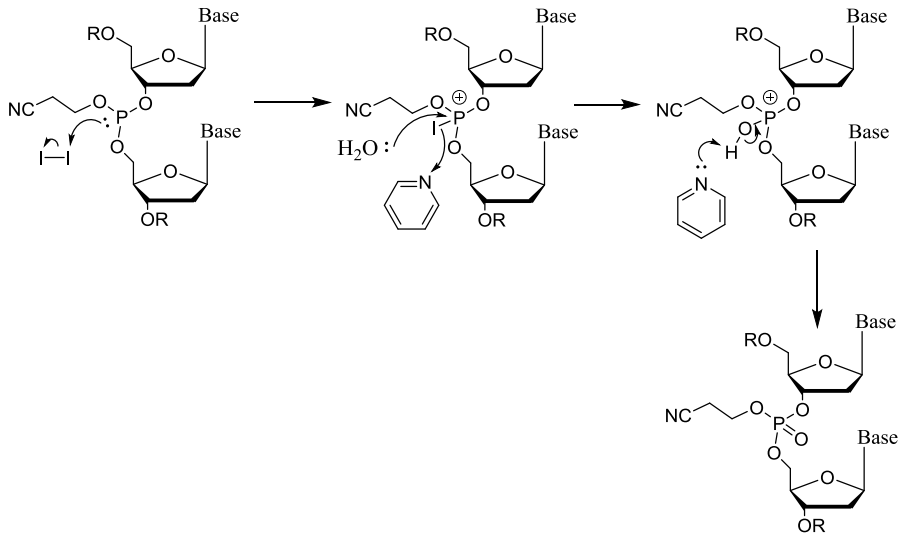

Scheme 1-4: Mechanism of step 4 of oligonucleotide synthesis: oxidation.

Once the oxidation is complete the cycle goes back to the first step and the 5’ hydroxyl is deprotected before another base can be added. This cycle continues until the full sequence is completed on the solid support.

Modified bases can be incorporated into a strand by adding them to the synthesiser. The modifications should be added to the synthesiser with the 5’ hydroxyl group protected and as a phosphoramidite. In this way, the modified base should react in the same was as described by the phosphoramidite oligonucleotide cycle. It is therefore possible to synthesise strands containing for example porphyrin and anthraquinone groups, but in fact almost any modifier can be introduced in this way. It is possible to incorporate the

modification at any point in the sequence and more than one modification can be added in each strand as desired. Many other modifications are possible using this method.

After the oligonucleotide synthesis is complete the DNA is removed from the solid support by ester hydrolysis as shown in Scheme 1-5. This is carried out by adding aqueous ammonia solution and passing it through the column for one hour.

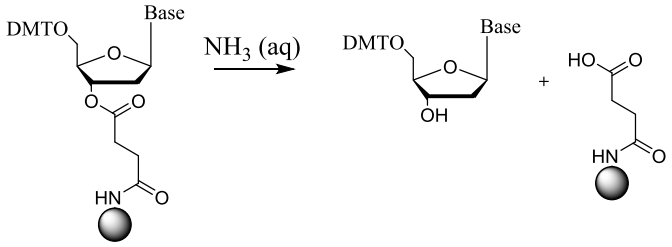

Scheme 1-5: Cleaving an oligonucleotide from the solid support using an aqueous ammonia solution.

After the oligonucleotide has been removed and dissolved in the aqueous ammonia solution, it is heated to remove the protecting groups. This can be done at 40 ºC for 24 hours, or at 55 ºC for 5 hours. Protecting groups on both the bases and the phosphate groups are removed. The cyanoethyl phosphate group is cleaved from the backbone, while the protecting groups on the bases are shown in Figure 1-6 in red. The primary amino groups on the bases adenine, cytosine and guanine are nucleophilic and therefore require protection throughout the oligonucleotide synthesis process. The cleavage of the protecting group from guanine has the slowest reaction time and is therefore the rate determining step. Thymine does not have a primary amino group and consequently does not require an additional protecting group.

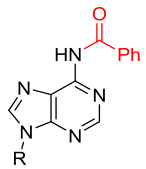

N(6)-benzoyl dA

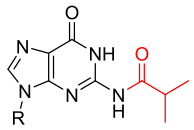

N(2)-isobutyryl dG

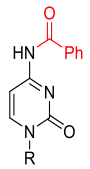

N(4)-benzoyl dC

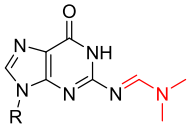

N(2)-dimethylforamidyl dG

Figure 1-6: Structures of the most common protecting groups used for oligonucleotide synthesis (in red). Where R is a sugar ring with 3’ and 5’ hydroxyl groups.

After the protecting groups of the bases have been cleaved the oligonucleotide is ready for purification. Details of which are discussed in a later section (3.3).

1.3 DNA Mutation and Methylation Leading to Cancer

DNA is vital to life and DNA replication constantly occurs in all living organisms. However, when there is an error in this process problems can arise. During the replication process of DNA, mutations and errors can occur. These mutations can occur in the gene promoter region. Single mutations are often corrected but they can be passed down to the daughter cells. Cancer specific mutations can occur anywhere in a gene. For example a mutation to the p53 tumour suppressor gene can lead to tumours and cancer [13].

DNA methylation is the addition of a methyl group to either adenine (N_6 on purine ring) or cytosine (C_5 or N_4 on pyrimidine ring), where mC occurs in humans and mA is limited to bacteria. The structures of these are shown in Figure 1-7. DNA methylation plays a crucial role in regulating gene expression. In cancer, hundreds of genes can be activated or silenced by mutations and methylation. For example, in bladder, prostate and lung cancer DNA methylation is used as a biomarker for detection of the diseases [14-18].

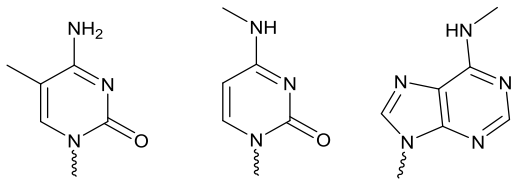

Figure 1-7: Structures of methylated cytosine and adenine.

CpG islands are areas where there is a high frequency of cytosine and guanine next to each other in the strand. Hypermethylation of the CpG islands at the promoter regions occur in cancer, which results in transcriptional silencing [19]. Once DNA methylation or DNA mutations are located and linked to specific types of cancer they can be detected as a form of cancer diagnosis.

1.3.1 Bladder Cancer

Bladder cancer (BC) is the fourth most common form of cancer [17]. Cystoscopy is currently used as the gold standard for detection of BC. Cystoscopy involves inserting a cytoscope, a thin tube with a light and camera on the end, into the urethra in order to investigate the bladder. Aside from being invasive for the patient, this method is expensive and not very specific. Estimated overall costs range between $89,287 and $202,203 per person in the US (long term), and are around £8,349 per person in the UK (annually), due to the high rate of recurrence and disease progression, which necessitates careful long-term monitoring for BC patients [20, 21]. As a result of this, BC turns out to be the most expensive cancer to treat per patient. Thus, a non-invasive, affordable and reliable detection system is required to reduce the BC screening cost, and to ease economic burden on societies. High methylated DNA content has been reported in BC patients compared to healthy individuals [16, 22]. Three genes that are commonly methylated in BC patients are epithelial cadherin (E. Cad), death associated protein kinase (DAPK), and retinoic acid receptor beta (RARβ). These three genes are known as a tumour suppressor gene (E. Cad), a mediator of cell death (DAPK) and a mediator of cell growth gene (RARβ) respectively. Detection of these methylated genes simultaneously in voided urine has been reported to diagnose BC with a 90.9% accuracy [16].

DNA methylation is a promising biomarker for cancer. With this epigenetic abnormality found in the promoter region of many genes, it is easier to use rather than mutations which can occur anywhere within a gene.

1.4 Methylation Specific Polymerase Chain Reaction

DNA methylation (5-MeC) is known to be a key epigenetic change in many different forms of cancer [23]. The hypermethylation of CpG islands, which occurs near the promoter region of a gene, is known to silence tumour suppressor genes and ultimately lead to the development of tumours. This phenomenon has led to extensive research efforts into DNA methylation patterns in order to identify the methylated DNA specific to different forms of cancer, which in turn can be used to assist in cancer diagnosis [19, 24, 25]. An enzyme, DNA methyltransferase, catalyses the transfer of a methyl group to the DNA base where the methyl donor is S-adenosyl methionine (structure shown in Figure 1-8).

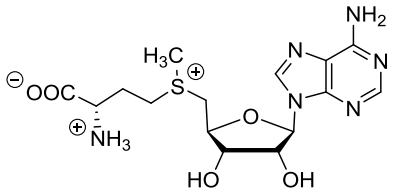

Figure 1-8: Structure of S-adenosyl methionine, methyl donor for DNA methylation.

To distinguish between methylated and unmethylated DNA, a commonly used method is methylation specific polymerase chain reaction (MS-PCR) [26, 27], but the process is not straight-forward. During MS-PCR, a bisulfite treatment is introduced that alters the unmethylated DNA sequence by transforming C to U through cytosine deamination, whereas the 5-MeC is refractory to bisulphite-mediated deamination. The amplification of U as T (and the concomitant G to A transformation in the complementary strand) then allows the methylated to be distinguished from unmethylated CpGs. The outline of this principle is shown in Figure 1-9. MS-PCR is also required to amplify the methylated DNA.

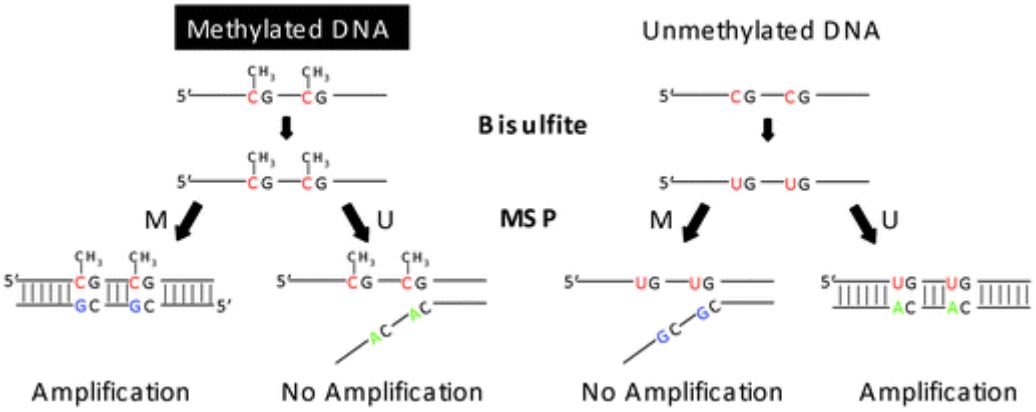

Figure 1-9: Outline of the principle of methylation specific PCR. Reproduced from [27] with permission of The Royal Society of Chemistry.

The bisulfite modification process is shown in Scheme 1-6 where the methylated cytosine remains unaffected.

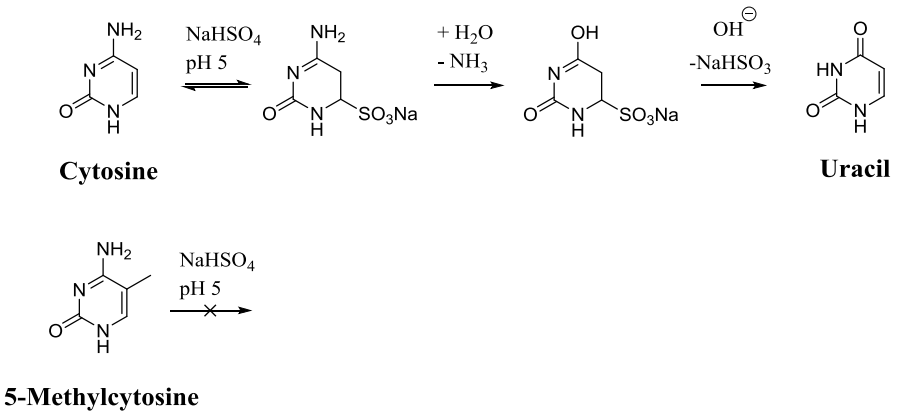

Scheme 1-6: Bisulfite modification of cytosine to uracil while methylated cytosine is not affected.

In addition to MS-PCR, methylated DNA can also be distinguished from unmethylated DNA using endonuclease digestion [28] or array/bead hybridisation [29-31]. However, the 'gold standard' remains with the robust MS-PCR. Research has been carried out to minimise this procedure on lab-on-a-chip technology, allowing the process to take place without the laboratory equipment. However, more research is required before it can have real world applications [32, 33].

1.5 Lab-on-a-chip Biosensors

Lab-on-a-chip (LOC) tends to be small devices that have the potential to be used as a point-of-care (POC) diagnostic application, allowing results to be obtained much faster at the patient site [34, 35]. Such devices can be designed to target a known molecular alternation in bladder cancer related DNA sequences. LOC can be used with very small volumes of sample (less than picolitres) and can be designed to carry out many different lab processes on one chip. Ideally, the previously discussed process of MS-PCR could be carried out on a chip, to eliminate the need for bulky equipment. Research is being done with LOCs in many areas, for example: chemical analysis, medical diagnosis and synthetic chemistry [36].

The advantages to LOCs are the low volumes required for use, which means for example that a smaller sample would be needed for diagnosis than a standard lab test. There would also be less waste and a lower reagent cost. Having the lab processes on one chip should also enable faster analysis times and also provide a better control over the processes used. The fabrication costs for the LOCs are feasible to enable mass production [37].

However, there are also some disadvantages to using LOC devices [37]. They are still being developed and have some physical and chemical problems. On a small scale, the chemical interactions of the surface of the chip and any other materials can become dominant. The surface will have a certain amount of roughness. LOCs can therefore be more complex than the laboratory. The signal to noise ratio can be low when the detection methods do not scale down in an efficient way.

Potentially, LOC systems could be used in developing countries for diagnosis, where a traditional laboratory is too expensive. Therefore the cost of the device is very important. Creating a POC diagnostic test in this way would be very beneficial because the results could be obtained faster and at the site of patient care with only a small amount of sample

required. There are a number of applications for DNA biosensors including: food analysis [38], pollution and environmental monitoring [39, 40], drug screening [41] and medical diagnosis [42].

Electrochemical sensors have attracted much attention due to their cheap production cost and potential to be miniaturised [43], while labelling a DNA probe with a redox marker allows for low detection limits [44]. The higher level of sensitivity with incorporating a redox marker into the design will be exploited in this work. For detection of DNA methylation a number of different methods have been researched with some of the methods detection limits compared in Table 1-1. These methods are described in the following sections.

Detection Method	**Nanomaterial**	**Detection Limit (M)**	**Reference**
Surface Plasmon Resonance		$2x10^{-9}$	Pollet et al 2009 [45]
Quartz crystal microbalance		$20x10^{-9}$	J. Wang et al 2013 [46]
DPV		$1.8x10^{-11}$	P. Wang et al 2012 [47]
Surface-enhanced Raman Scattering	Gold nanoparticles	$5x10^{-13}$	Y. Wang et al 2015 [48]
Photoelectrochemical	Bi_2S_3 nanorods and Au nanoparticles	$3.5x10^{-14}$	Yin et al 2014 [49]
CV	Fe_3O_4/TMC/Au nanocomposites	$2x10^{-15}$	Daneshpour et al 2015 [50]

Table 1-1: Comparison of different methods of DNA methylation detection with their detection limits.

1.5.1 Surface Plasmon Resonance

Surface plasmon resonance (SPR) is a technique used to monitor real time interactions between a metal surface, such as gold or silver, with a sample (for example: antibodies, proteins or nucleic acids). SPR was discovered in 1968 by Otto and commercialised in 1990 by Biacore® for applications related to biomolecular interactions [51, 52].

The basic principle of SPR is that a change to the metal surface induces a difference in the refractive index which can be seen by a shift in the relative SPR signal. A metal surface is required so that there are free electrons that can be excited by the polarised light. The three main SPR configurations are denoted Grating, Otto and Kretschmann methods. The incident light for the Grating method travels through the sample solution, while for the Otto and Kretschmann methods the light travels through a prism [52]. For the Biacore® X100 machine used in this project, the Kretschmann configuration is used. A diagram of the Kretschmann configuration is shown in Figure 1-10.

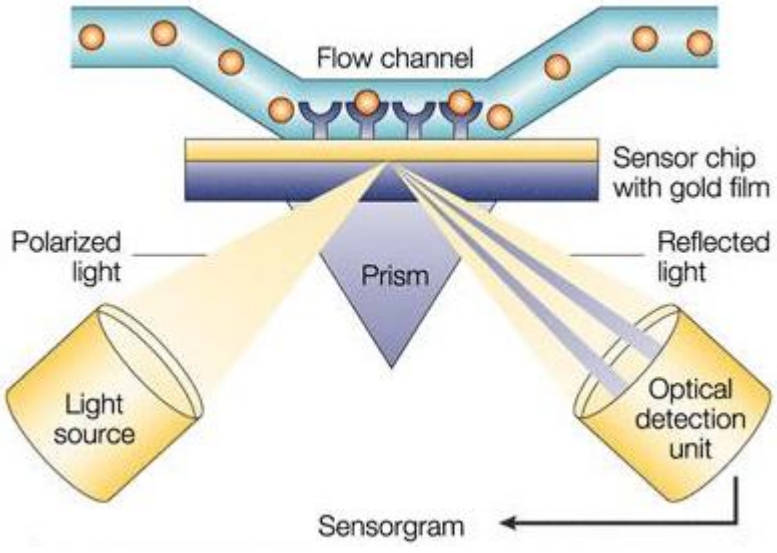

Figure 1-10: Diagram of the Kretschmann configuration as used in the Biacore® X100. Reprinted from [34] with permission from Nature Publishing Group.

SPR can be used for detecting direct molecular adsorption. For example it finds applications with polymers, proteins and DNA [34]. When DNA is immobilised onto the surface of the gold chip a change to the relative SPR signal is observed. A thiol linker attached to the DNA provides an efficient means of immobilisation due to direct spontaneous bonding between the thiol and the gold surface. If a thiol linker is unavailable other methods can be used, for example streptavidin and biotin bind strongly, and therefore the gold chip can be functionalised with streptavidin while the DNA can be modified with biotin. As SPR is a sensitive technique, the DNA sample is often diluted from the running buffer. An example SPR chromatogram of a binding cycle can be seen in Figure 1-11.

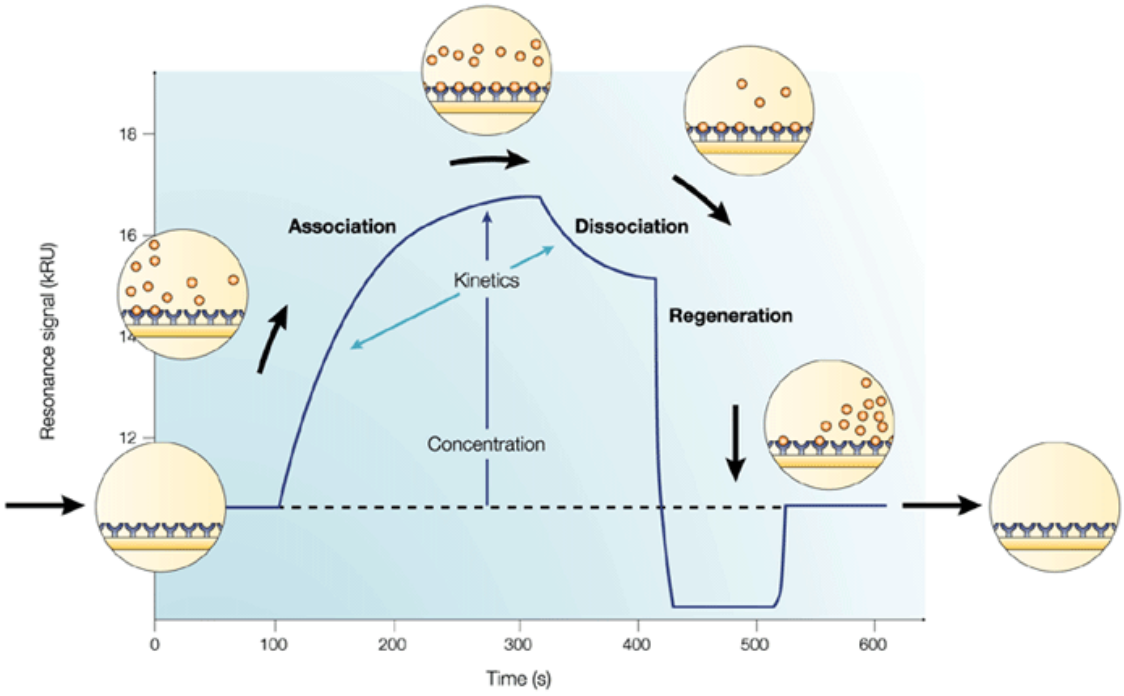

Figure 1-11: Example SPR chromatogram for a typical binding cycle. Reprinted from [34] with permission from Nature Publishing Group.

Pollet et al carried out DNA hybridisation detecting using SPR and found a limit of 2 nM [45]. However, SPR requires a bulky machine and does not have the potential for miniaturisation to develop a lab on a chip device using the technique.

1.5.2 Cyclic Voltammetry

Cyclic voltammetry (CV) is an electrochemical method where a potential is cycled back to the initial potential as many times as is required. The current from different potentials is recorded and is observed from the movement of electrons in a redox species that is present as it is oxidised/reduced. The peak at positive current is due to oxidation while the peak at negative current is due to reduction of the redox species. Changes to the peak current observed can be used to monitor DNA hybridisation and therefore the corresponding DNA methylation status (after bisulfite treatment of the DNA). Figure 1-12 shows an example CV where $[Ru(NH_3)_6]^{3+}$ was used as the redox species [47].

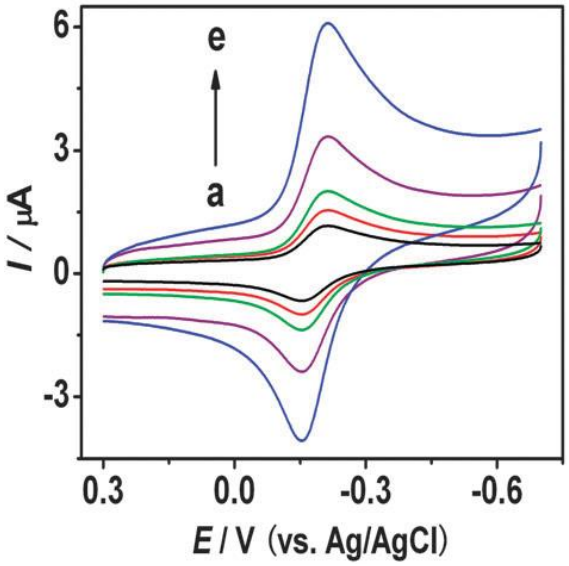

Figure 1-12: CV of hybridisation with different methylated targets a to e (where e contains more methlation sites). Reproduced from [47] with permission from The Royal Society of Chemistry.

1.5.3 Differential Pulse Voltammetry

Differential pulse voltammetry (DPV) is an electrochemical measurement which is similar to staircase voltammetry. Voltage is pulsed regularly with the current being measured before each change in the potential. The current is produced from a redox species undergoing oxidation/reduction as the voltage is applied over the required range specific to the redox species. Unlike in CV where the potential is swept in both directions, DPV potential only goes one way. DPV can provide a better peak resolution over CV with a higher current sensitivity. *Wang et al* successfully used DPV combined with bisulfite conversion for DNA methylation detection [47]. Figure 1-13 shows DPV of DNA hybridisation of methylated DNA targets with different concentrations ranging from 50 pM to 96 nM where the redox species used was $[Ru(NH_3)_6]^{3+}$. The limit of detection was found to be 18 pM [47]. CV and DPV both have the potential to be miniaturised and used in a lab on a chip device.

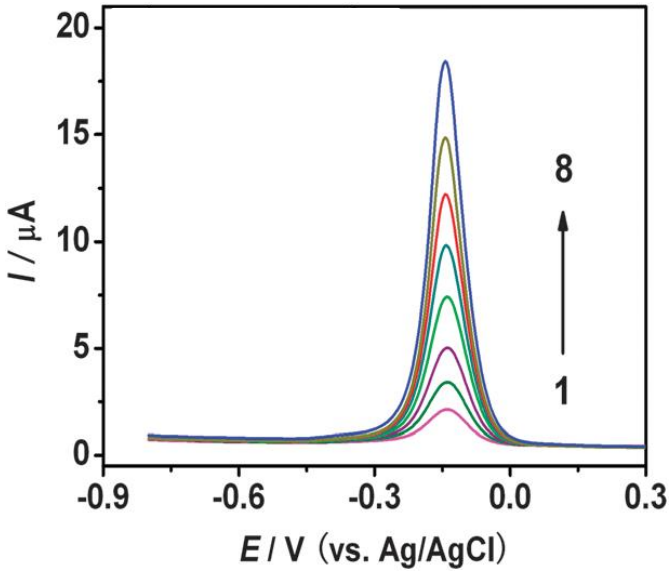

Figure 1-13: DPV of hybridisation with methylated DNA targets with increasing concentration 1 to 8 (where the concentrations were: 50, 100, 200, 600, 1800, 5400, 18000 and 96000 pM). Reproduced from [47] with permission from The Royal Society of Chemistry.

1.5.4 Electrochemical Impedance Spectroscopy

Electrochemical impedance spectroscopy (EIS) can be used to monitor surface changes. EIS is plotted as a Nyquist graph from which the charge transfer resistance (R_{ct}) can be calculated from a semicircle measurement directly from the plot. An increase in R_{ct} indicates binding to the surface of the chip, therefore an increase in R_{ct} is expected upon immobilisation of the DNA probe with a further increase after complementary DNA is added and hybridises with the probe. Figure 1-14 shows an example Nyquist plot where the R_{ct} value is the diameter of the semicircles.

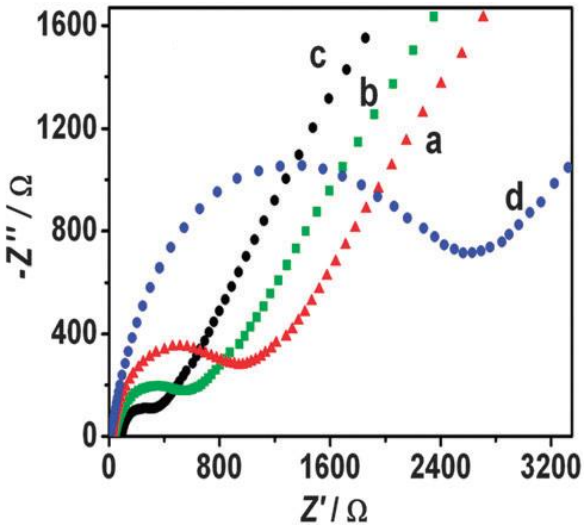

Figure 1-14: Nyquist graph of the different stages of constructing the biosensor. Reproduced from [47] with permission from The Royal Society of Chemistry.

1.5.5 Quartz Crystal Microbalance

Quartz crystal microbalance (QCM) is a detection method that measures the real time frequency shift at the surface. QCM is comprised of a piezoelectric quartz crystal disc and a gold film. The resonance frequency can be measure and upon the addition of a material this frequency will be reduced. *Wang et al* used QCM as a detection method for DNA methylation [46]. A methylation-sensitive restriction endonuclease was used in order to digest unmethylated sequences. The methylated sequences underwent PCR and were injected into the QCM sensor chamber. Thiol modified DNA probes (attached to the gold film) hybridised to the methylated DNA which causes a real time frequency shift. The limit of detection was found to be 20 nM with the advantages of avoiding using labour intensive gels which can be highly toxic. Figure 1-15 shows the QCM curves with 5 different concentrations of target DNA.

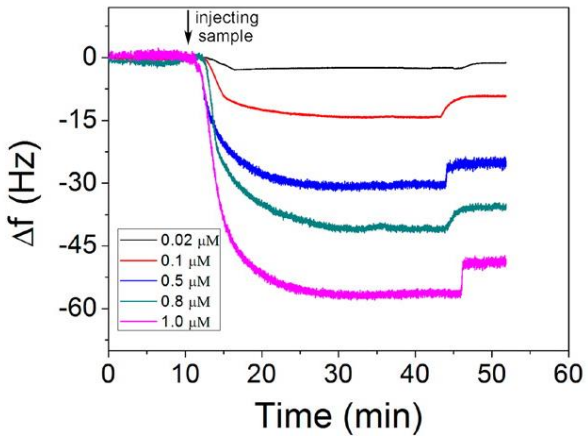

Figure 1-15: QCM curves when target DNA is added. Five difference concentrations shown. Reprinted with permission from [46]. Copyright 2013 American Chemical Society.

1.5.6 Surface-enhanced Raman Scattering

Surface-enhanced Raman scattering (SERS) is a technique which has the capability of detecting single molecules. By performing SERS after DNA undergoes a bisulfite treatment methylated DNA can be detected. *Wang et al* carried out sensitive DNA methylation analysis using SERS and obtained a limit of detection of 50 pM [48]. Figure 1-16 shows a schematic of this methylation analysis. The DNA was labelled with gold nanoparticles in order to enhance the sensitivity of detection. An advantage of SERS detection is the multiplexing potential due to the Raman bands having distinctive and narrow bandwidths.

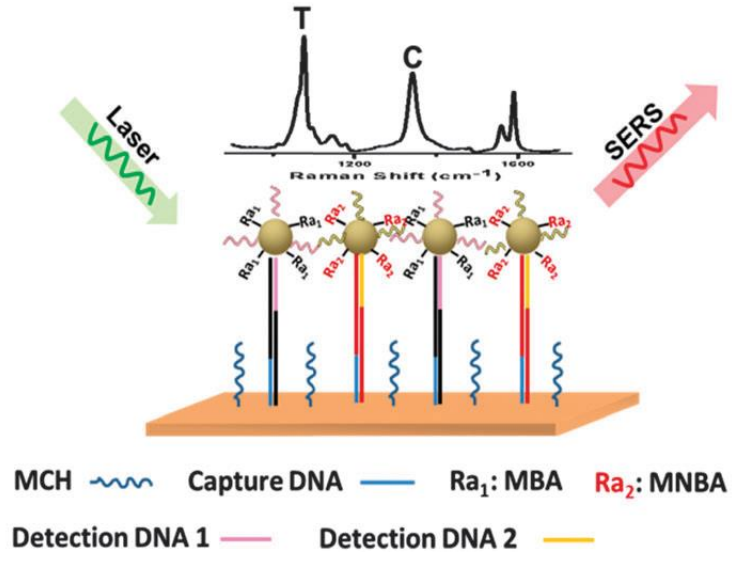

Figure 1-16: Schematic showing DNA methylation analysis via SERS on a gold surface. Reproduced from [48] with permission from The Royal Society of Chemistry.

1.6 Electrochemical and Fluorescent Tags

Biosensors can be combined with electrochemical or fluorescent tags in order to enhance detection. The following sections introduce tags which can be used for electrochemical or fluorescence detection. The tags can be covalently incorporated into a DNA strand.

1.6.1 Anthraquinone

Anthraquinone can be used as an electrochemical tag [53]. It is an aromatic compound with the structure of the most common isomer used (9,10-anthraquione) shown in Figure 1-17, which is formed by the oxidation of anthracene.

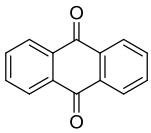

Figure 1-17: Structure of 9,10-anthraquinone.

While anthraquinone has many reported uses, including the stabilisation of triplex-forming oligonucleotides [54] and the detection of induced duplex melting [55]; it has also been used as an electrochemical tag for DNA hybridisation [56]. Previous work with using anthraquinone for DNA detection obtained a limit of 0.32 pM [57].

The redox reaction for anthraquinone is shown in Figure 1-18.

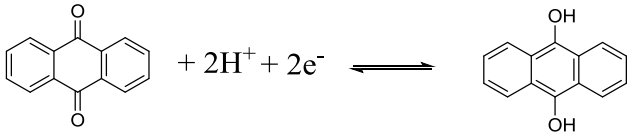

Figure 1-18: Redox reaction for anthraquinone

Anthraquinone modified nucleobases with a sufficiently long linker can maintain the B-form DNA, allowing the anthraquinone to reside in the major groove [58]. Therefore the anthraquinone will be attached to the nucleobase via a short chain with an amide bond to the nucleobase. Anthraquinone can be commercially bought as anthraquinone-2-carboxylic acid which allows it to be joined to a nucleobase with an extended amine chain. The synthesis of an anthraquinone monomer is discussed and investigated in 3.1.1.

1.6.2 Porphyrin

Porphyrin is a macrocyclic molecule that can potentially be used as either an electrochemical or a fluorescent tag. Porphyrins, which are naturally occurring, are essential for both plant and human life. In plants, chlorophyll plays a role in photosynthesis in which the plants can absorb energy from light. Chlorophyll is a magnesium metalloporphyrin with the structure of the most common form (chlorophyll c_2) shown in Figure 1-19. Porphyrins are also found in blood where they transport oxygen around the body. The most common form of the iron metalloporphyrin (haem B) is shown in Figure 1-19.

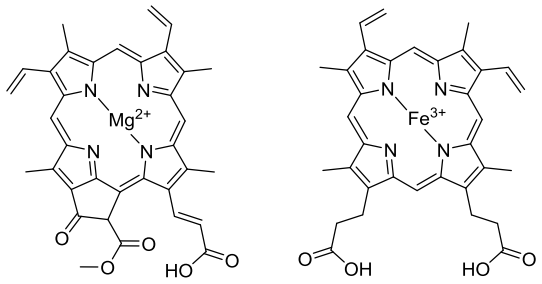

Figure 1-19: Structures of the most common forms of Chlorophyll (Chlorophyll c_2) and Haem (Haem B).

Porphyrins obey Huckel's law (4n + 2) for aromaticity in which they contain 18π delocalised electrons around the planar macrocycle. There is a small energy gap between the highest occupied molecular orbital and lowest unoccupied molecular orbital due to the large number of conjugated bonds. Thus, porphyrins have intense absorptions and are brightly coloured.

Transition metals can be added to porphyrins, which bind to the internal nitrogens, in order to change their optical and electronic properties. The internal cavity of porphyrin is approximately 4 Å wide allowing small transition metals (e.g. Mg^{2+}/Fe^{3+}) to sit inside, while bigger metals (e.g. Re^{+}/Hf^{4+}) distort the ring and sit above the cavity. The addition of a metal to the porphyrin increases symmetry and therefore the absorbance spectra differs. In free base porphyrin, where there is no metal present in the cavity, the UV spectra shows a large Soret band and four small Q bands. In metalloporphyrin only two Q bands are present due to the increased symmetry which is shown in Figure 1-20.

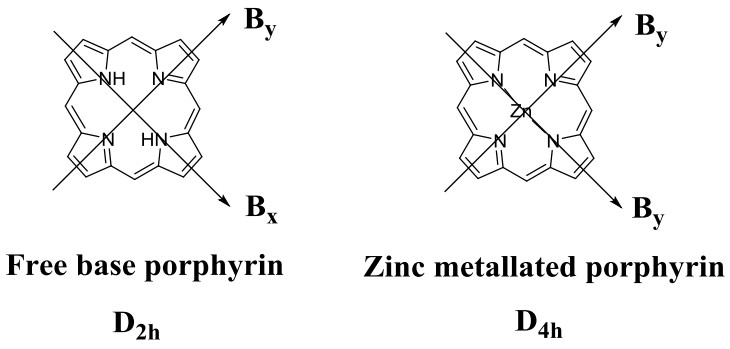

Figure 1-20: Structures to show the difference in the transition dipole moments which are present in free base porphyrin (D_{2h}) and zinc metallated porphyrin (D_{4h}).

An absorbance spectrum for free base porphyrin showing the Soret band (420 nm) and four Q bands (500-700 nm) is shown in Figure 1-21.

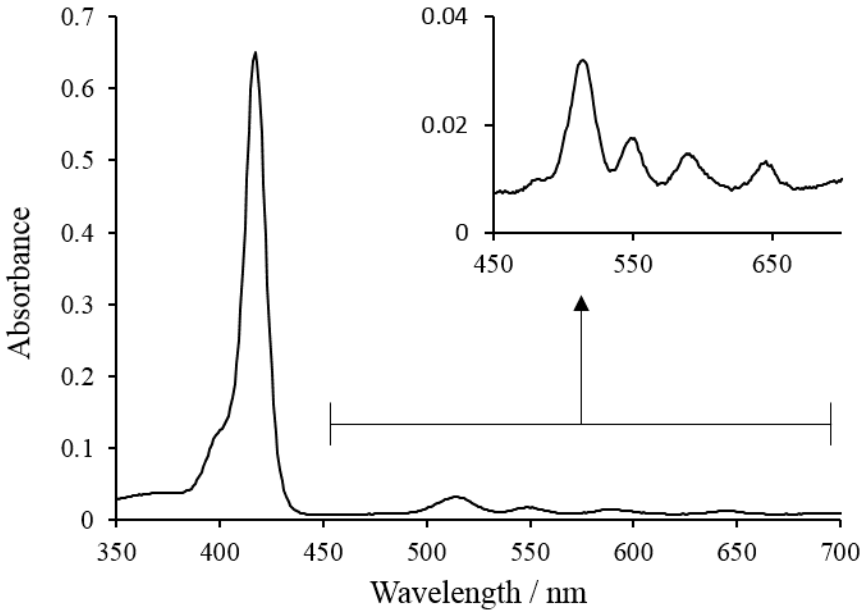

Figure 1-21: Absorbance of free base porphyrin with the Soret band (420 nm) and inset of four Q bands (500-700 nm).

Porphyrin synthesis has been reported and improved by Rothemund and Adler [59-61]. Their work mainly focused on simple symmetric porphyrins. Lindsey then synthesised unsymmetrical porphyrins using a mixture of aldehydes [62]. A method has been developed by the Stulz group to synthesise the mono-substituted porphyrin in a higher yield [63]. This is discussed in more detail in 3.1.2, but the key point is the ratio 6:6:1 of benzaldehyde:pyrrole:methyl-4-formylbenzoate to maximise the mono-substituted porphyrin. The basic mechanism of porphyrin synthesis is shown in Scheme 1-7.

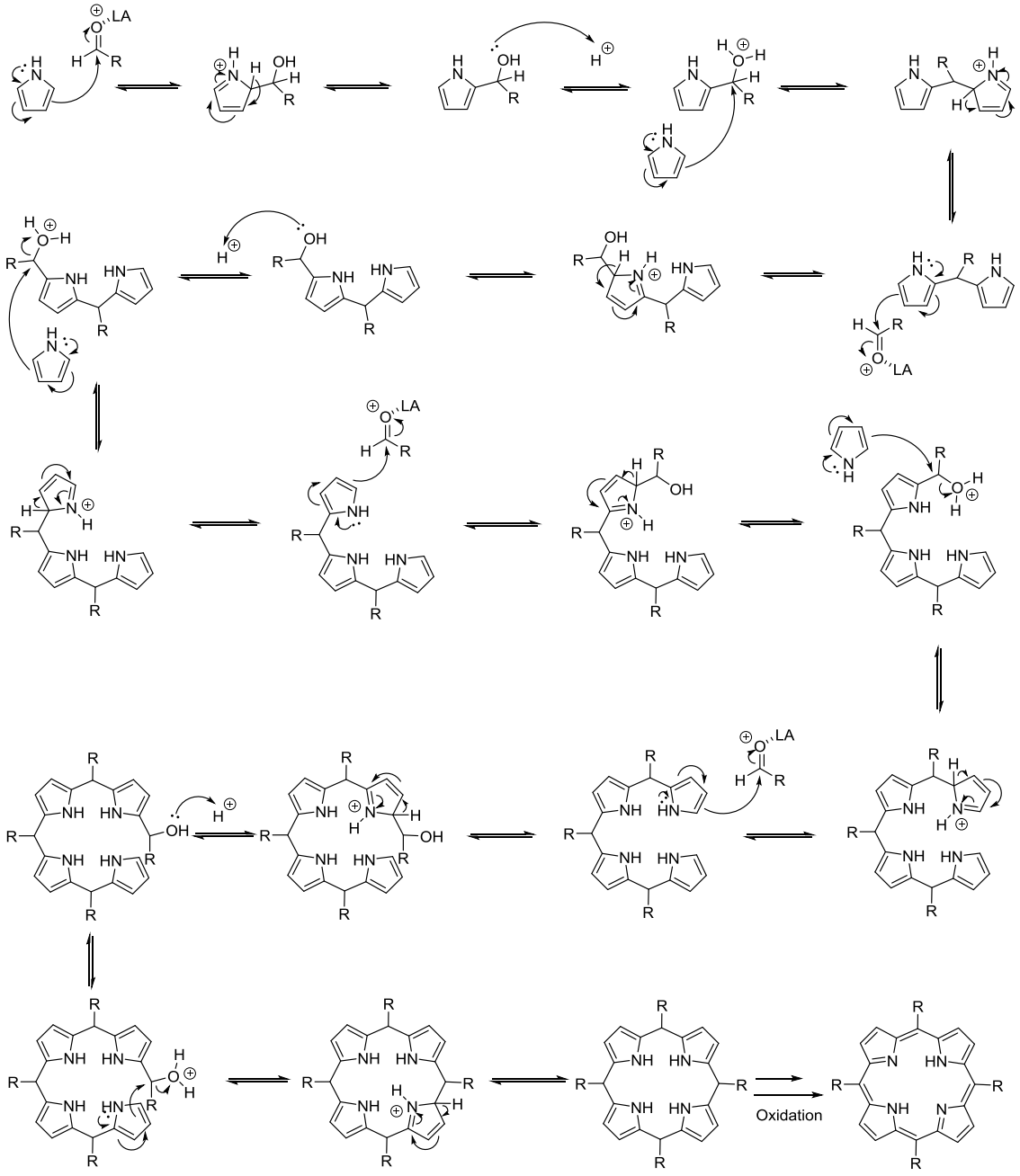

Scheme 1-7: Mechanism of porphyrin synthesis where possible reagents could be: benzaldehyde, pyrrole and boron trifluoride diethyl etherate (Lewis acid).

The ring structure that is synthesised by combining four pyrroles is then oxidised into the porphyrin. This is often carried out from the use of 2,3-dichloro-5,6-dicyano-*p*-benzoquinone (DDQ) as the oxidising agent. The oxidation mechanism is shown in Scheme 1-8.

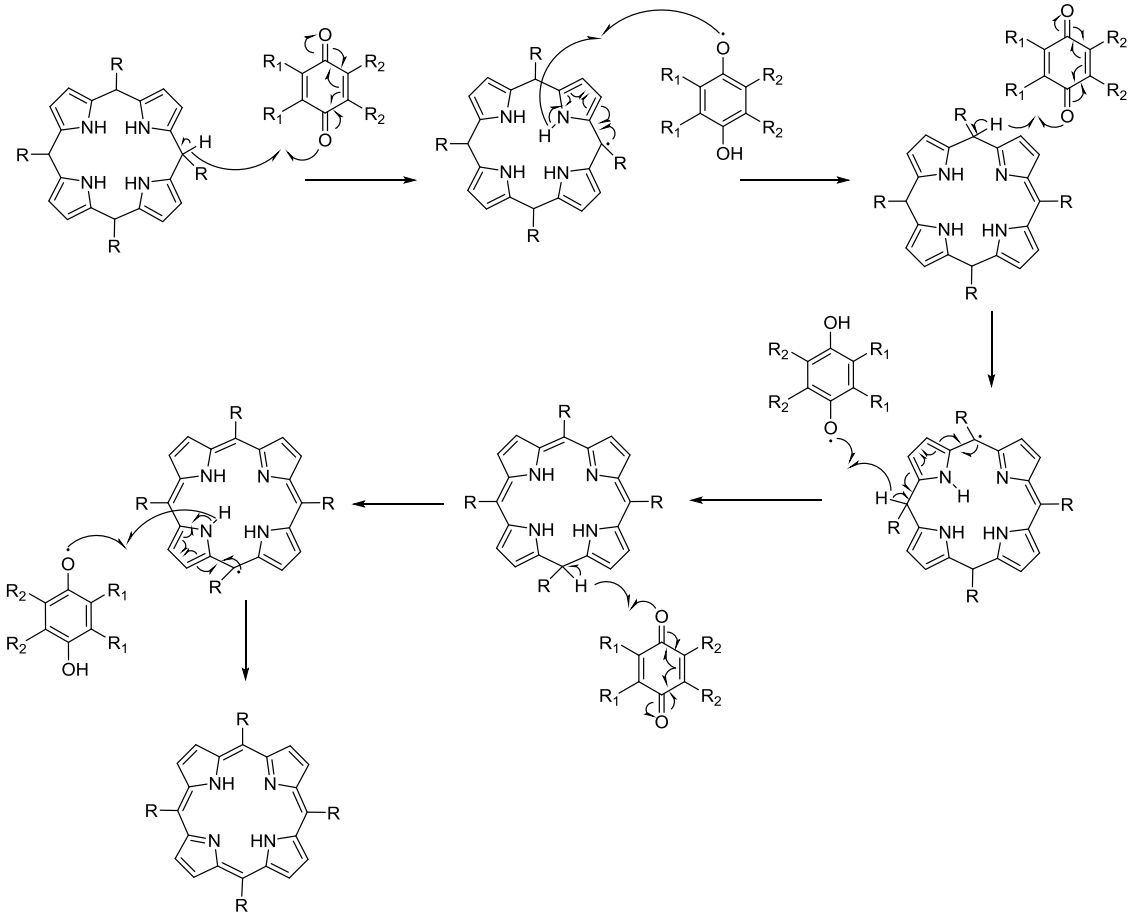

Scheme 1-8: Oxidation of porphyrin mechanism where DDQ is used.

The porphyrin will be attached to the nucleobase, as with the anthraquinone modification, via a short chain with an amide bond. For details see 3.1.

It has been shown that cobalt porphyrin-tagged DNA provides an ideal probe to detect DNA with a detection limit ~20 fM (accounting to 1000 DNA molecules on the microelectrode) using the electrochemical sensing of the porphyrin [64]. A linear probe design was used where the porphyrin is buried in the major groove as the target DNA is added causing a double stranded DNA to hybridise. The linear probe is discussed in the future section 1.7.

As the porphyrin is electrochemically active, it makes it a very versatile internal redox marker for electrochemical measurement, and it can easily be detected using cyclic voltammetry (CV) while avoiding addition of external redox markers and washing steps. Therefore this combination of porphyrin-tagged DNA with an electrochemical sensor could potentially be applied for high sensitivity of methylated DNA detection, which could in turn assist in rapid cancer diagnosis. The redox reaction for free base porphyrin is under discussion with one possibility shown in Figure 1-22. An alternative reaction would be the loss of an electron from the aromatic ring with the resulting charge being spread over the ring. However, when a metal is present the redox process takes place on the metal within the cavity. For example, cobalt can be added to the cavity where the redox reaction is Co(II)/Co(III) which will have a different electrochemical potential than free base porphyrin. This means that porphyrin monomers can be used with different metals corresponding to different sequences to enable multiplex detection to be carried out.

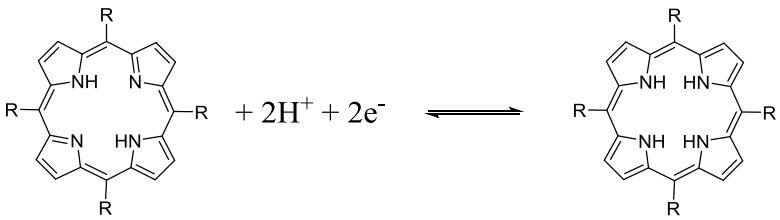

Figure 1-22: Redox reaction of free base porphyrin

1.6.3 Methylene Blue

Methylene Blue is a commercially available electrochemical tag with the structure shown in Figure 1-23. It can be synthesised by the use of a starting material dimethyl-4-phenylendiamine

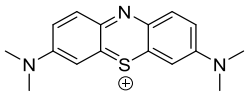

Figure 1-23: Structure of methylene blue.

Methylene Blue can be linked with DNA covalently and non-covalently [65-67]. Methylene Blue is known to be an electrochemical redox marker by previous work [44, 65, 68, 69]. As a commercially available tag it can be compared with other tags which are made synthetically. Figure 1-24 shows the redox reaction for methylene blue.

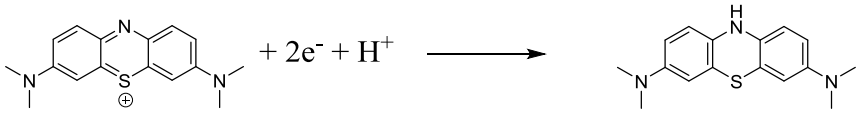

Figure 1-24: Redox reaction for methylene blue.

1.6.4 Ferrocene

Ferrocene ($Fe(C_5H_5)_2$) is comprised of an iron atom which is sandwiched between two cyclopentadienyl rings. Ferrocene can be oxidised where is loses a single electron to become $Fe(C_5H_5)_2^+$. It can be conjugated with DNA to be used as sensor for DNA hybridisation detection [70, 71]. Figure 1-25 shows the structure of ferrocene and its linker to the DNA as used by *Nakayama et al* [70].

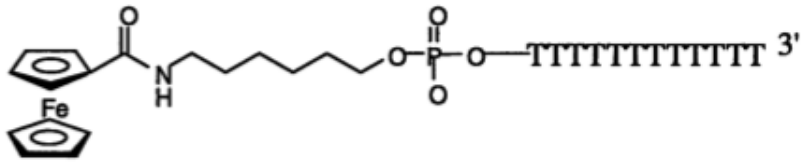

Figure 1-25: Structure of the ferrocene tagged DNA. Reprinted from [70] with permission from Elsevier.

Kang et al compared methylene blue and ferrocene directly with use in an electrochemical sensor [44]. Both redox active tags show sensitive DNA detection, however, there is a difference in stability between the two tags. It was shown that methylene blue is more stable and repeated cycles can be carried out. Ferrocene was observed to lose approximately 50% of the original signal upon regeneration [44].

1.6.5 Acetyacetonate

For multiplex detection being able to tune the redox active tag to a different electrochemical potential is a big advantage. As previously discussed, the electrochemical potential of the porphyrin tag (see 1.6.2) can be altered by the addition of a metal to the cavity and adding substituents. The same was seen by *Weizman et al* by the development of acetyacetonate complexes using Ru and Os as the metal centres [72]. It was found that nucleotide was readily incorporated into DNA allowing it to have a possible future in DNA detection / diagnostics. Figure 1-26 shows the structures and electrochemical potentials of these complexes.

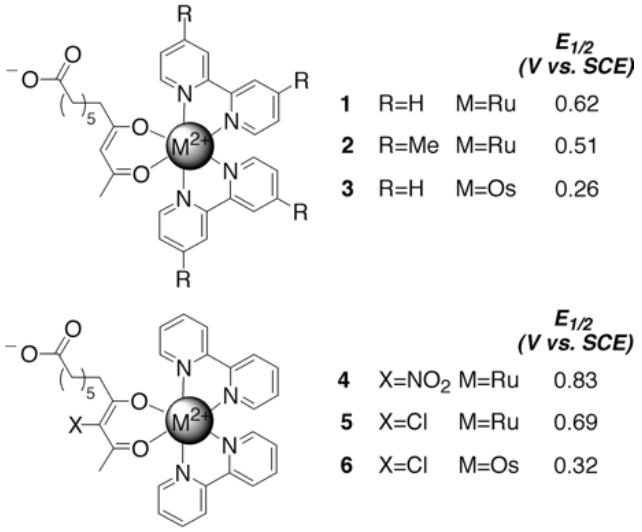

Figure 1-26: Structures of acetyacetonate complexes (including electrochemical data) with a functionalised linker for attaching to a nucleotide. Reprinted with permission from [72]. Copyright 2002 American Chemical Society.

1.7 Molecular Beacon Design

One way of detecting methylated DNA is to use a molecular beacon approach. DNA can be synthesised to have a tag on one end, and the opposite end modified to attach to the surface of the chip used. A hairpin loop can be designed so that when the probe is immobilised to the surface the chemical tag is in close proximity of the surface. After hybridisation with the target DNA, the chemical tag should then move away from the surface. Potentially both a fluorescent and electrochemical tag could be used. This design can be seen in Figure 1-27 with a porphyrin tag used as an example.

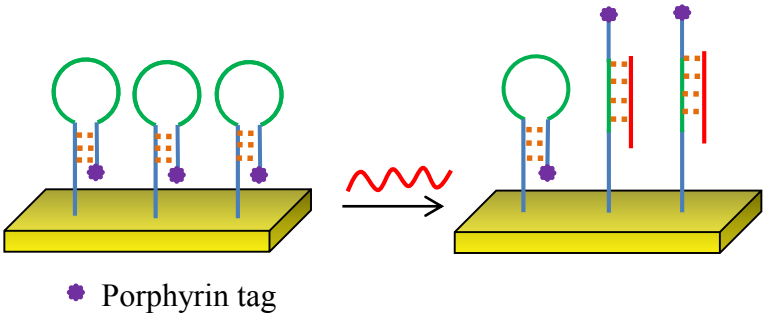

Figure 1-27: Schematic of the working principle of the hairpin DNA probe before and after hybridisation with complementary target DNA, with the chemical tag, in this case porphyrin, moving away from the surface.

For an electrochemical device, a gold chip can be used where the output observed is current. A 5'-thiol modification can be added which spontaneously forms a bond with the gold surface, as seen in Figure 1-28, attaching the DNA to the gold surface. This can either be a thiol or a dithiol modification.

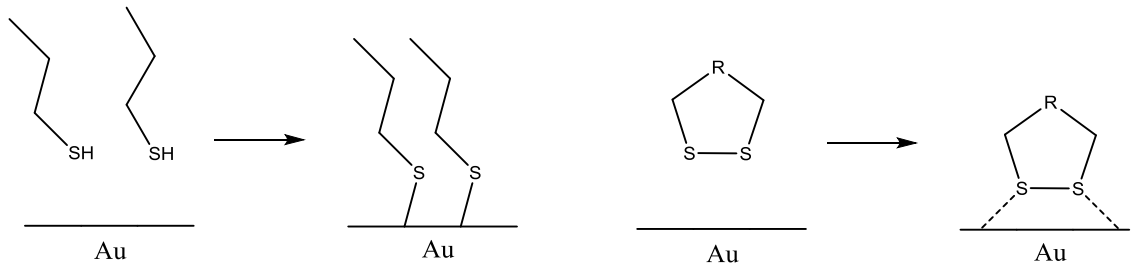

Figure 1-28: Thiol and dithiol modification spontaneously attaches to a gold surface.

The trend of the current response, with a gold electrochemical sensor, of the proposed probe (hairpin design) and hybridised target DNA is presented in Figure 1-29.

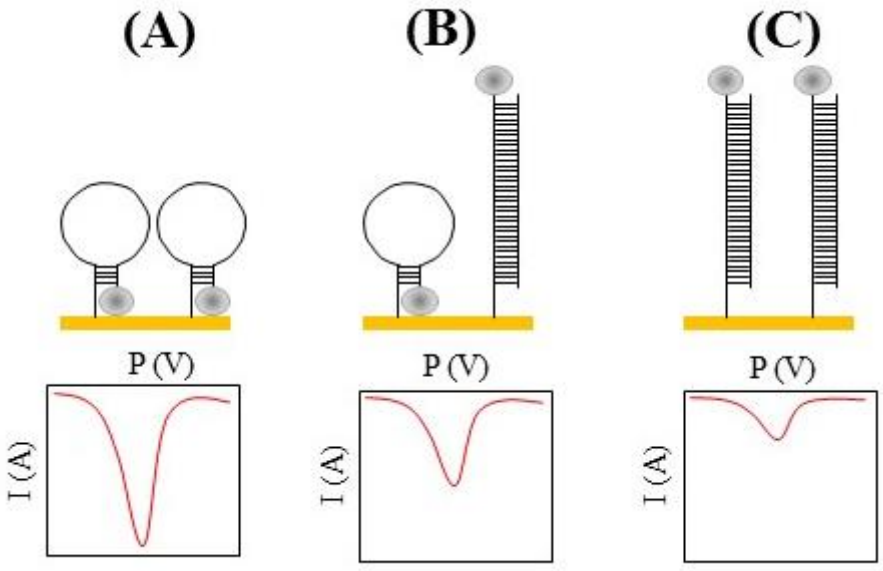

Figure 1-29: (A) Probe immobilised onto gold surface, high current response. (B) Low concentration of complementary target DNA, reduction in current response. (C) High concentration of complementary target DNA, large reduction in current response.

The chemical tag can be either used for electrochemical or fluorescence experiments, depending on the properties of the tag. With the fluorescence experiments when the tag is close to the gold surface of the device the fluorescence is quenched as presented in previous work [73, 74]. After the target DNA is added and it hybridises with the probe DNA the fluorescent tag is then at a greater distance from the surface and so the fluorescence will be observed. This should enhance the sensitivity of the device. Work from Huang *et al* showed that their fluorescent setup had a limit of detection (of 0.3 nM) one order of magnitude lower than previous work [75]. As well as synthetically made fluorescent tags, commercial dyes have also been used [76]. An electrochemical tag, for example an anthraquinone, porphyrin or ferrocene tag [44] could also be used with a reduction in current after hybridisation.

In addition to hairpin designs, a linear design can also be used for DNA detection (Figure 1-30). In such a design the porphyrin tag can be buried within the hydrophobic major groove of the dsDNA which means that they are not as accessible, which leads to a lower current response [77]. The porphyrin on a single strand will have a higher signal so in this case a lower current response would be expected upon hybridisation.

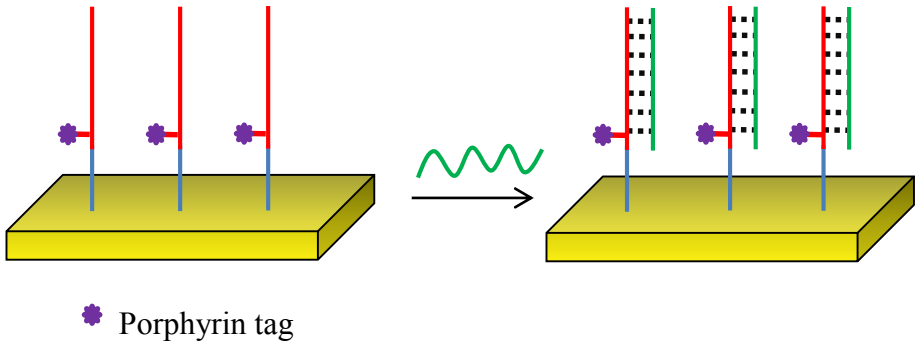

Figure 1-30: Schematic of a linear probe design and the addition of complementary target DNA.

2. Aims and Objectives

The aim of this project was to synthesise chemically modified DNA probes (tagged with porphyrin or anthraquinone) to enhance the detection sensitivity of DNA hybridisation. This was then compared with a commercially available tag (methylene blue). Molecular beacons were used where a hairpin and linear sequences were designed. Different sensors were investigated in order to find the most compatible one for the system proposed.

In bladder cancer, three genes (DAPK, E. Cadherin and RARβ) are found to be methylated in the promoter region [16]. Simultaneous detection of these three genes is essential for bladder cancer diagnosis. Therefore, what is required is a highly sensitive multiplex sensor, able to detect several DNA sequences in parallel, which eventually can be combined with MS-PCR. A section of this project develops a multiplex sensor which was used together with chemically tagged DNA probes. Previous work within A*STAR (Singapore) carried out MS-PCR 'on-chip' distinguishing between methylated and unmethylated DNA [32, 33]. Therefore this project will detect the product of the MS-PCR with the aim of enhancing this detection for an increased sensitivity.

Strands in which the recognition section is contained solely in the loop of the hairpin design, and strands where the recognition section is incorporated into the stem of the hairpin design were then compared. In addition to the hairpin probes, a linear probe was also investigated. These are based on the designs discussed in 1.7.

Alongside DNA methylation, mutations specific to bladder cancer are also investigated. The detection of bladder cancer specific miRNA directly in a patient's sample was explored with the use of Surine (urine negative control).

The project was split between the University of Southampton and A*STAR, Singapore – where an equal time was spent in both. The probes were synthesised within the University before being sent to Singapore where the testing was carried out.

3. Chemically Tagged Oligonucleotides

To enhance the sensitivity of DNA detection, oligonucleotides were synthesised with an incorporated redox active tag for electrochemical and fluorescence detection. The specific position of this redox active tag within the oligonucleotide sequence was discussed in 1.7. The sequences of the probes were based on three methylated bladder cancer genes (DAPK, E. Cadherin and RARβ) which were chosen to demonstrate the system. This chapter discusses the synthesis and purification of anthraquinone and porphyrin oligonucleotides alongside the attempted synthesis of a phthalocyanine monomer.

3.1 Synthesis of Redox Active Tags for Incorporation into Oligonucleotides

3.1.1 Synthesis of Anthraquinone Phosphoramidite

The first step of the anthraquinone synthesis shown in Scheme 3-1 was to protect the 5'-hydroxyl group of the ribose in the starting material 5-iodo-deoxyuridine, so it would be unreactive in future reactions, to give the DMT-protected product (**1**). This was done using 4,4'-dimethoxytrityl chloride (DMT-Cl); the DMT-protecting group is standard in automated solid-phase DNA synthesis (see 1.2). The 5'-hydroxyl is more reactive than the 3'-OH as it is the least sterically hindered, and also a primary alcohol *vs* secondary alcohol at the 3'-position. However, an unwanted bis-product can form when there is an excess of DMT-Cl present, therefore the DMT-Cl was added portion-wise over several hours to ensure that only a single DMT was substituted. An additional measure taken to avoid the bis-product was that the reaction was not left for an extended period of time and was worked up after 30 minutes.

With the 5'-position protected, the next step was to carry out a Sonogashira coupling reaction between (**1**) and progargylamine. This cross-coupling reaction forms a carbon-carbon bond to introduce the propargylamine at the 5-position of uridine (**2**). The Sonogashira coupling is moisture sensitive so oven dried glassware was used along with 3 Å molecular sieves.

An amide coupling was then carried out to attach the anthraquinone group to form the desired product (**3**). The amide couping was carried out using standard carbodiimide coupling reagents (DIC, HOBt) with the commercially available anthraquinone-2-carboxylic acid. The modified base could then be incorporated into DNA synthesis after it had been transformed into the corresponding 2'-phosphoramidite using 2-cyanoethyl *N*,*N*-diisopropylchlorophosphoramidite (CEP-Cl). Phosphoramidites are very reactive towards nucleophiles and are therefore used in solid phase DNA synthesis, as discussed in 1.2. Phosphitylation is highly sensitive to oxygen, as the phosphorous (III) ideally wants to be oxidised to the more stable phosphorus (V), and to moisture as the P-Cl bond is labile to hydrolysis. Therefore the reaction was performed under inert conditions and the product was used immediately on the DNA synthesiser to prevent degradation. The phosphoramidite (**4**) was dissolved in acetonitrile, the same solvent as used with the natural nucleobases, and added to the DNA synthesiser.

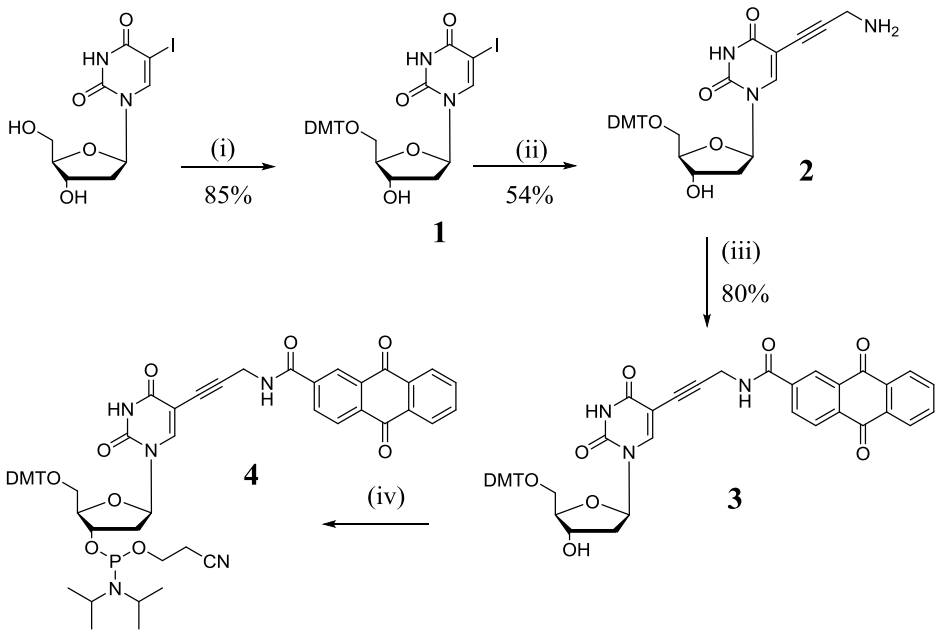

Scheme 3-1: Synthetic route to anthraquinone phosphoramidite [78] (**4**). (i) DMT-Cl, Pyridine (ii) Propargylamine, CuI, $Pd(PPh_3)_4$, DMF, TEA (iii) Anthraquinone-2-carboxylic acid, HOBt, DIPEA, DIC, DMF (iv) CEP-Cl, DIPEA, DCM.

3.1.2 Synthesis of Porphyrin Phosphoramidite

Porphyrins have the potential to be used as an electrochemical or a fluorescent tag, thus providing a dual role modifier. The 'one-pot' synthesis mechanism is shown in 1.6.2. The synthesis of the porphyrin nucleoside is discussed below.

The synthetic route carried out to obtain the porphyrin nucleoside is shown in Scheme 3-2. In brief, this involved an amide coupling reaction between (**2**) and (**6**) (see Scheme 3-2) to form the porphyrin monomer (**7**), which was then phosphitylated using CEP-Cl to give the phosphoramidite (**8**). This phosphoramidite (**8**) was then incorporated into DNA using automated SPS (see section 3.2).

In detail, the ratio 6:6:1 of benzaldehyde:pyrrole:methyl-4-formylbenzoate was used to synthesise the mono substituted porphyrin (**5**). Previous work by the Stulz group had shown this to be the best ratio to produce the methyl ester, suppressing the formation of the higher substituted porphyrins which would make purification difficult. The methyl ester porphyrin was produced in a yield of 15%. This would be a very low yield in other synthetic chemistry, however, in porphyrin synthesis this is acceptable as a yields of less than 10% are often reported [79].

A strong base (KOH) was used in a large excess to convert the methyl ester porphyrin (**5**) to the carboxylic acid (**6**). To shorten the reaction time the reaction mixture was heated to 40 °C. During the work-up procedure a small amount of acid was added. This was to neutralise the solution as the deprotonated porphyrin is slightly soluble in water. The neutralised porphyrin is soluble in the organic layer and this enables separation to be carried out with more ease. However, care was taken not to add too much acid in order to prevent the dark purple solution turning bright green. The bright green colour change would occur due to the protonation of nitrogen in the porphyrin ring. This causes the porphyrin to buckle and moves the phenyl groups into the same plane as the porphyrin.

Hence the conjugation of the molecule greatly increases, which is indicated by the bright green colour. A yield of 70% was obtained for this reaction.

The carboxylic acid porphyrin (**6**) was then coupled with the amine nucleoside (**2**) analogously to the synthesis of (**3**), which produced the porphyrin nucleoside (**7**) with a yield of 78%. Care was taken while monitoring the reaction as the starting material and product have similar R_f values (0.52 (**6**) compared to 0.49 (**7**) where the solvent used was 10% MeOH in DCM). To distinguish between the starting material and product, longer TLC plates were used (10 cm length compared to 5 cm).

The porphyrin nucleoside (**7**) was then transformed into the phosphoramidite monomer (**8**), for incorporation into a DNA strand during DNA synthesis. As with the previous phosphoramidite reaction (to form (**4**)), the product was immediately used for DNA synthesis to avoid degradation of the product. However, a small sample was taken for analysis by ^{31}P NMR spectroscopy. The reagent used, CEP-Cl, was found to contain a single peak (180.63 ppm) while the porphyrin monomer (**8**) was found to contain two peaks (149.71 ppm, 149.35 ppm). This was due to the product being diastereomeric, as indicated by separate peaks in NMR, while the reagent is a racemate which only shows a single peak.

The phosphoramidite (**8**) was dissolved in a 1:1 mixture of DCM and acetonitrile. This was due to (**8**) being insoluble in acetonitrile alone, which is the preferred solvent for DNA synthesis. DCM alone would be unreliable to use, as the high vapour pressure of the solvent showed to cause problems in the DNA synthesiser, as the solution was passed too quickly through the column.

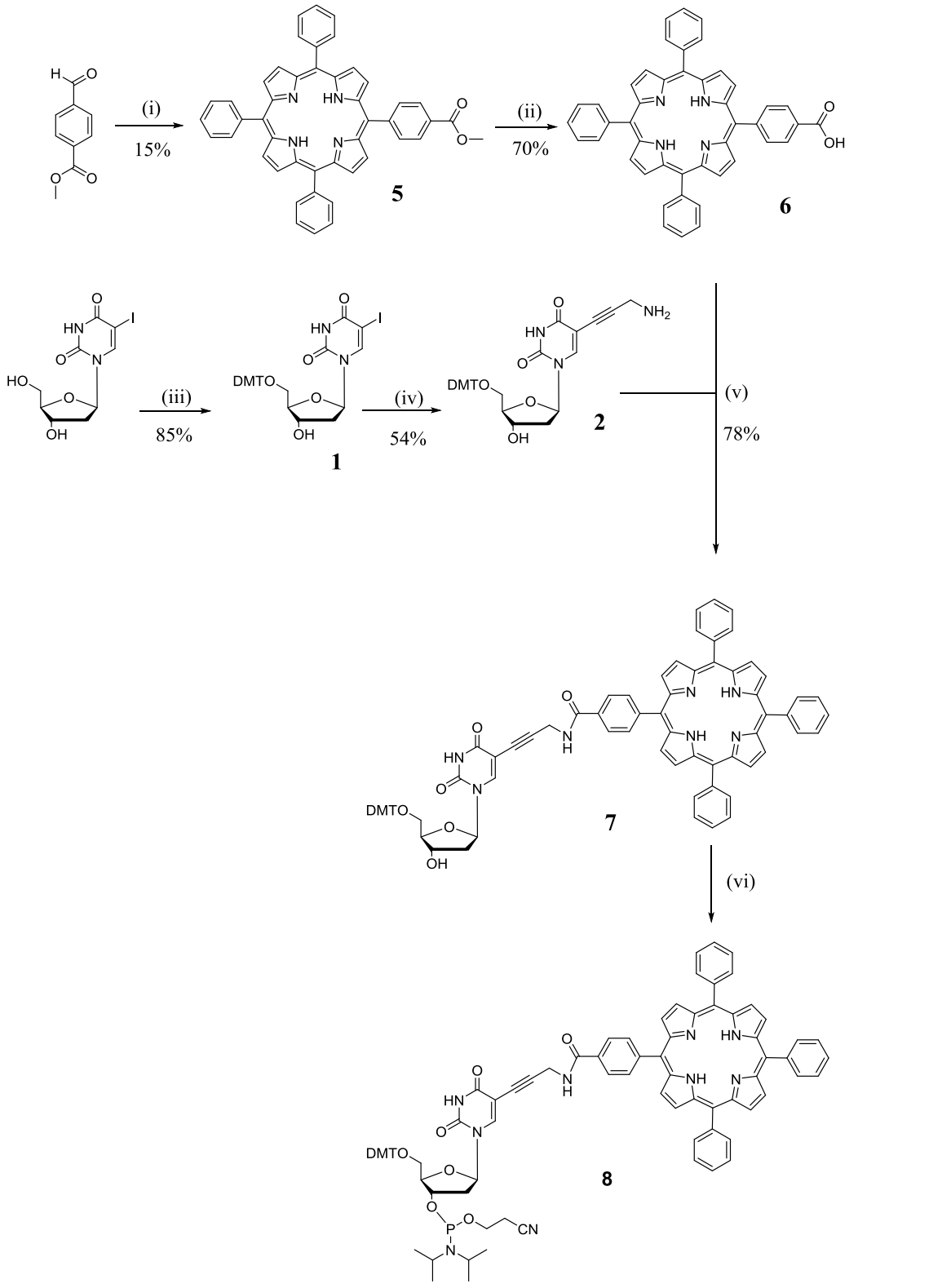

Scheme 3-2: Synthetic route to porphyrin phosphoramidite [63] (**8**) (i) Benzaldehyde, Pyrrole, $CHCl_3$ 1. $BF_3.Et_2O$, 2. DDQ (ii) KOH, Pyridine, H_2O (iii) DMT-Cl, Pyridine (iv) Propargylamine, CuI, $Pd(PPh_3)_4$, DMF, TEA (v) HOBt, DMAP, DIC, DCM (vi) CEP-Cl, DIPEA, DCM.

3.1.3 Synthesis of Phthalocyanine monomer

In addition to the synthesis of anthraquinone and porphyrin monomers ((**4**) and (**8**) respectively) a phthalocyanine monomer was also attempted. This proved to be challenging with a lack of solubility of the phthalocyanine being the main problem. Phthalocyanine is a macrocycle that has an intense blue/green colour. It is related to porphyrin as shown in Figure 3-1, and also closely related to tetrabenzoporphyrin and porphyrazine. Initially the desired product was a mono substituted phthalocyanine similar to the porphyrin carboxylic acid (**6**) that has been previously described [80, 81]. It could then be coupled via an amide bond with the modified nucleobase (**2**). A phthalocyanine monomer has a different excitation and emission wavelength than the porphyrin monomer which could prove useful for fluorescence work. If both porphyrin and phthalocyanine are used with different sequences, but at the same time, then depending on the wavelength of light detected different target sequences could be determined.

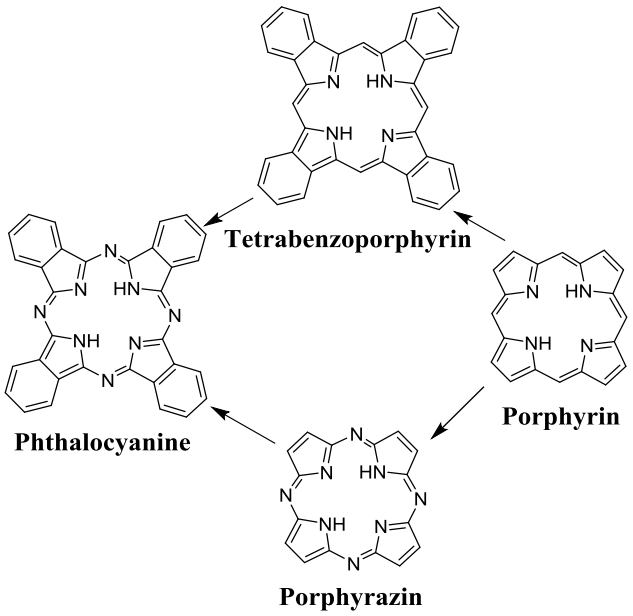

Figure 3-1: Structures of porphyrin, tetrabenzoporphyrin, porphyrazine and phthalocyanine to show the relationship between them.

The first synthetic route that was attempted is shown in Scheme 3-3 [81]. The starting materials and reagents (phthalic anhydride, trimellitic anhydride, urea, $Zn(OAc)_2$, $(NH_4)_2MoO_4$ and NH_4Cl) were finely grounded using a pestle and mortar before being transferred to the reaction flask. As with the porphyrin synthesis, a ratio of 6:1 (phthalic anhydride:trimellitic anhydride) was used in an attempt to optimise the amount of 2-carboxypthalocyanine zinc produced. The solvent free reaction was then heated to 170 °C for 4 hours. The reaction started as a white powder and after heating a cloudy solution was produced. Throughout the 4 hours this changed from yellow to light green and finally dark green. After the workup of washing with 0.5 M HCl, then washing with water until the filtrate was neutral, a dark green solid was produced. The second reaction in Scheme 3-3 shows the addition of 1 M of KOH which was refluxed for 24 hours. The reaction mixture was washed with 0.5 M of KOH until the filtrate was clear. It was then washed with 1M of HCl before washing with water until the filtrate was neutral. The blue solid produced was then dried and found to be only fully soluble in pyridine.

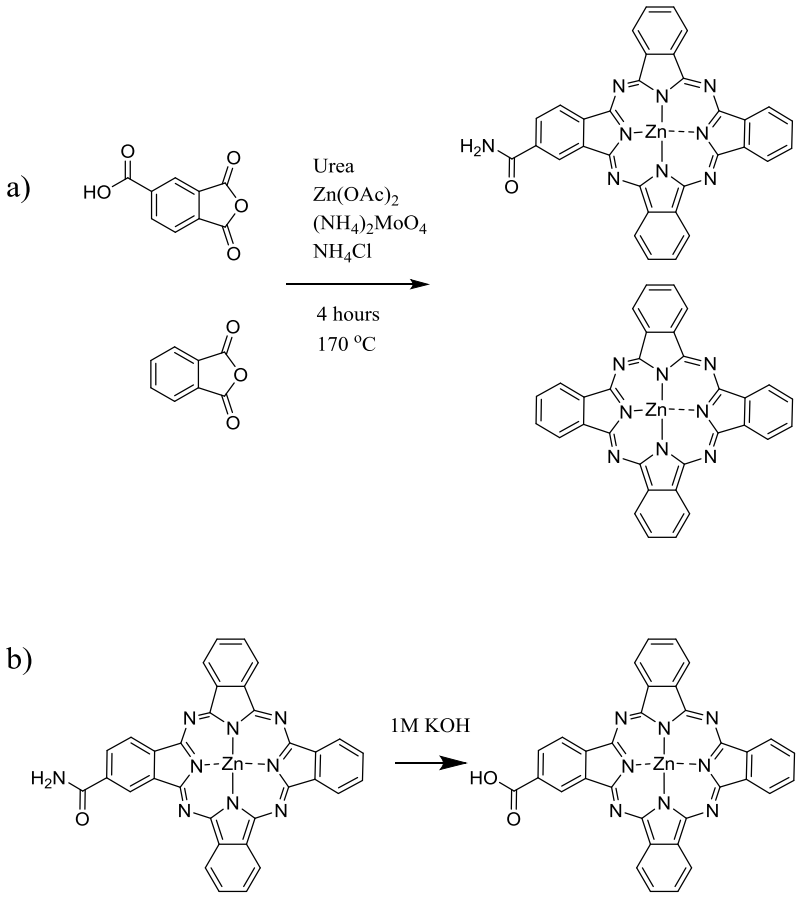

Scheme 3-3: Attempted synthetic route to 2-carboxyphthalocyanine zinc.

The compound produced by the phthalocyanine reaction was not soluble in the solvents used in DNA synthesis and therefore not suitable to be used in DNA synthesis. However, substituents can be added to increase the solubility. The same synthetic route was attempted using 4-*tert*-butyl phthalic anhydrous in place of phthalic anhydride. The added non-polar *tert*-butyl substituents should increase the solubility of the phthalocyanine produced. Despite the reaction being carried out on a relatively large scale (2 g of 4-*tert*-butyl phthalic anhydrous) the product was brown and minimal. Several attempts were made before deciding that another route should be conducted.

Two different synthetic routes were attempted using information found in literature [82-84]. The first alternative synthetic route is shown in Scheme 3-4. A variety of zinc compounds were used as the template for the reaction including: zinc chloride, zinc acetate and zinc trifluoromethanesulfonate.

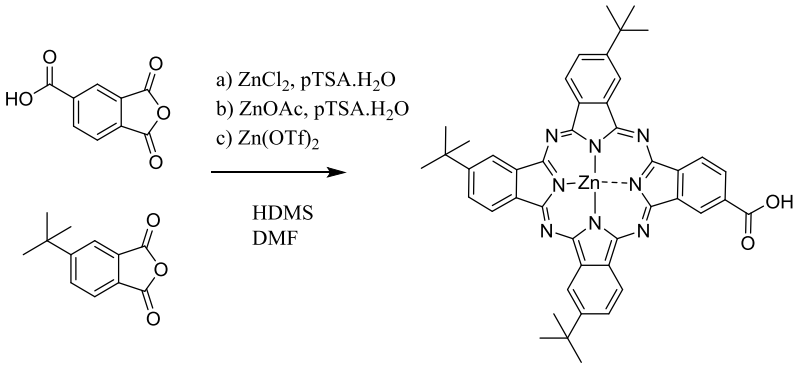

Scheme 3-4: Attempted synthetic route for *tert*-butyl carboxylic acid phthalocyanine.

The second alternative synthetic route is shown in Scheme 3-5 was also attempted. Instead of obtaining a mono carboxylic acid group on the phthalocyanine an amine was considered.

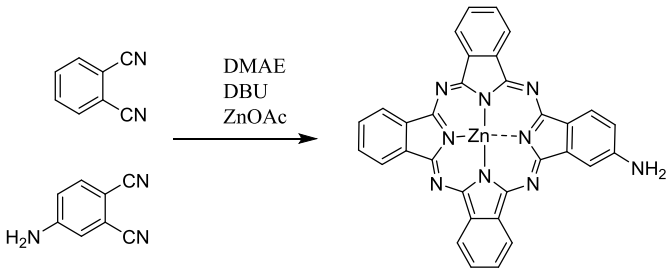

Scheme 3-5: Attempted sythnthetic route to mono-amino phthalocyanine.

The proposed product shown in Scheme 3-5 could then be reacted with the compound shown in Figure 3-2, which can synthesised by the reaction of 5-Iodo-2'-deoxyuridine with propiolic acid.

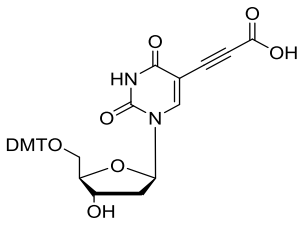

Figure 3-2: Structure of proposed nucleic acid containing a carboxyl group.

Neither synthetic routes were successful. Due to time restraints in the preparation of samples in order to transport them to Singapore this avenue was abandoned, therefore a maximum amount of anthraquinone and porphyrin modified DNA could be synthesised for further experimentation. If time had allowed, an alternative method for phthalocyanine synthesis could have made use of a microwave oven [85, 86].

3.2 Porphyrin and Anthraquinone Oligonucleotides

As both porphyrin and anthraquinone phosphoramidites ((**4**) and (**8**)) have successfully been synthesised they could be incorporated into DNA strands during DNA synthesis. As previously discussed, in section 1.7, the design of the DNA was a hairpin probe with the redox active tag positioned near the 3'-end, allowing it to be in close proximity to the surface after immobilisation. The coupling times used for the synthesised monomers ((**4**) and (**8**)) were extended to 5 minutes to maximise the amount of monomer coupled. The optimum coupling time was previously found by the Stulz group in order to increase coupling efficiency without wasting material. The 5'-end was modified with an amine or thiol group to allow it to attach to either a silicon or gold surface respectively. The modifiers were left to dissolve for 10 minutes in anhydrous acetonitrile with occasional movement to ensure that the modifier was fully dissolved. Standard coupling times were used for the purchased amine and thiol modifiers. This is further discussed in 3.2.1.

The sequences of the DNA probes are based on the three methylated genes in bladder cancer (DAPK, E. Cad and RARβ) as discussed in 1.3.1 with the sequences taken from [18]. The DNA probes are complementary with the methylated target after MS-PCR, with the sequences shown in Table 3-1; where the stem is underlined, the loop is in bold and the monomer is labelled as X. In addition to the anthraquinone and porphyrin monomers synthesised, strands with methylene blue incorporated into the same position were purchased.

Probe	**Sequence 5'-3'**
DAPK	Y<u>AAGGCGC</u>**GGAGGATAGTCGGATCGAGTTAACGTC**<u>GCGCCXT</u>
E. Cad	Y<u>AAGGCGC</u>**TAATTTTAGGTTAGAGGGTTATCGCG**<u>GCGCCXT</u>
RARβ	Y<u>AAGGCGC</u>**GGTTAGTAGTTCGGGTAGGGTTTATC**<u>GCGCCXT</u>

Table 3-1: List of sequences of the DNA probes synthesised where X is porphyrin or anthraquinone and Y is a single 5'-C6 amine or two 5'-dithiol modifications. Underlined bases for the stem of the hairpin design while bases in bold represent the recognition section of the sequence.

Unmodified targets were also synthesised. These were complementary to the recognition section of the DNA probe. The sequences of the synthesised targets are shown in Table 3-2. Sequences labelled as unmethylated are used as mismatched DNA where the base difference is shown in bold. The unmodified target sequences represent the product of the MS-PCR where the cytosine undergoes bisulfite modification as discussed in 1.4.

Target	**Sequence 3'-5'**
DAPK unmethylated	CCTCCTATCA**A**CCTA**A**CTCAATTGCAG
DAPK methylated	CCTCCTATCA**G**CCTA**G**CTCAATTGCAG
E. Cad unmethylated	ATTAAAATCCAATCTCCCAATA**A**C**A**C
E. Cad methylated	ATTAAAATCCAATCTCCCAATA**G**C**G**C
RARβ unmethylated	CCAATCATCAA**A**CCCATCCCAAATA**A**
RARβ methylated	CCAATCATCAA**G**CCCATCCCAAATA**G**

Table 3-2: Sequences of target DNA synthesised. Unmethylated targets will be used as mismatched DNA. Mismatched bases from MS-PCR are shown in bold.

3.2.1 Amine and Thiol 5’-modifications

To attach the DNA probe to the required surface a 5’-modification is needed. Different surfaces require different modifications. For this project, both silicon and gold surfaces can be used and therefore DNA probes with 5’-amine and 5’-dithiol modifiers, respectively, were synthesised. These were purchased from Cambio UK and used as received.

The best modification for DNA to attach to a silicon surface is a 5’-amine modification. Two alternative 5’-amine modifications (protected with trifluoroacetic acid (TFA) or 4-methoxytriphenylmethyl (MMT)) are shown in Figure 3-3.

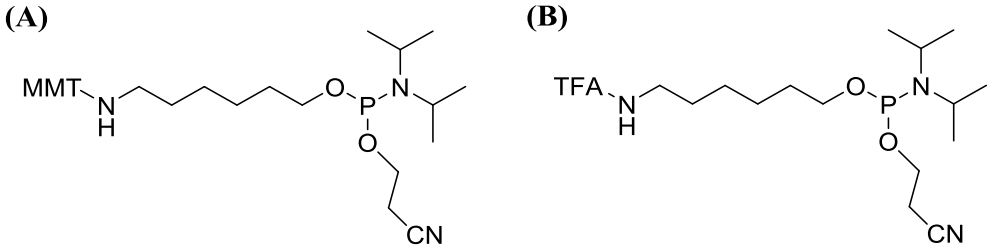

Figure 3-3: Structures of 5’-amine modification for attaching to silicon surface : (A) 5’-MMT-amino-modifier C6-CE phosphoramidite, (B) 5’-TFA-amino-modifier C6-CE phosphoramidite.

For gold surfaces a 5’-dithiol modification is necessary. More than one dithiol group increases the stability of the DNA probe on the gold surface, which avoids the oligonucleotide being cleaved from the gold surface. Therefore two dithiol serinol phosphoramidites were used. The structure of a single dithiol phosphoramidite is shown in Figure 3-4.

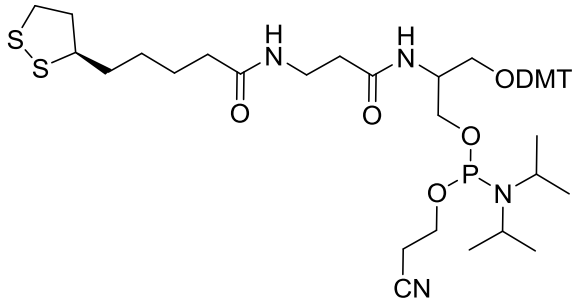

Figure 3-4: Structure of the 5'-thiol modification for attaching to a gold surface: Dithiol serinol phosphoramidite.

All modifiers were used as recommended by the supplier. They were dissolved in the required volume of anhydrous acetonitrile and vortexed before adding to the DNA synthesiser.

3.3 Oligonucleotide Purification

After the protecting groups have been cleaved from the bases (see 1.2) the strands were purified using a Glen Pak column. When setting up the synthesis the choice of whether to leave the 5'-DMT on the last base can be made. If Glen Pak purification is to be used then the strands are synthesised DMT-ON. When the DNA is loaded onto the Glen Pak column the DMT group that remains will be retained to the reverse-phase column. This enables the failure sequences to be washed through the column. After the failure sequences have been removed the DMT group is cleaved using 2% TFA. The desired DNA can then be collected from the column.

Amine modified strands were synthesised with TFA or MMT as the 5'-protecting group (Figure 3-3). When MMT was present a lower temperature of 40 ºC for 24 hours was used to deprotect the bases in an aqueous ammonia solution. This was in comparison to 55 °C for 5 hours as discussed in 1.2.4. The procedure for the Glen Pak columns remained as standard except 4% TFA was used, with an extended contact time of five minutes. Care was taken to not leave the acid on the column for too long in order to prevent damaging the DNA as high acidic conditions can break down the phosphodiester bonds or lead to depurination. The mechanism for this is shown in Figure 3-5.

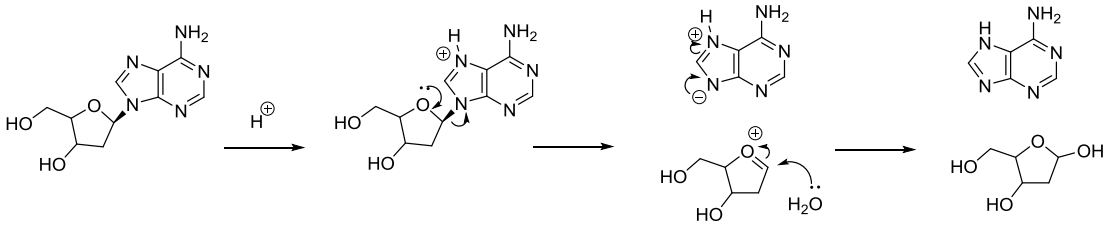

Figure 3-5: Mechanism of depurination with adenine as an example.

TFA is also used to protect the 5'-amine modification. TFA is base labile and will therefore be removed in the aqueous ammonia solution (used when deprotecting the nucleobases). This means that Glen Pak purification is unsuitable as all of the DNA will be washed through the column. However, when porphyrin has been incorporated into a strand Glen Pak purification can still be used. As the column is reverse phase the porphyrin will be retained by the column allowing strands that do not contain a porphyrin to be washed through. Porphyrin DNA can then be collected from the column. While HPLC is still needed to remove the failure sequences which contain porphyrin, the process will be simplified by the unmodified DNA being removed prior to this. Therefore TFA should be used with the porphyrin strands to ease purification and provide a convenient method to separate porphyrin DNA from unmodified DNA. However, anthraquinone DNA was not found to be retained to the Glen Pak column so MMT was used.

DNA probes that contained the 5'-thiol modification (dithiol serinol phosphoramidite) were purified by Glen Pak as standard. For the porphyrin DNA the sequences were synthesised DMT-OFF to allow the porphyrin to bind to the Glen Pak column. However, the anthraquinone DNA was synthesised DMT-ON in order for the strand to be retained on the Glen Pak column without being washed through. Further purification was then carried out as discussed in the next section (3.3.1).

3.3.1 High Performance Liquid Chromatography

High performance liquid chromatography (HPLC) was carried out to further purify the DNA modified with a redox active tag. Unmodified DNA strands were analysed using mass spectrometry to ensure that the correct strand was synthesised, and no further HPLC purification was required. During HPLC the starting buffer was 8.6 mM TEA/100 mM HFIP with 0.5 mM EDTA and moved into methanol.

As previously discussed, in section 3.2.1, two different protecting groups for the 5-amine modification (TFA and MMT) were used. After Glen Pak purification, HPLC was carried out on both to compare samples. It was seen, from comparing Figure 3-6 and Figure 3-7, that the sample protected with MMT (Figure 3-6) contained a much higher proportion of unmodified DNA. The peak corresponding to the unmodified DNA appeared with a retention time of between 25-30 minutes while the peak corresponding to porphyrin DNA was present at 50-55 minutes. The chromatogram shown in Figure 3-6, MMT protected 5-amine modification, had no major porphyrin DNA peak and therefore further purification was required.

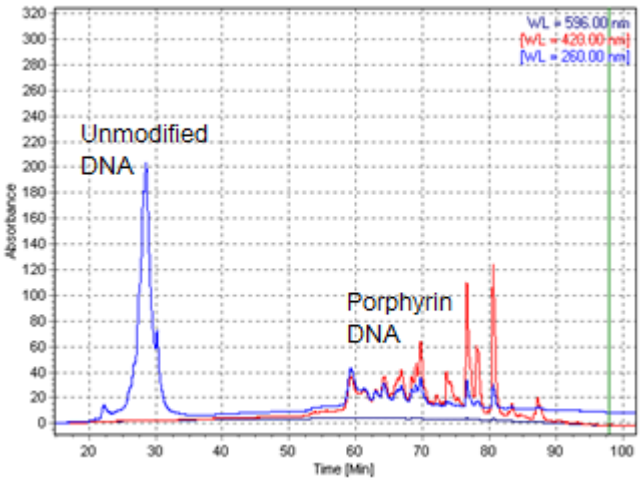

Figure 3-6: HPLC trace of RARβ, 5'-MMT-Amino-Modifier C6 modified porphyrin DNA. Blue line shows absorbance measured at 260 nm while the red line absorbance at 420 nm.

Figure 3-7, TFA protected 5'-amine modification, clearly showed a defined porphyrin DNA peak at 50 minutes and could be collected, giving a sample containing a single porphyrin DNA peak.

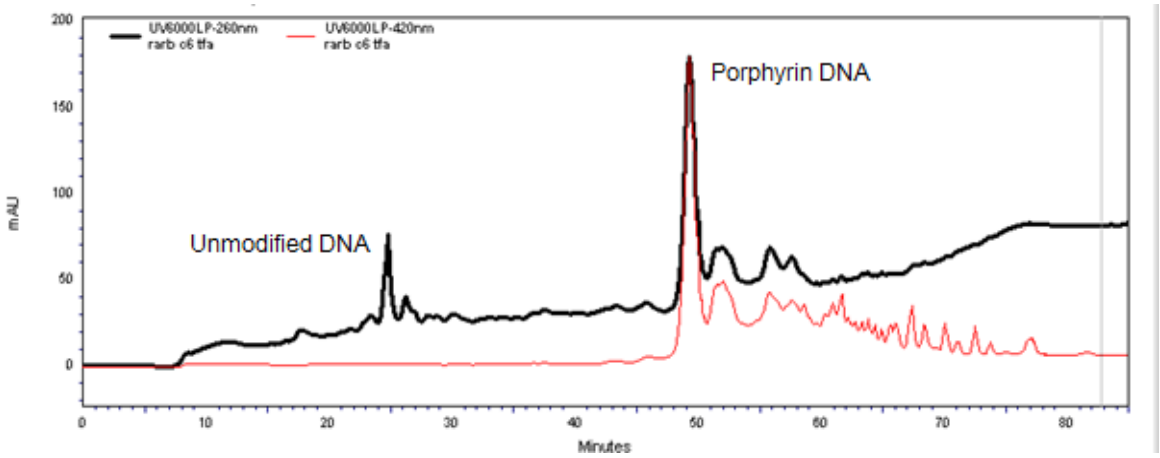

Figure 3-7: HPLC trace of RARβ , 5'-TFA-Amino-Modifier C6 modified porphyrin DNA. The black line shows absorbance at 260 nm while the red line shows absorbance at 420 nm.

Further purification for the MMT protected 5'-amine modified DNA was carried out using polyacrylamide gel electrophoresis (PAGE) followed by a 'crush and soak' method for extraction of the modified DNA (for full experimental details see 9.9). PAGE was carried out as standard with the gel being imaged using a BIO-RAD imager. The main band was cut out of the gel and into small pieces. An eluting solution was added, which contained MeOH and NaCl, and left overnight in a thermomixer at 36 °C. The supernatant was then carefully removed, after 8000 rpm for 15 minutes, before being washed with water. The sample was desalted using a Glen Pak. Figure 3-8 shows HPLC chromatograms for before and after PAGE with the 'crush and soak' method for a porphyrin DAPK sequence with a MMT protected 5'-amine modification. It can be seen

that after PAGE and ‘crush and soak’ purification there is a distinct porphyrin DNA peak which was then collected and isolated to achieve a pure porphyrin DNA sample.

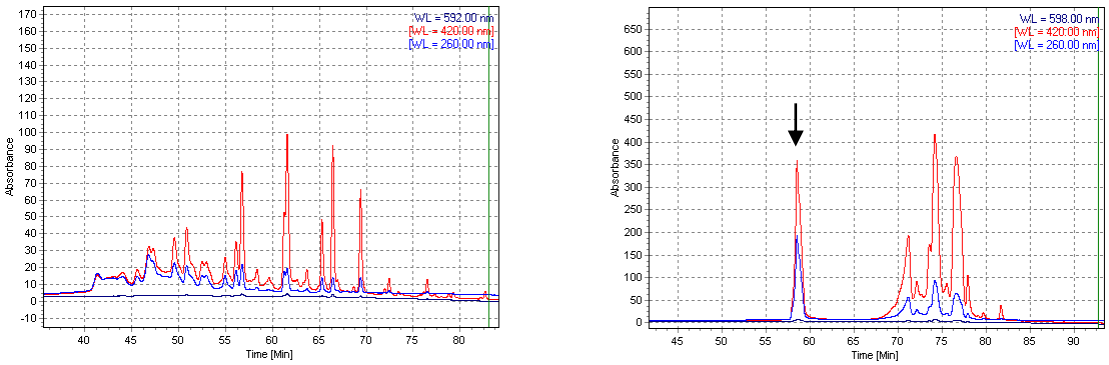

Figure 3-8: HPLC trace (40-80 minutes) of porphyrin DAPK with MMT protected 5-amine modification, Left – Before PAGE purification and ‘crush and soak’ extraction, Right – After PAGE purification and ‘crush and soak’ extraction. The first porphyrin band (shown with arrow) was then collected and isolated. The blue line shows absorbance at 260 nm while the red line shows absorbance at 420 nm.

However, even with the PAGE purification followed by the ‘crush and soak’ extraction method for the MMT modification the TFA modification gave a purer porphyrin DNA sample. This is due to the porphyrin DNA attaching to the Glan Pak column as discussed in section 3.3. Therefore the MMT protected 5’-amine modification was only used for anthraquinone DNA. As previously discussed (see 3.3) TFA deprotection cannot be used with anthraquinone therefore MMT is required for the 5’amine modification. Figure 3-9 shows a HPLC trace for RARβ anthraquinone DNA with MMT 5’-amine modification. Two distinct peaks corresponding to unmodified DNA (27 minutes) and anthraquinone DNA (30 minutes) were seen, which was confirmed by mass spectrometry. The anthraquinone DNA peak was collected.

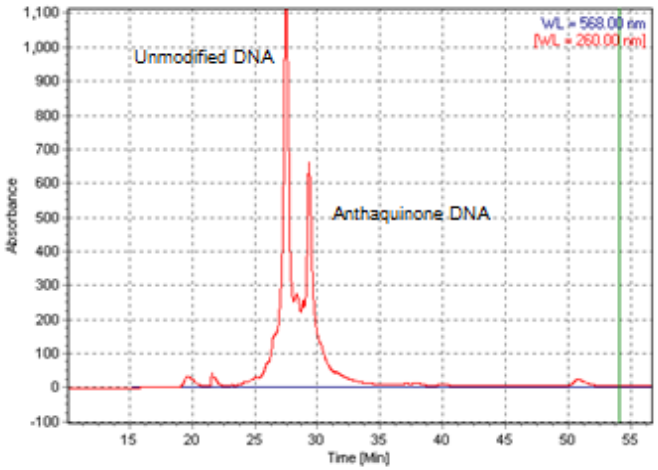

Figure 3-9: HPLC trace of RARβ anthraquinone DNA with MMT protected 5'-amine modification. Red line shows absorbance from 260 nm.

In addition to the 5'amine modification, 5'-thiol modified DNA was also synthesised (see 3.2.1 and 3.3) with a DMT protecting group. Anthraquinone or porphyrin was incorporated as the redox active tag. The strands were purified by HPLC, the main porphyrin DNA or anthraquinone DNA was collected as previously discussed in this section. The anthraquinone DNA was confirmed by mass spectrometry. Previous work with synthesised porphyrin modified DNA have been unable to obtain mass spectrometry results [87, 88].

3.3.2 Calculating number of moles of oligonucleotides synthesised

After Glen Pak purification, the concentrations of the oligonucleotides were calculated, using the Beer-Lambert Law, allowing the number of moles synthesised to be determined.

$$A = \varepsilon c l$$

Where A is the absorbance, ε is the extinction coefficient ($M^{-1}cm^{-1}$), c is the concentration (M) and l is the path length (cm).

UV-Vis spectroscopy was used to measure the absorbance of a DNA sample. The path length is a known value (1 cm) and the extinction coefficient is obtained using the ATDBIO oligonucleotide calculator. An example UV-vis spectra of DAPK porphyrin modified DNA (5'-thiol modification) is shown in Figure 3-10 where peaks at 260 nm and 420 nm correspond to the DNA and porphyrin (Soret band) respectively.

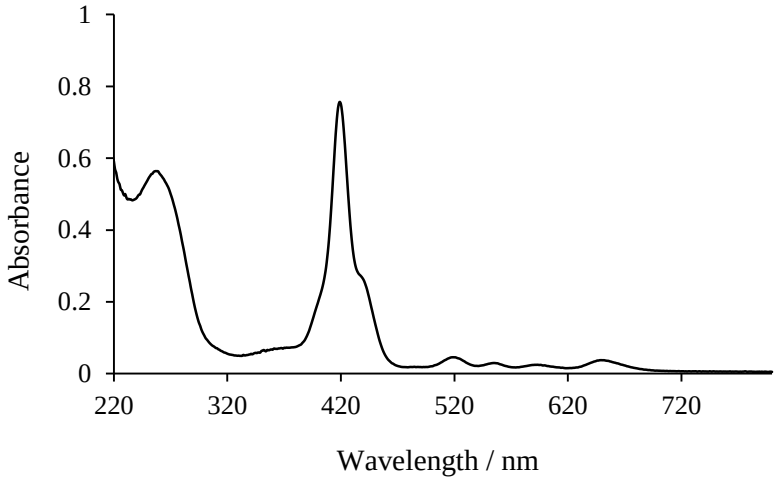

Figure 3-10: UV-Vis spectrum of DAPK porphyrin modified DNA with 5'-thiol modification with a peak at 260 nm for DNA and another at 420 nm corresponding to the soret band of the porphyrin.

Once the concentration of the oligonucleotides had been calculated the number of moles of DNA that have been synthesised can be determined using the equation below.

$$Number\ of\ moles = volume \times concentration$$

The volume used is known so the number of moles obtained is a simple calculation. The number of moles of anthraquinone modified DNA is shown in Table 3-3 while the number of moles of porphyrin modified DNA is shown in Table 3-4.

As seen in Table 3-4 the number of moles of porphyrin modified DNA is low (<10 nmoles). This is due to the porphyrin monomer being added to the solid support directly after the preloaded base at the 3' position. However, this was necessary as a thiol/amine modification was required at the 5' position. The extra base after the porphyrin modification stops the porphyrin from getting as close as possible to the surface in the closed hairpin form. A possible way of avoiding this could be to use a universal support where there is no preloaded base. The anthraquinone modified DNA (Table 3-3) also has low yields (~10 nmoles) except for two entries. The similar absorbance wavelength of DNA (260 nm) and anthraquinone monomer (255 nm) could have affected these concentration calculations.

	MMT 5'-amine modified	DMT 5'-thiol modified
DAPK	7.76	7.13
E.Cad	53.56	12.67
RARβ	55.08	9.66

Table 3-3: Number of nmoles of anthraquinone modified DNA that have been synthesised.

	TFA 5'-amine modified	DMT 5'-thiol modified
DAPK	3.37	3.77
E.Cad	4.97	1.92
RARβ	9.09	3.18

Table 3-4: Number of nmoles of porphyrin modified DNA that have been synthesised.

In addition to the modified DNA synthesised, unmodified target DNA (sequences in Table 3-2) were also synthesised, with the number of moles of each sequence shown in Table 3-5. The values observed were higher than for the modified DNA which was as expected.

	Unmethylated Target	Methylated Target
DAPK	257.72	92.69
E.Cad	325.61	42.76
RARβ	300.86	35.77

Table 3-5: Number of nmoles of unmodified target DNA synthesised.

3.4 Conclusions: Chemically Tagged Oligonucleotides

Anthraquinone and porphyrin modified DNA were successfully synthesised and purified as a hairpin design (see 1.7). 5'-amine and 5'-thiol modifications were added for attachment to silicon and gold surfaces respectively. The number of moles were calculated and samples sent to Singapore for electrochemical and fluorescence detection.

Glen Pak columns were carried out on all synthesised DNA strands before unmodified DNA sequences were confirmed via mass spectrometry, while the modified DNA underwent further purification. PAGE and a 'crush and soak' method were used in order for HPLC purification to be carried out for DNA which did not have a defined porphyrin DNA peak. The defined peak for porphyrin and anthraquinone modified DNA was then collected.

In addition to the anthraquinone (**4**) and porphyrin (**8**) phosphoramidites that were synthesised, a phthalocyanine monomer was attempted. Several routes were investigated, however the compound had low solubility and not suitable for DNA synthesis. Other routes, which included the addition of *tert*-butyl substituents (to increase the solubility), did not produce the desired product. Therefore, (as the DNA samples were required to be sent to Singapore) the phthalocyanine synthesis was stopped, with the focus solely on anthraquinone and porphyrin modified DNA.

4. Unmodified DNA Probes for DNA Detection

Different detection methods for DNA hybridisation with unlabelled DNA probes were investigated in order to compare the limit of detection of each. This will then be compared with chemically tagged (redox active tag) DNA probes (Chapter 5), which should enhance the sensitivity of detection.

The oligonucleotides used in this section were purchased from Integrated DNA technologies, where they were purified by HPLC, and used as received. The sequences used are shown in Table 4-1. Devices with a gold surface were used and therefore a 5'-thiol (C6) modification was used. The sequences of the probes were the same as in Chapter 3 and were based on the biomarkers for bladder cancer (as discussed in 1.3.1). The synthesised targets used are shown in Table 3-5.

	Sequence 5'-3'
DAPK un	XAAGGCGC**GGAGGATAGTCGGATCGAGTTAACGTC**GCGCCTT
E. Cad un	XAAGGCGC**TAATTTTAGGTTAGAGGGTTATCGCG**GCGCCTT
RARβ un	XAAGGCGC**GGTTAGTAGTTCGGGTAGGGTTTATC**GCGCCTT

Table 4-1: Sequences purchased from Integrated DNA technologies. X is a 5'-C6 thiol linker. Underlined bases form the stem of the hairpin design while bases in bold show the recognition section of the sequence.

4.1 Silicon Biophotonic Sensor

Previous work within the group in A*STAR (Singapore) used a silicon biophotonic sensor to measure DNA hybridisation [18, 89]. A silicon ring resonator was used where DNA hybridisation causes a resonant wavelength shift. A shift of picometres was observed for concentrations ranging between 25 nM to 1 µM of target DNA [89]. Figure 4-1 shows a representation of this process.

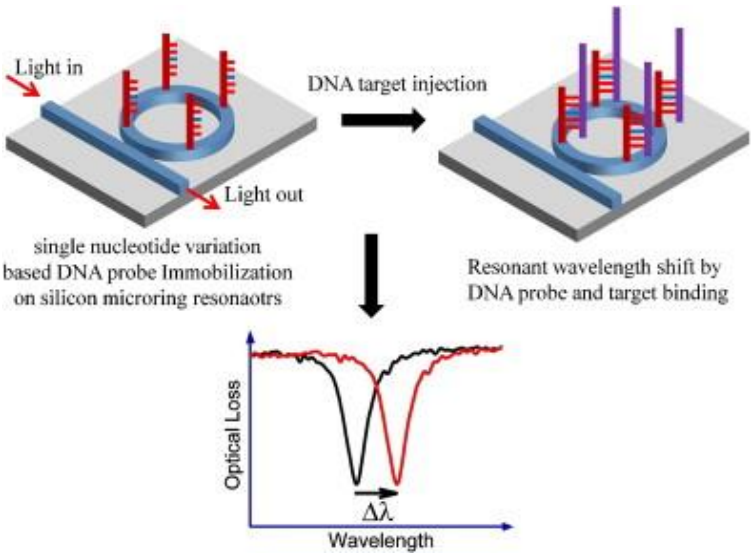

Figure 4-1: Representation of silicon ring resonator and the wavelength shift caused by DNA hybridisation. Reprinted from [89] with permission from Elsevier.

As the resonant wavelength shift is in the region of picometres, different sensors were investigated, to find a greater difference after hybridisation with unlabelled DNA in order to compare the systems. Three different devices for detection of DNA hybridisation will now be discussed and compared to previous work.

4.2 Surface Plasmon Resonance

Surface plasmon resonance (SPR) as introduced in 1.5.1 is a detection method that can monitor real time surface interactions. Using unlabelled DNA probes the limit of detection was found as a comparison.

4.2.1 Detecting DNA Hybridisation Using SPR

All three bladder cancer probes (DAPK, E. Cad and RARβ) were tested in order to find a detection limit for SPR. The DNA probes (1 μM in PBS) were immobilised onto a blank gold chip over six injections of 1080 seconds. After the DNA probe had been immobilised, 6-mercapto-1-hexanol (MCH, 1 mM) was injected for 600 seconds in order to block the gold surface from non-specific binding. This immobilisation process is shown in real time in Figure 4-2.

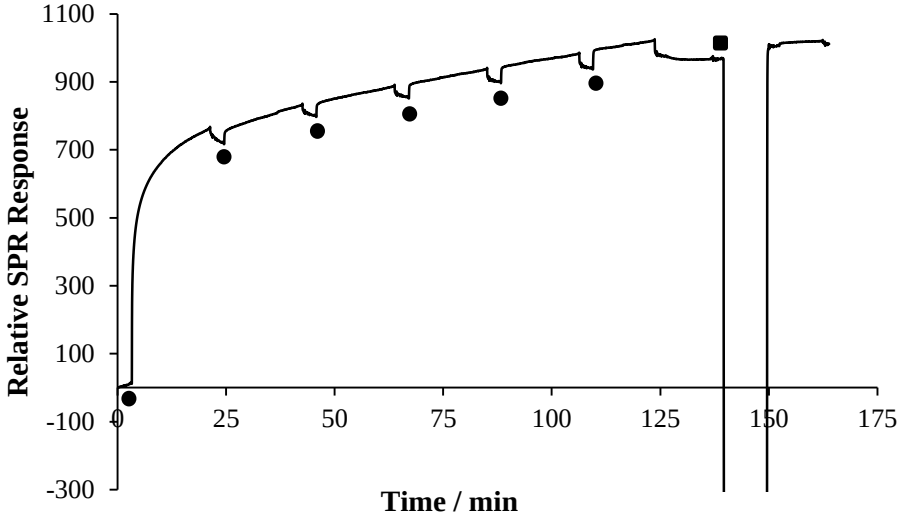

Figure 4-2: Immobilisation of DAPK probe where ● shows the injection of probe and ■ shows the injection of MCH.

After the addition of MCH the relative SPR response increased by approximately 50-60 RU, indicating that MCH had bound to the gold surface and blocking it to future non-specific binding.

Different concentrations of complementary target DNA were then injected for 1080 seconds in a range of 1 nM to 300 nM. This range was chosen to determine the limit of detection with the higher concentrations used to show the full capabilities of the detection method. The gold surface was regenerated after addition of target DNA by injecting 50 mM NaOH for 100 seconds. The hydrogen bonds between the base pairs of the dsDNA were broken and the target DNA was washed away. The real time addition of target and regeneration is shown in Figure 4-3.

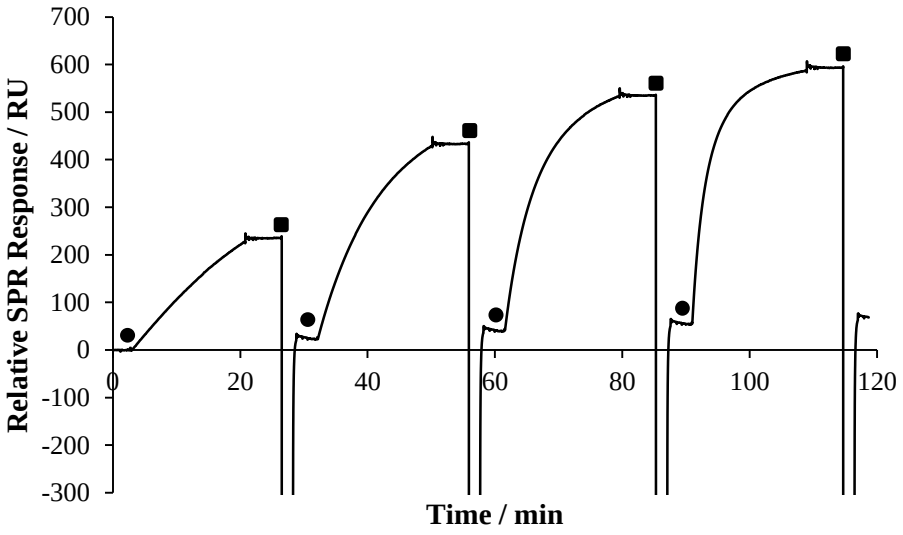

Figure 4-3: Real time graph of (●) injection of DAPK target in a range of concentrations – 40 nM, 60 nM, 90 nM, 150 nM – and (■) injection of the regeneration solution with 50 mM NaOH.

As seen in Figure 4-3, increasing the concentration of target increased the relative SPR response. While the regeneration is effective to remove the target DNA, it can be observed that the baseline increased before each injection of target DNA. After the fourth injection/regeneration cycle, the baseline was 70 RU. This occurred because the

regeneration of the gold chip was not 100% effective, meaning that the gold chip should not be used for multiple cycles, as the response will not be as accurate. However as the final device would likely be a single use the increase in baseline was only when comparing different concentrations of target DNA on the same chip.

Figure 4-4(A) shows the relative SPR signal from the concentration range of complementary target DNA used (RARβ probe and target) from 12.5 nM to 300 nM. As before it was seen that as the concentration of the target DNA increased so did the relative SPR signal. Figure 4-4(B) shows the different concentrations of complementary target DNA with their respective relative maximum SPR signal values. It is seen from Figure 4-4(B) that while the concentration of the complementary target DNA increases, the relative maximum SPR signal increases, but not at a linear rate.

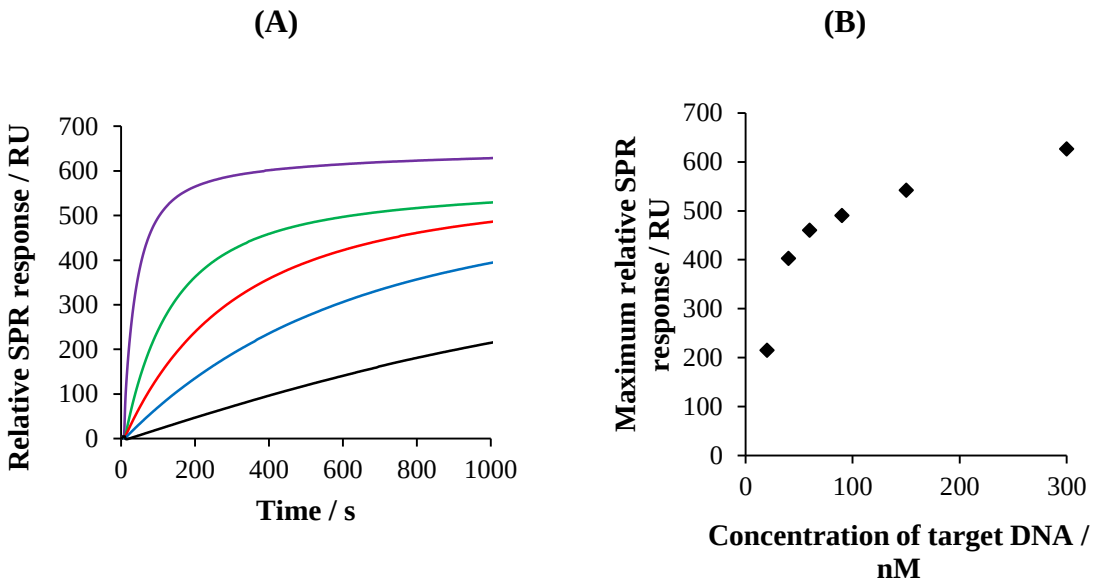

Figure 4-4: (A) Real time relative SPR response for a range of increasing concentrations of complementary target DNA. 12.5 nM (black), 25 nM (blue), 50 nM (red), 100 nM (green), 300 nM (purple). (B) Relationship between maximum relative SPR responses over a range of complementary target DNA concentrations. RARβ probe and target used.

In addition to the complementary target, mismatched DNA was also injected. The sequences of complementary and mismatched DNA are shown in Table 3-2. This was to ensure that the increased SPR response was from the DNA hybridisation rather than non-specific binding. Figure 4-5 shows mismatched DNA was added with a concentration of 300 nM and a maximum SPR shift of 159 RU was observed compared with 748 RU for the fully complementary target DNA of the same concentration. The limit of detection was found to be 5 nM, as below this concentration the response observed was in the same region as the mismatched DNA.

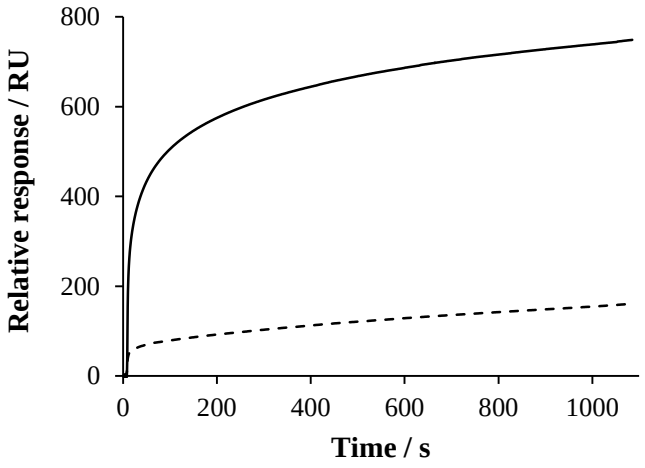

Figure 4-5: Relative SPR signal response of 100 nM complementary target DNA (solid line) and 100 nM mismatched DNA (dashed line) where a RARβ DNA probe/target was used.

The data collected for SPR allows for real time spectra to be recorded. Using the same concentration range as for the known silicon ring resonator allows the two methods to be directly compared. It can be seen that a relative shift in SPR signal is easily observed for DNA hybridisation. However, the size of the SPR Biacore® machine makes it unsuitable as a point-of-care device. Therefore, even though the limit of detection is similar, additional systems were investigated.

4.3 Nanoplasmonic Sensor

Another type of sensor which can be used to monitor surface interactions is a nanoplasmonic sensor. It has been shown, from previous work within the group, that a wavelength shift in the range of nanometres can be detected for the monitoring of bacterial growth [90]. The principle of the nanoplasmonic sensor, as used for monitoring bacterial growth, is shown in Figure 4-6.

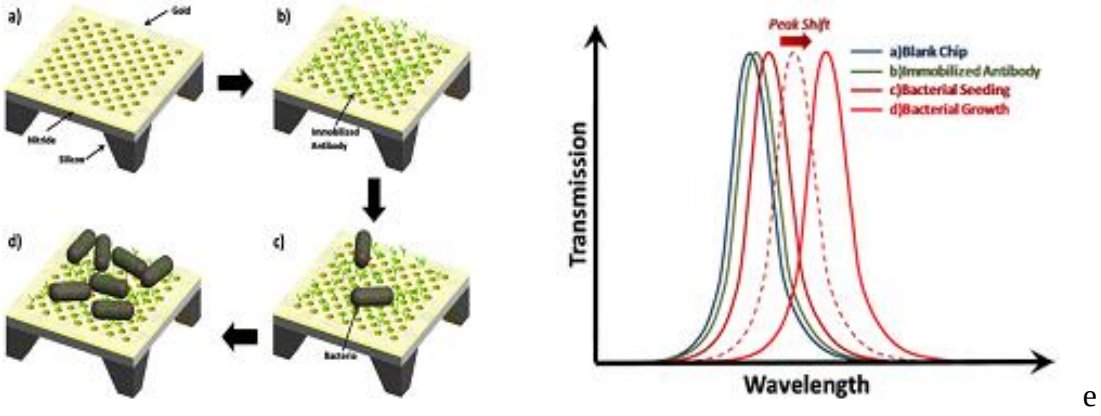

Figure 4-6: Outline of bacterial growth monitoring. (a) Blank sensor, (b) Antibody immobilised on surface of sensor, (c) Bacterial seeding on the sensor, (d) Bacterial growth on sensor and (e) Transmission spectrum of the processes a-d. Reprinted from [90] with permission from Elsevier.

The nanoplasmonic sensor has a wavelength shift in the region of nanometres upon bacterial growth. This is a larger shift in comparison to the silicon micro ring resonator where a shift of picometres observed. Therefore, the nanoplasmonic sensor was tested with DNA in order to see if hybridisation also gives a response shift in the region of nanometres. The detection of DNA hybridisation with a nanoplasmonic device without the use of nanoparticles was novel and is presented in the following sections.

4.3.1 Fabrication and Setup

Conventionally, scanning beam lithographies are used when plasmonic nanohole sensors are fabricated. However this is generally a slow process so it cannot be used in mass fabrication. Deep Ultra-Violet (DUV) lithography, on the other hand, is faster and still gives the high resolution required to make nanohole arrays. The fabrication process to develop the plasmonic nanohole device was carried out in A*STAR (Singapore) by a member of staff. The outline of this process is shown in Figure 4-7.

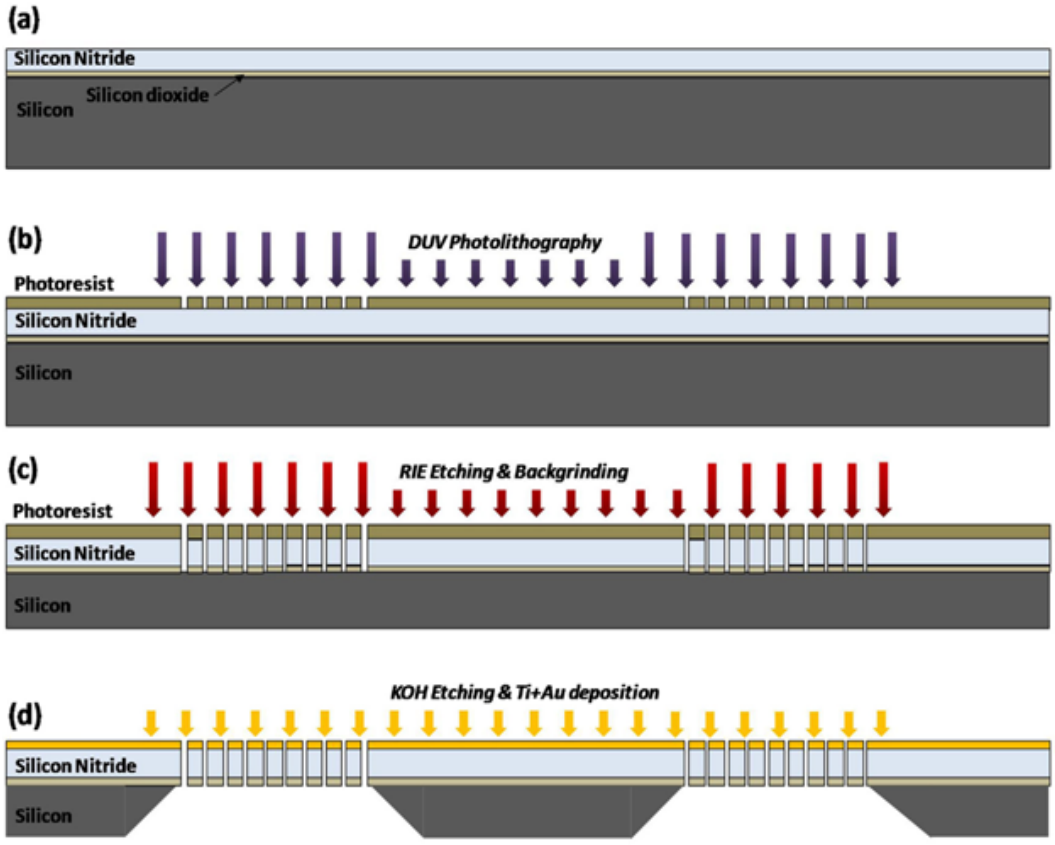

Figure 4-7: Outline of the fabrication process carried out by a member of staff within IME for the nanoplasmonic sensor using DUV lithography. Reprinted from [90] with permission from Elsevier.

A silicon wafer was first oxidised (wet oxidation) to form a layer of SiO_2 approximately 300 Å thick. Low pressure chemical vapour deposition was then used to form a layer of Si_3N_4 about 1.5 kÅ thick. DUV lithography was used to produce an array of holes which were subsequently transferred to the silicon nitride and silicon oxide layers using a reactive ion etching process. Backgrinding was carried out on the wafer until it was 400 µm thick, before KOH etching underneath the wafer to form a free standing membrane with the dimensions of 100 µm x 100 µm. A sputtering method was used to finish with an adhesion layer of titanium (10 nm) and layer of gold (100 nm).

SEM images were taken and shown in Figure 4-8(A) revealing that the device had a smooth gold surface. The whole device used is shown in Figure 4-8(B).

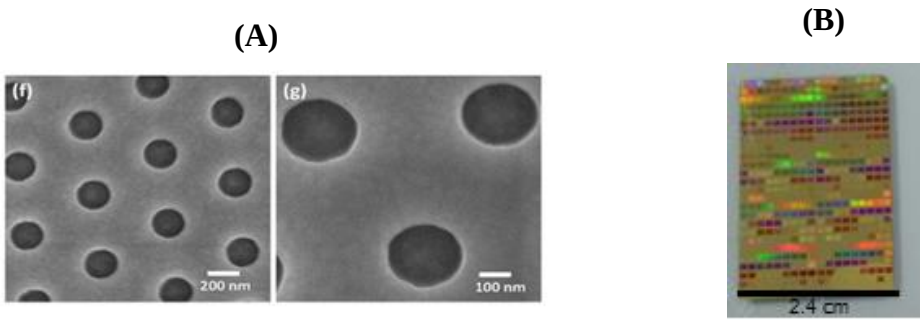

Figure 4-8: (A) SEM images of the device after gold deposition where the diameter of the nanohole is 200 nm and the pitch is 550 nm. Reprinted from [90] with permission from Elsevier, (B) Image of the whole device

The transmission of light through an array of subwavelength holes has an enhanced local intensity due to phenomenon called extraordinary optical transmission (EOT). In 1998 *Ebbesen et al* reported on EOT for the first time [91]. It has been shown that this phenomenon occurs in both regular and random nanohole arrays [92-94]. Gold is well suited for this application and by changing the shape of the hole the transmission intensity can be altered [91, 95]. As this occurs with subwavelength holes, this theory is well suited to the miniaturisation process required for a POC device to be made.

The device was placed over a halogen light source while a fibre optic cable was positioned on top and manoeuvred into the precise position with the help of a microscope. This setup can be seen in Figure 4-9. The wavelength of the light transmitted through the nanohole can then be recorded and monitored during immobilisation and hybridisation of DNA.

(A) **(B)**

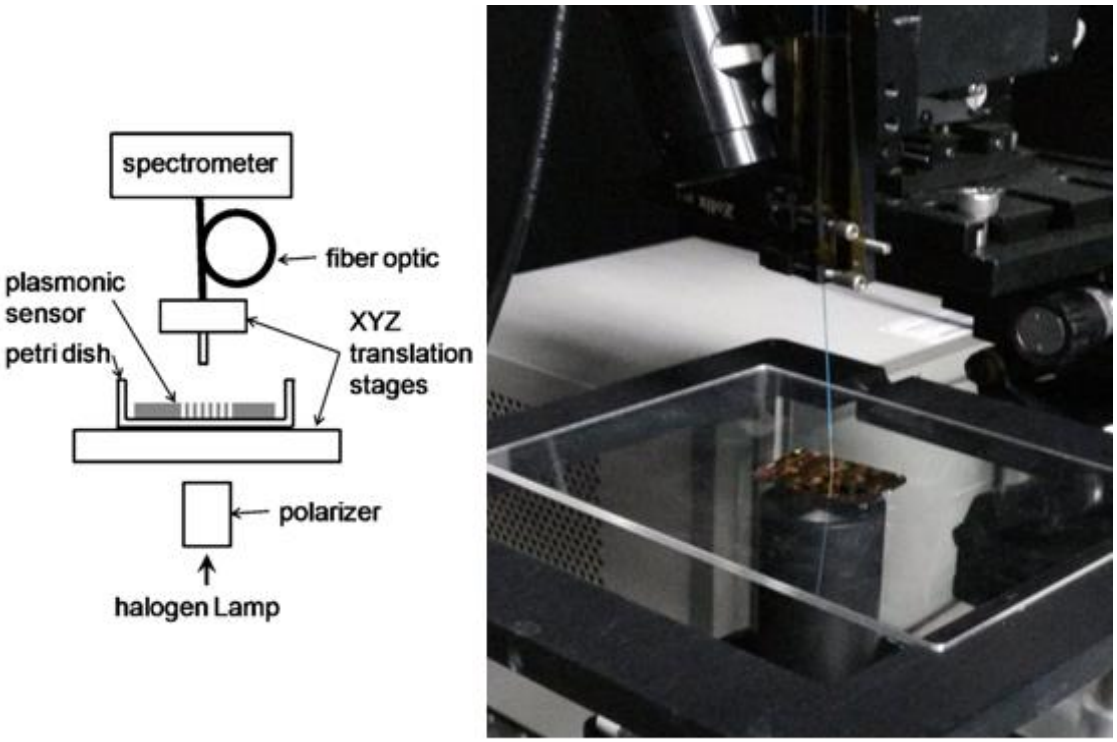

Figure 4-9: (A) Outline of the setup used. Reprinted from [90] with permission from Elsevier, (B) Image of the setup used.

The transmission spectrum was recorded and a Gaussian fit was applied to enable the position of the peak to be found with increased accuracy as shown in Figure 4-10. The data was then normalised in order to find the maximum. This was done for all the transmission data recorded including immobilisation of the DNA probe and hybridisation of the target DNA.

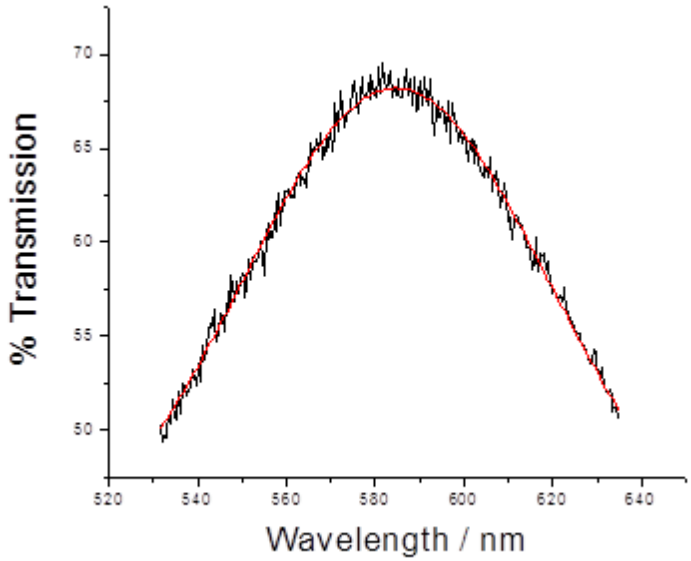

Figure 4-10: Gaussian fit (red line) overlaid on an example sample (E.Cad probe, 1 μM) to find the transmission wavelength peak.

4.3.2 Surface Sensitivity

Initial characterisation was carried out to determine the surface and bulk sensitivity of the nanoplasmonic device. Full experimental details can be found in 9.11.

The surface sensitivity of the nanoplasmonic device was tested using deposition of polyelectrolyte multilayers of reproducible thickness [96-98]. This was done by alternatively adding layers of positively charged (polyallyamine hydrochloride, PAH) and negatively charged (polysodium styrene sulfonate, PSS) polymers. The polymer thin film is suitable to measure the sensitivity and reproducibility of a new device. Results from this test are shown in Figure 4-11(A).

The bulk sensitivity of the nanoplasmonic device was determined by measuring the transmission wavelength when the device was immersed in a range of concentrations of aqueous NaCl. The change in refractive index of the different solutions cause a shift in the observed peak. Results from this test are shown in Figure 4-11(B). Both the surface and bulk sensitivity were as expected and so DNA hybridisation experiments were carried out [90].

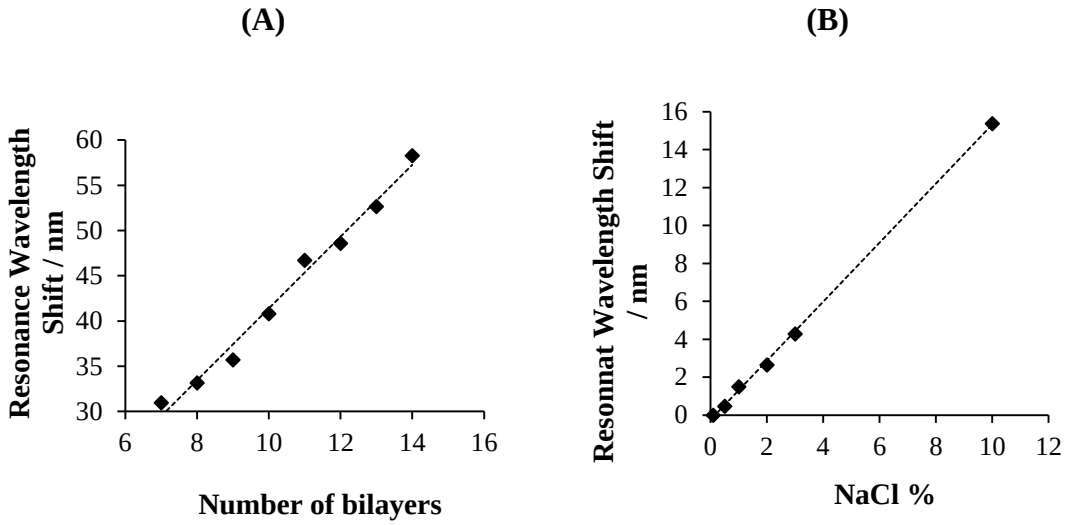

Figure 4-11: (A) Surface sensitivity of the nanoplasmonic sensor by the addition of PAH/PSS bilayers. (B) Bulk sensitivity of the nanoplasmonic sensor by measuring the wavelength in different concentrations of NaCl.

4.3.3 Detecting DNA Hybridisation Using a Nanoplasmonic Sensor

Each of the three DNA probes (E.Cad, DAPK, RARβ) were immobilised onto the gold surface (1 µM in PBS), of previously cleaned chips. To limit non-specific binding on the gold surface MCH (1 mM) was added, similar to the SPR experiments. For full details see 9.11. Complementary target DNA, with the concentration ranging from 10 nM to 500 nM, was then added to the chip and the transmission wavelength was monitored. Figure 4-12, which has the RARβ sequence as the DNA probe, compares the highly concentrated complementary target (400 nM) with a low concentration of complementary target DNA (10 nM). It was observed that when a lower concentration of complementary target DNA was used there was more noise from the nanoplasmonic device than seen using SPR. Although the trend was still increasing, when 10 nM of target DNA was used, the data was not completely reliable as seen for the higher concentrations of target DNA.

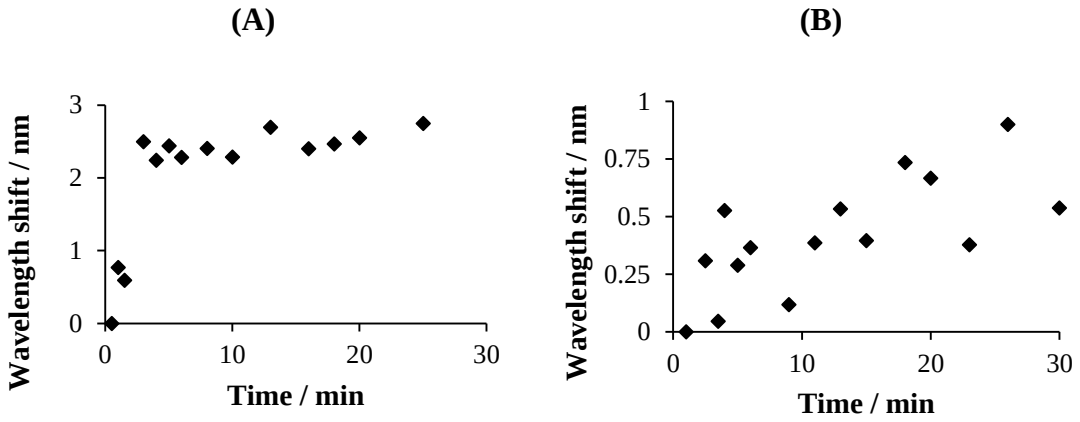

Figure 4-12: Real time wavelength shifts from the plasmonic nanohole device using different concentrations of complementary target DNA, (A) 400 nM, (B) 10 nM (RARβ was used as probe and target DNA).

Figure 4-13 compares the different concentrations of complementary target DNA used with the relative wavelength shift observed. There is a positive correlation that shows that as the concentration increases the wavelength shift also increases.

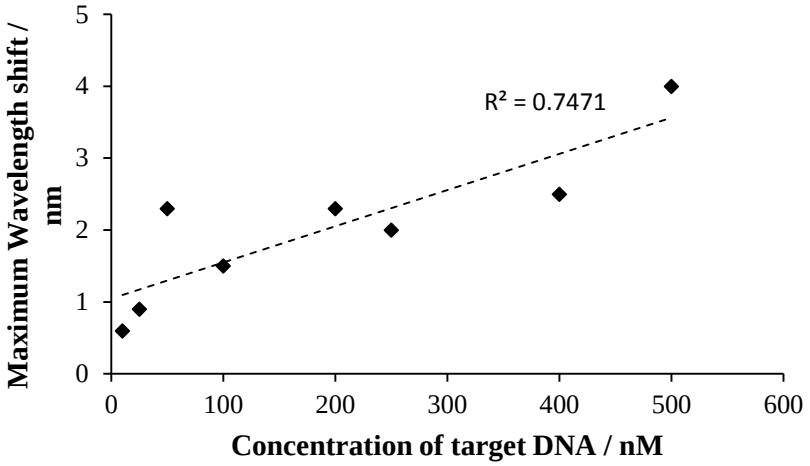

Figure 4-13: The relationship between the maximum wavelength shift and concentration of target DNA when using RARβ

As previously described in this chapter for the SPR experiments, the surface was regenerated using 50 mM NaOH. The device underwent three hybridisation/regeneration cycles before it was cleaned using a piranha solution (H_2O_2:$3H_2SO_4$) to remove all DNA. After the cleaning process the device can be reused. After 3 regeneration cycles the data was no longer consistent. As with the SPR experiments the regeneration is not 100% effective and so only 3 cycles were carried out for both SPR and the nanoplasmonic device.

Mismatched DNA was also tested using the nanoplasmonic device, with the sequences shown in Table 3-2. Using the RARβ probe and a concentration of 100 nM of complementary target DNA, a wavelength shift of 1.5 nm was observed. However when the mismatched DNA was added, a shift of only 0.5 nm was seen. The limit of detection found for the nanoplasmonic sensor was 10 nM, as below this concentration the noise from the device, was too high and the overall shift was less than 0.5 nm. This limit of detection is in the same region as the limit of detection found for the silicon micro ring resonator (25 nM) and previous SPR results (5 nM) [18]. Therefore as the limit of detection is not more sensitive this avenue was dropped.

4.3.4 Fluorescence Detection Using the Nanoplasmonic Device

The nanoplasmonic sensor can also be used for fluorescence experiments by replacing the halogen light source with an X-CITE light source, which gives a uniform fluorescence light using a 120 watt lamp. This should enable excitation of a dye to allow the fluorescence to be observed.

To observe fluorescence, the light transmitted through the device is required to be equivalent to the excitation wavelength of the molecule which exhibits fluorescence. Therefore several experiments were carried out to ensure that a selected membrane on the device would correspond to the excitation wavelength. The experiments, run on each membrane, showed the shift of the transmitted wavelength of light after DNA immobilisation and binding steps had occurred to be approximately 10 nm. This figure was then combined with the blank reading, to enable the appropriate membrane to be chosen, so that the excitation wavelength matched the wavelength transmitted through the device. This was found to be in the range of 590 nm to 650 nm. The excitation wavelength of the porphyrin tag synthesised, in chapter 3, is 420 nm. Unfortunately, this is incompatible with the system (as it is not within the experimental range needed) so oligonucleotides with commercial dyes were considered for use. Several fluorescent dyes have excitation wavelengths in the correct region and commonly used ones are shown in Table 4-2.

Name	**Excitation λ / nm**	**Use of fluorophore**
Alexa Fluor Dyes	5 in range from 590 – 650	Cell and tissue label
Allophycocyanin (ACP)	652	Fluorescent protein
ATTO Dyes	10 in range from 590 – 650	DNA and RNA label
Cy5	650	Biomedical imaging
DRAQ5, DRAQ7	600/647, 599/644	Cellular imaging
mPlum	590	Fluorescent protein
mRaspberry	598	Fluorescent protein
Texas Red	589	DNA and RNA label
TOTO-3, TO-PRO-3	642	Cellular imaging

Table 4-2: A list of commonly used fluorescent dyes with excitation wavelengths of between 590 nm to 650 nm.

For use in this project the fluorescent dye is required to label DNA. Therefore a selection of ATTO dyes were used. The ATTO dyes are patented by a German company called ATTO-TEC. They have been shown to have a strong stable absorption in comparison with other dyes as shown in Figure 4-14 and they have a high extinction coefficient with a high quantum yield (QY). The quantum yield is the ratio of photons emitted through fluorescence by the photons absorbed. For example Cy5 has a QY of 0.27 compared to ATTO 594 which has a QY of 0.85. The increased lifetime of the ATTO dyes allows for real time measurements to be carried out. The high fluorescence yield and high photostablilty of the dyes provides an excellent option for the fluorescence tag.

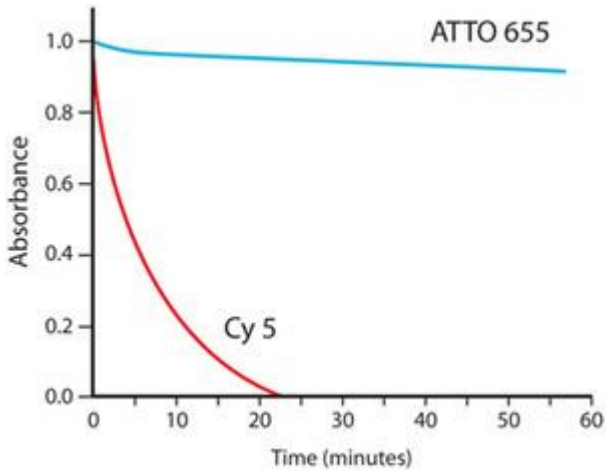

Figure 4-14: Comparing absorbance over time for ATTO 665 (blue line) and Cy 5 (red line) dyes [99]. ATTO 665 has a substationally longer lifetime then Cy 5.

The selection of ATTO dyes that were tested in the experiments are listed in Table 4-3 with the associated excitation and emission wavelengths. The exact structures of these dyes are not published.

Name	**Excitation λ / nm**	**Emission λ / nm**
ATTO 594	601	627
ATTO 633	629	657
ATTO 647	645	669

Table 4-3: Excitation and emission wavelengths of the ATTO dyes used.

Oligonucleotides with 5'-thiol (C6) modification and 3'-ATTO dye modification (via an amino link) were obtained from Integrated DNA technologies. They were used as received. The sequences of the strands are shown in Table 4-4.

	Sequence 5'-3'
DAPK-ATTO 594	XAAGGCGC**GGAGGATAGTCGGATCGAGTTAACGTC** GCGCCTT ATTO 594
DAPK-ATTO 633	XAAGGCGC**GGAGGATAGTCGGATCGAGTTAACGTC** GCGCCTT ATTO 633
DAPK-ATTO 647	XAAGGCGC**GGAGGATAGTCGGATCGAGTTAACGTC** GCGCCTT ATTO 647

Table 4-4: List of sequences purchased from Integrated DNA technologies where X is 5'-thiol (C6) modification and the 3'-ATTO dye was attached via an amino link. The underlined bases form the stem of the hairpin design while the bases in bold show the recognition section of the sequence.

As seen in Table 4-3, for all three ATTO dyes, the wavelength shift between the excitation and emission wavelengths is only between 24 and 28 nm. The transmission graph that was obtained using ATTO 594 has a broad peak (Figure 4-15) and therefore if a new emission wavelength peak is present it cannot be seen. This was the same for all ATTO dyes tested.

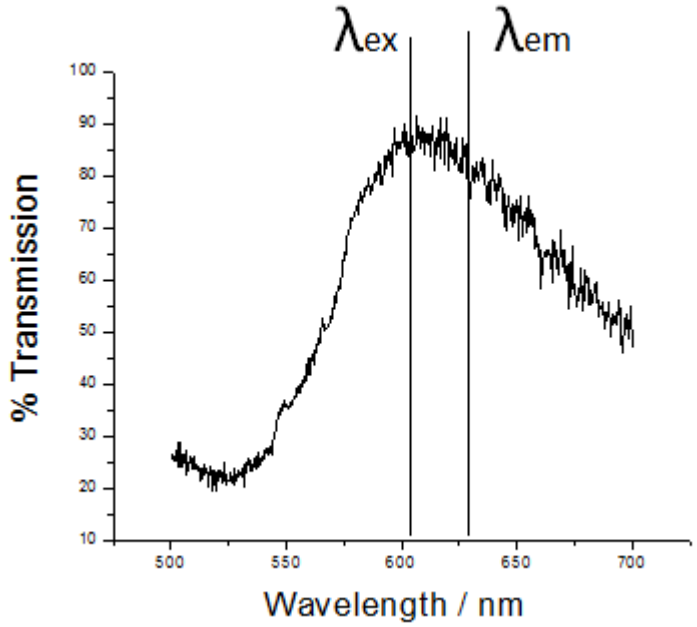

Figure 4-15: Example fluorescence data marking on the position of the excitation and emission wavelengths.

The current system is not sensitive enough to detect the new fluorescence that should be produced upon hybridisation. Possible methods to move forward with fluorescence detection could be to synthesise a dye which has an excitation wavelength in the correct region and an emission wavelength that has a far greater difference than the ATTO dyes which have already been investigated.

A different system using a silicon biophotonic sensor could be developed where the light originates from a different plane to the observed fluorescence. Therefore the fluorescence could be observed as an on-off switch type approach. This could be done by filtering out different wavelengths so only the desired wavelength due the fluorescence would be detected. However, the silicon biophotonic sensor would not be able to be fabricated in time by A*STAR during my attachment in Singapore. Due to time and location restraints it was decided that the next avenue to investigate would be electrochemical sensors.

4.4 Electrochemical Sensor

Electrochemical sensors can be used for measuring DNA hybridisation by cyclic voltammetry (CV) and differential pulse voltammetry (DPV). CV and DPV measures the current when a voltage is applied, with CV cycling the voltage while DPV provides a linear sweep voltage. Initially the electrochemical sensor was used to detect TNF-α from undiluted human serum [100] before moving onto the detection of DNA hybridisation. The latter is explored in this chapter.

4.4.1 Chip Fabrication

All chips used were fabricated by members of staff within A*STAR (Singapore) using methods previously described [100-104].

A silicon wafer was used to fabricate a gold electrode array. Electron beam evaporation was used to deposit a layer of Ti/Au of thickness 0.1 μm/1 μm. This process takes place in a vacuum where the source material was heated until it evaporated onto the desired surface. An electron beam was directed to the source material whereby the intense beam heats the source material from energy transfer to the atoms on the surface. It is a physical vapour deposition (PVD) technique which are often used instead of chemical vapour deposition (CVD) as it is cheaper and has fewer risks associated with it for depositing metals. PVD does not require a high temperature, specialised precursors or by products which can be corrosive or toxic.

A series of processes were carried out to pattern the sensing microelectrodes, connecting route lines and bond pads. These include photoresist spin coating and photolithography through a chrome mask. In order for the photolithography process to take place, a

photoresist coating is initially required. There are three main ways for this process to occur which are spin coating, spray coating and electrodeposition of the photoresist. Spin coating, used herein, is a simple process where the thickness can be controlled by changing the spin speed. Photolithography can then take place, where a chrome mask is used to pattern a substrate containing a light sensitive photoresist coating.

The unpatterned metal regions were etched with gold etchant (Au-600, CLC) and titanium etchant (Ti-890, CLC). The photoresist coating was then stripped off using solvent. Sulphuric acid and hydrogen peroxide were then used in a 4:1 ratio to clean the wafers. This was done at 125 °C to remove any contamination.

The wafer, apart from the gold electrodes, was passivated with a moisture barrier layer of silicon dioxide and silicon nitride with a thickness of 0.8 µm/0.2 µm. This was carried out using plasma enhanced chemical vapour deposition (PECVD). To stop any inter-diffusion of titanium into the gold surface, the PECVD was conducted at 200 °C. Reactive ion etching (RIE) exposed the bond pads and the array of sensing microelectrodes for use using CF_4.

After fabrication, the chips were cleaned and used (see 9.12 for details). A chamber was made using a laser cutter to contain the probe/target solution. The chip can be seen in Figure 4-16. The comb structure of the sensing part of the working electrode is magnified and also shown.

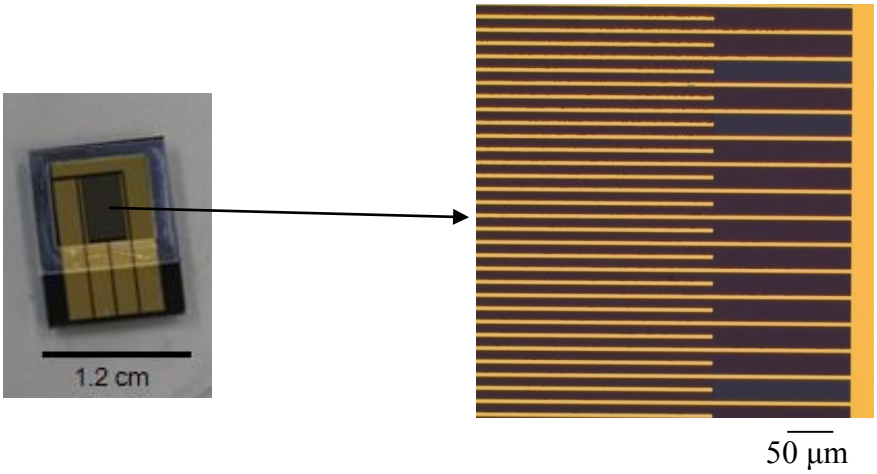

Figure 4-16: Single electrode chip used for the electrochemical experiments with a chamber made from double sided tape cut using a laser machine. Inset – magnified image of the sensing part of the electrode. Scale bar included.

4.4.2 Detecting DNA Hybridisation Using an Electrochemical Sensor

The electrochemical sensor was then used for DNA detection, for full experimental details see 9.12. 5-Thiol modification was again chosen due to its ability to spontaneously bond with gold. After the chip was cleaned with UV-ozone for 20 minutes, a baseline CV was conducted. This was done by adding a redox probe solution of 5 mM $[Fe(CN)_6]^{3-/4-}$, pH 7.4, to the chip 1 minute before the measurement was taken. 5'-Thiol modified DNA (1 µM) was then immobilised onto the chip and a repeat CV was run. Complementary target DNA was added and the CV was repeated. The difference observed between probe and target is seen in Figure 4-17(A). The experiment was repeated using DPV and a range of concentrations from 5 nM to 100 nM with representative data shown in Figure 4-17(B). As the target concentration increased the observed current response decreased. CV and DPV are introduced in 1.5.2 and 1.5.3 where the peaks observed correspond to the oxidation/reduction of the redox species – in this case $[Fe(CN)_6]^{3-/4-}$.

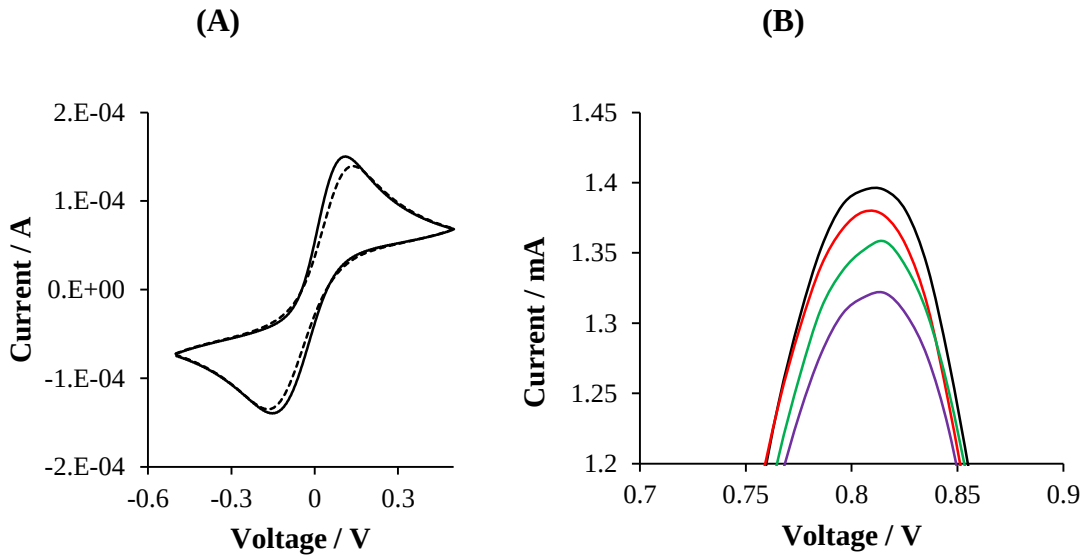

Figure 4-17: (A) CV of RARβ probe (solid line) and 100 nM complementary target DNA (dashed line). (B) DPV of RARβ probe (black) and increasing complementary target DNA, 10 nM (red), 50 nM (green) and 100 nM (purple).

As shown in Figure 4-18, mismatched DNA (100 nM) was found to shift the DPV by 0.08 mA compared with 0.7 mA when complementary target DNA (100 nM) was used. The limit of detection was found to be 5 nM, as below this concentration the current response was in the same region as the mismatched DNA. To enhance the sensitivity the probes were tagged with a redox active marker (see Chapter 3). Experiments run with these probes were investigated in the following sections (Chapters 5 and 6).

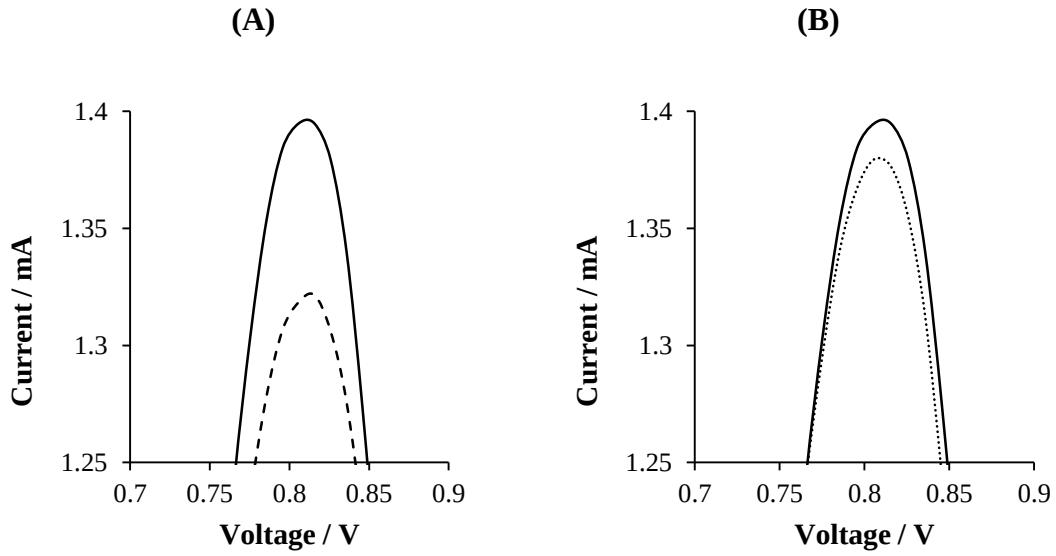

Figure 4-18: (A) DPV data of DAPK probe (solid line) and 100 nM complementary target DNA (dashed line). (B) DPV data of DAPK probe (solid line) and 100 nM mismatched DNA (dotted line).

4.5 Conclusions: Unmodified Oligonucleotide Sensors

Limits of detection of the methods examined are compared in Table 4-5. It was seen that the limit of detection of all sensors with unlabelled DNA probes were very similar. However, as SPR cannot be miniaturised into a POC device, this was not investigated further.

Method of Detection	**Limit of detection**
Silicon biophotonic	25 nM
SPR	5 nM
Nanoplasmonic	10 nM
Electrochemical sensor	5 nM

Table 4-5: Comparison of the limit of detections of the methods discussed in this chapter.

Fluorescence work was attempted with the nanoplasmonic device, however, the excitation and emission wavelength of the ATTO dyes were found to be too close together for accurate measurements. Previously synthesised porphyrin modified DNA, with excitation wavelength of 420 nm, was unsuitable as the excitation wavelength required was 590 nm – 650 nm. A dye could be synthesised with a greater difference between the excitation and emission wavelength, with the excitation wavelength within the region for the device. Alternatively, a silicon biophotonic sensor could be developed in which the plane of incident light is orthogonal to the fluorescent emission. Hence, a fluorescence based approach could be used as an on/off switch type detector. However, time and location constraints meant that this would be unrealistic in the time frame within (A*STAR, Singapore).

In addition to the work with DNA, the protein TNF-α was also detected using the electrochemical sensor. This shows the capability and versatility of the device and further applications that it can be used for. The electrochemical sensor can now be used with the DNA synthesised in chapter 3 where a redox active probe is incorporated into the sequence. This should enhance the sensitivity of the sensor and eliminate the need of an external redox active solution to be added.

5. Electrochemical Sensor with Chemically Tagged DNA Probes

The electrochemical sensor described in section 4.4 was used with the chemically tagged DNA probes synthesised in Chapter 3. The incorporation of redox active tags into bladder cancer genes (DAPK, E. Cad and RARβ), should enhance the sensitivity of the electrochemical sensor in addition to not requiring an external redox solution, eliminating several washing steps. The hairpin design, as described in section 1.7, allows the redox active probe to be in close proximity to the gold surface upon immobilisation. Complementary target DNA hybridisation will then move the redox active tag further from the surface, hence causing a decrease in the observed current response. The sensitivity of detection should be enhanced from section 4.4.3 where unlabelled DNA probes were used. Sequences of the complementary and mismatched DNA are shown in Table 3-2.

5.1 Anthraquinone and Porphyrin Tagged DNA Probes

Before attempting electrochemical detection, the synthesised chemically tagged DNA probes (described in Chapter 3) were initially tested using SPR to ensure probe immobilisation on a gold surface (as in 4.2). SPR is an efficient and rapid method that additionally allows the hybridisation efficiencies of immobilised oligonucleotides to be observed. This method confirmed that the probe binds efficiently to the gold surface and recognises the complementary DNA strand selectively before attempting electrochemical detection. The SPR experiments, as seen in Figure 5-1, showed the same increase in signal response as the concentration of complementary target DNA increased as previously discussed in 4.2.1.

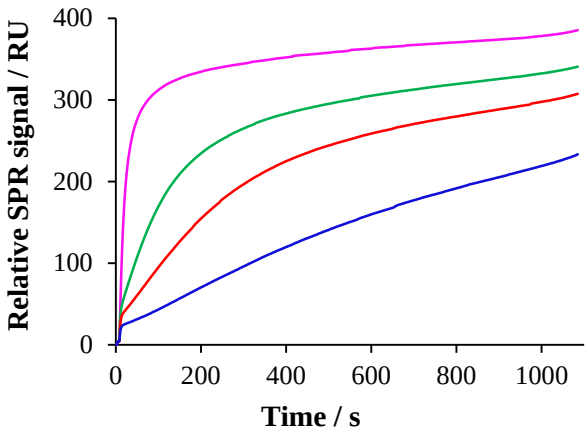

Figure 5-1: Real time relative SPR response for a range of increasing concentrations of complementary target DNA (E. Cad porphyrin modified DNA probe). Where: 20 nM (blue), 50 nM (red), 100 nM (green), 300 nM (pink).

Representative data demonstrating the selective hybridisation of the immobilised DNA probe is shown in Figure 5-2. This compared 300 nM of complementary target DNA with 300 mM of mismatched DNA (E.Cad porphyrin modified probe, 1 μM). The maximum relative SPR signal for 100 nM complementary DNA was 382 RU compared to 69 RU for the mismatched DNA.

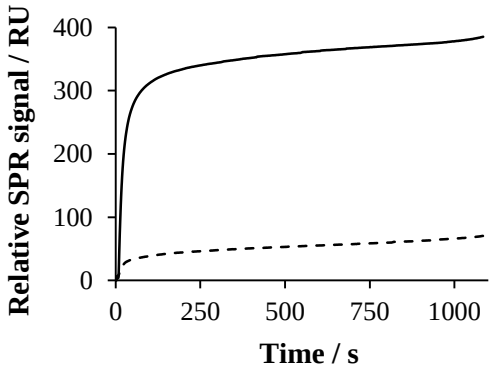

Figure 5-2: Relative SPR signal response of 300 nM complementary target DNA (solid line) and 300 nM mismatched DNA (dashed line) where E. Cad porphyrin modified DNA with a 5'-thiol modification probe was used.

Before the electrochemical sensor was functionalised with the chemically modified DNA probe, the sensor was cleaned as previously described in 4.4. Briefly, the chip was immersed in acetone and sonicated for 10 minutes before it was rinsed with IPA (5 mL) and water (20 mL). The chip was then treated with UV/ozone for 20 minutes before the chemically modified DNA probe was added immediately.

As the chemically tagged probes contain a redox active molecule the redox probe solution, as used with the unlabelled DNA probes, was not necessary. Instead the peak observed is from the redox active tag being oxidised/reduced.

Preliminary experiments using both the porphyrin and anthraquinone modified DNA probes allowed for a range of immobilisation times (Figure 5-3), scan rates (Figure 5-6) and buffer solutions (Figure 5-5) to be optimised. It was observed that increased immobilisation time (24 hours) did not benefit the current response obtained. The peak from the porphyrin is shown where the longer immobilisation time reduced the definition of the desired peak. Therefore a lower immobilisation time of 5 hours was used. Measurement of complementary (or mismatched) DNA target was carried out after 1 hour.

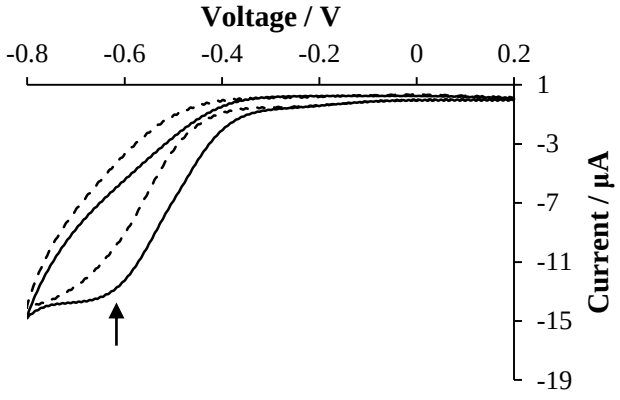

Figure 5-3: CV of porphyrin modified DNA (E. Cad) with 24 hour immobilisation (dashed line) and 5 hour immobilisation time (solid line).

The initial CVs of both the anthraquinone and porphyrin modified DNA probe is shown in Figure 5-4, where the same concentration is used for each probe (1 µM). The porphyrin modified DNA probe gave a higher current response (-12.7 µA) than the anthraquinone modified DNA probe (-9.4 µA). The current response is lower than observed with the unlabelled probes (µA compared to mA) due to the signal only coming from the redox active tag and not an additional redox solution. However, this avoids numerous washing steps and allows the results to be collected rapidly.

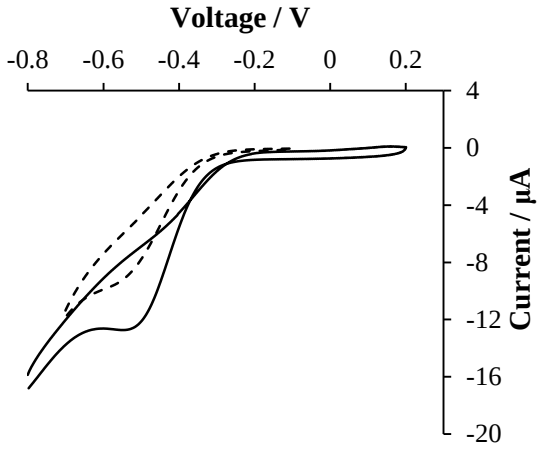

Figure 5-4: Comparison CV of porphyrin modified DNA probe (solid line) and anthraquinone modified DNA probe (dashed line) with a scan rate of 100 mV/s. Both probes had 5'-thiol modifications.

A comparison was made between PBS and 1 M sodium chloride/0.1 M sodium citrate buffers with the latter having been used previously with porphyrin modified DNA [77]. As seen in Figure 5-5 the current response was higher (1.5 µA) with the sodium chloride/sodium citrate buffer and hence was used for all further CV and DPV experiments.

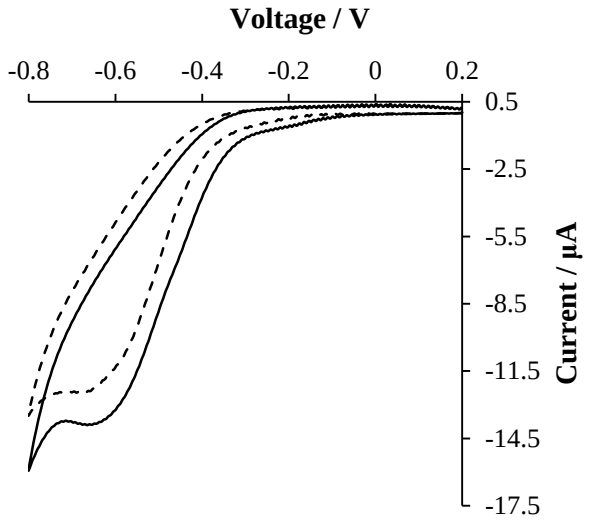

Figure 5-5: CV of free base porphyrin modified DNA (RARβ) in PBS (dashed line) and sodium chloride/sodium citrate buffer (solid line).

A range of CV scan rates from 25 mV/s to 800 mV/s was run with both the porphyrin and the anthraquinone modified DNA probes. Representative data of DAPK anthraquinone modified DNA (with 5'-thiol modification) is shown in Figure 5-6. Increasing the scan rate decreased the definition of the reduction peak while an oxidation peak could be clearly seen, solely in the higher scan rate (500 mV/s).

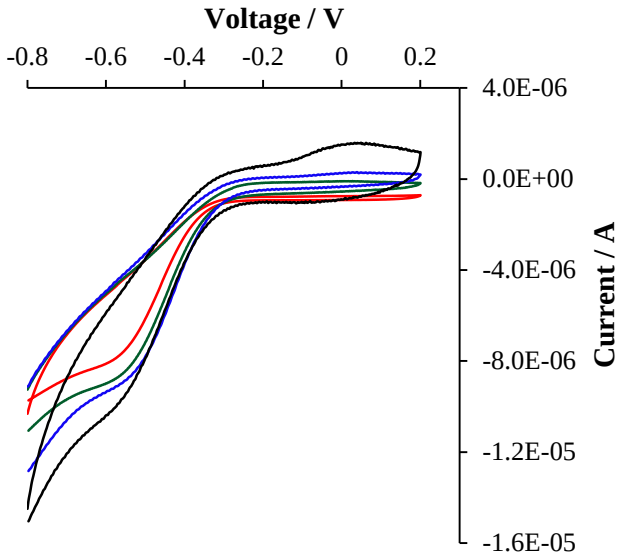

Figure 5-6: Representative CV of increasing scan rates used with an anthraquinone modified DNA probe (DAPK). 25 mV/s (red), 50 mV/s (green), 100 mV/s (blue) and 500 mV/s (black).

In order to determine whether the electrochemical reaction of the redox active marker was surface dependant or diffusion dependent, the peak current for each scan rate was obtained from the corresponding CVs. If the peak current is proportional to the inverse of the scan rate, the reaction would be diffusion dependant. However, if the peak current is proportional to the scan rate the reaction is surface dependant. Figure 5-7 shows the relationship of the peak current with both anthraquinone and porphyrin modified DNA probes (E.Cad) was proportional to the scan rate. Therefore, the electrochemical reaction is surface dependant, which indicated that the probe was immobilised onto the surface of the sensor, since the design of the hairpin probe brings the redox marker into close proximity of the sensor.

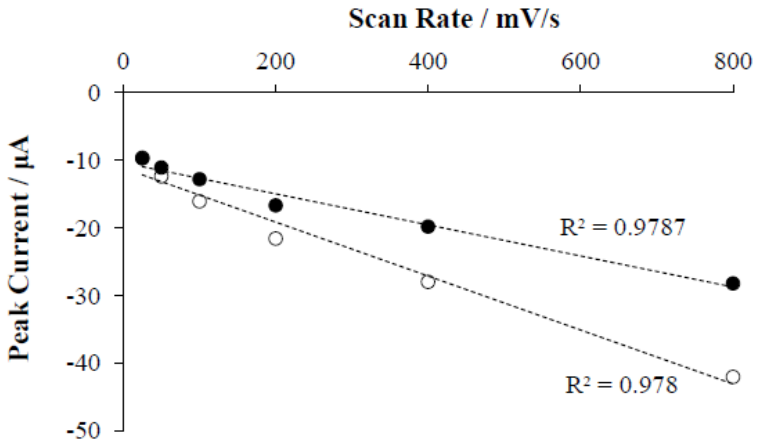

Figure 5-7: Linear relationship between the scan rate and the peak current for porphyrin (○) and anthraquinone (●) modified DNA probes (E.Cad probe).

The lack of the oxidation peak and the reduction in signal on repeated scans (Figure 5-8) suggested that the porphyrin and anthraquinone modified DNA probe was being desorbed from the gold chip surface. This observation was in agreement with the previous reports that thiol DNA at negative voltages can be desorbed from the gold surface [105, 106]. Possible reasons including the sulphur being oxidised and electrostatic repulsion of the DNA. Unfortunately this makes it a single use system, as the results are not reliable after the first scan due to some of the DNA probe desorbing from the gold surface and into the bulk solution. The second scan may be useable after a separate calibration, however in this work the focus will be on the first scan.

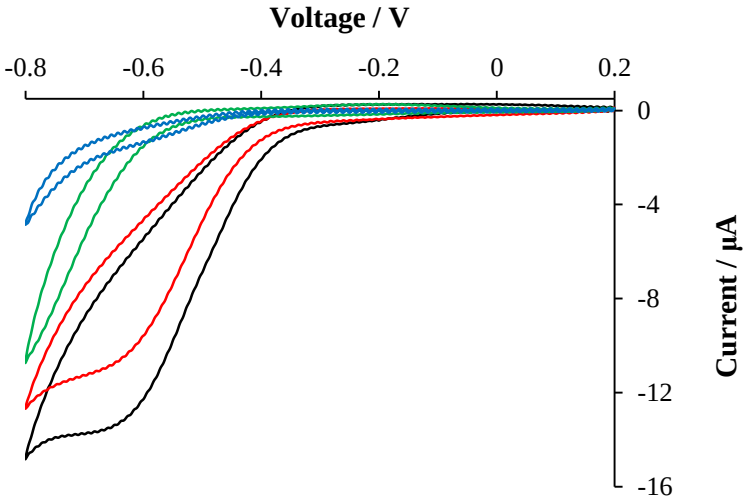

Figure 5-8: CV showing the reduction in current response with a repeated scan, with scan 1 (black), scan 2 (red), scan 3 (green) and scan 4 (blue). RARβ porphyrin modified DNA probe.

Due to the reduced signal of repeated scans, the first scan of each chip was used. A test was carried out to check that there is a difference in signal between the immobilised probe and hybridisation with a complementary target. Figure 5-9 shows that a clear difference can be seen between the probe and complementary target using CV. The signal decreases after the target DNA is introduced. This agrees with the proposed idea that by adding the target the chemical tag is moved away from the gold surface. Therefore confirming feasibility of the proposed system. In addition to the complementary target used, mismatch DNA (which is not fully complementary to the probe) was also tested. As seen in Figure 5-9 the mismatch DNA showed only marginal difference to the specific probe (0.02 µA) indicating good probe specificity.

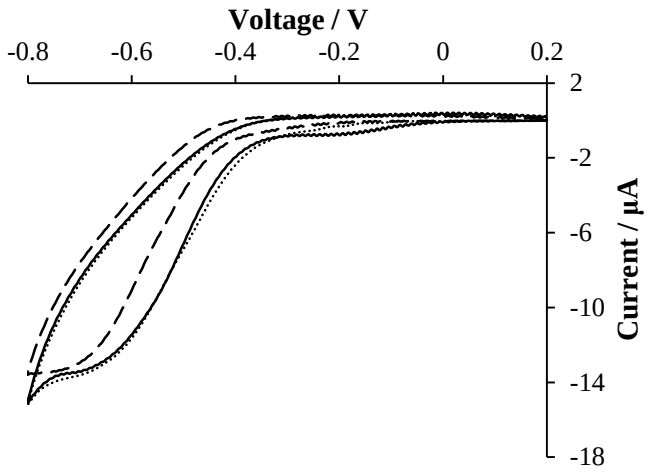

Figure 5-9: CV showing the difference in signal between immobilised probe (solid line) and the addition of complementary target DNA (dashed line) and mismatch DNA (dotted line)

As with the unlabelled DNA, CV can distinguish between the DNA probe and the DNA probe with complementary target. However to find the limit of detection (LOD) DPV, which is a more sensitive technique than CV, was carried out using a range of target concentrations (50 fM to 100 nM). Both the porphyrin and anthraquinone modified DNA probes decreased the signal as the concentration of the target solution was increased. This was as expected due to the hairpin design of the DNA probes. As previously described (see 1.7) when the probe is immobilised onto the gold surface the redox active tag is close to the gold surface. Hybridisation of the complementary target DNA with the immobilised probe opens the hairpin design, and in doing so, moves the chemical tag away from the gold surface. This larger distance is represented by the decrease in the current response observed. Representative data with a porphyrin modified DNA probe is shown in Figure 5-10(A).

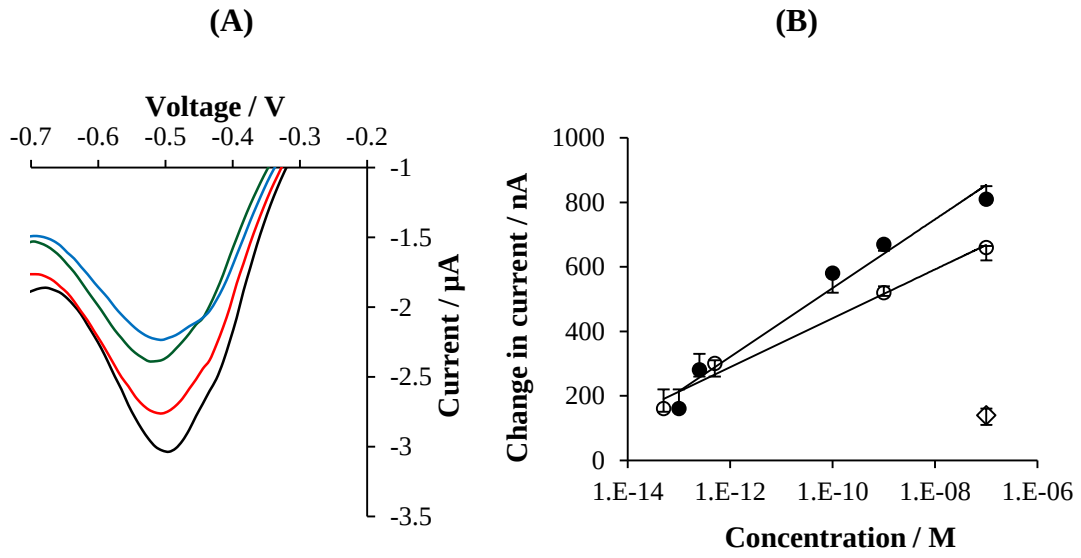

Figure 5-10: (A) Example DPV data of porphyrin modified DNA probe (5'-thiol modification) over a range of target concentrations: probe (black), 250 fM (red), 100 pM (green) and 100 nM (blue). (B) Peak current comparison of porphyrin (●), anthraquinone (○) in a dynamic target concentration range (50 fM to 100 nM) with (◊) mismatched target DNA shown.

Figure 5-10(B) compares the change in current response between the peak current for the probe and the peak current for the complementary target, for both anthraquinone and porphyrin modified DNA. Mismatched DNA (for sequences see Table 3-2) was also added and showed that the limit for anthraquinone modified DNA was 50 fM compared with 100 fM for porphyrin modified DNA. These LODs are in the biologically relevant range and is greatly enhanced over the results with unlabelled DNA probes (discussed in 4.5). As seen in Figure 5-10(B) at a higher concentration of complementary target DNA porphyrin modified DNA had a larger current response change after hybridisation (810 nA compared with 660 nA). However, at a lower concentration of target DNA the anthraquinone had a lower LOD, making it more sensitive for DNA detection. The detection limit of these probes in the femtomolar range performs well against other methods as seen in Table 1-1. Therefore this system with porphyrin and anthraquinone probes are worth exploring.

5.2 Methylene Blue Tagged DNA Probes

As a comparison to the porphyrin and anthraquinone modified DNA probes, oligonucleotides using the commercially available methylene blue tag were purchased (from IBA Life Sciences, Germany). Methylene blue has been used previously as an electrochemical tag [44, 65, 66, 69]. As similar to the porphyrin and anthraquinone modified DNA probes, the methylene blue internal modification is based on thymine (Figure 5-11).

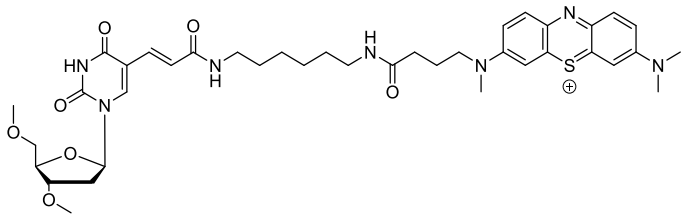

Figure 5-11: Structure of methylene blue attached to the deoxynucleoside thymidine.

Two different designs for the methylene blue modified DNA hairpin probes were purchased. The first design was the same as used previously, see sequences in Table 3-1, in which the recognition section of the hairpin was solely in the loop. This allows for direct comparison with the synthesised porphyrin and anthraquinone modified DNA probes. The second design, however, incorporated part of the recognition section into the stem of the hairpin design. By having part of the recognition section in the stem of the hairpin could allow the hairpin to open more readily and therefore could have a lower limit of detection. The position of the methylene blue tag remained in the same position for both designs and hence the current response was expected to be reduced upon hybridisation with the complementary target DNA. The sequences of both designs, based on DAPK, are shown in Table 5-1.

	Sequence 5'-3'
MB-1	YAAGGCGC**GGAGGATAGTCGGATCGAGTTAACGTC**GCGCCXT
MB-2	YTATGACG**GGAGGATAGTCGGATCGAGTTAACGTC**AXA

Table 5-1: Sequences of methylene blue modified DNA probes, where X is the methylene blue and Y is the 5'-Thiol C6 modification. The bases underlined form the stem of the hairpin while the bases in bold represent the recognition section.

As with the synthesised porphyrin and anthraquinone modified DNA probes, the methylene blue modified DNA probes underwent CV at varying scan rates (25 mV/s to 800 mV/s). Figure 5-12 shows that the peak current was proportional to the scan rate indicating that the electrochemical process is surface dependent. These results were as expected as they are similar to the previous results with porphyrin and anthraquinone modified DNA probes (see Figure 5-7).

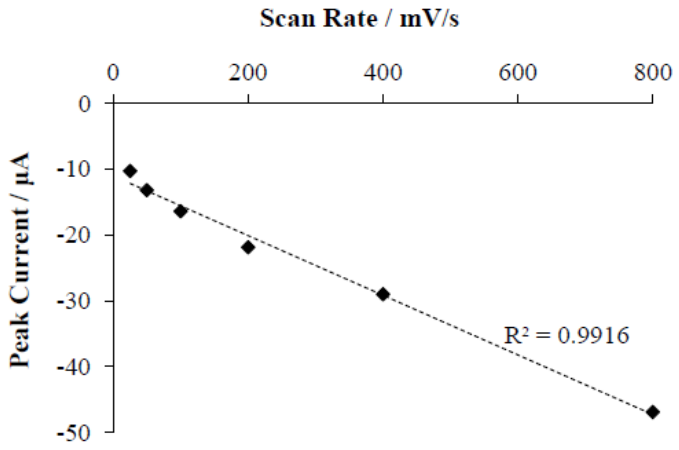

Figure 5-12: CV showing a linear relationship between scan rate and the peak current for methylene blue modified DNA probes.

In addition to the CV carried out on the methylene blue modified DNA probes, DPV was performed to find the limit of detection. Representative DPV data, shown in Figure 5-13(A), showed MB-1 probe and the current reduction observed upon DNA hybridisation with complementary target DNA. An increased concentration of the complementary target DNA caused an increased reduction of the current response. Figure 5-13(B) shows how different concentrations of complementary target DNA effected the current response for both MB-1 and MB-2.

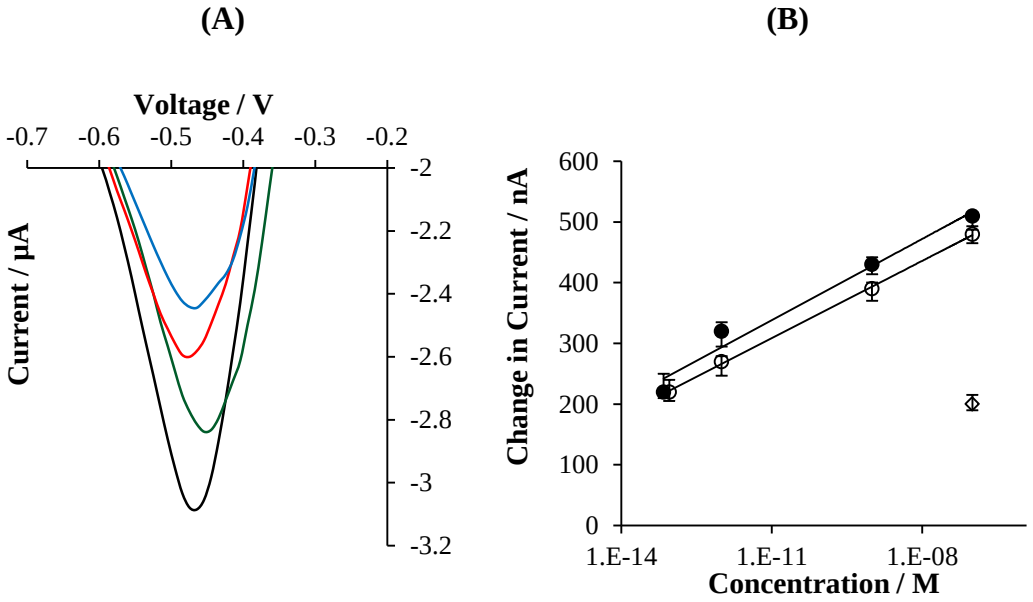

Figure 5-13: (A) Representative DPV of MB-1 to show increasing concentration of complementary target decreases the peak current. Probe (black), 500 fM (green), 1 pM (red) and 100 nM (blue). (B) Peak current change over dynamic concentration range where (●) MB-1, (○) MB-2, (◊) mismatched target.

Figure 5-13(B) shows a small difference (approximately 40 nA) between the two different designs, where the MB-1 design used gave a slightly higher change in the current response than MB-2. A similar limit of detection was recorded for both designs with MB-1 having a LOD of 70 fM while MB-2 had a LOD of 90 fM. As MB-2 had part of the recognition section incorporated into the stem of the hairpin design, it was thought that it would have

a lower detection limit as the hairpin design would open with more ease. However, as determined above this was not the case. At a higher concentration of target DNA MB-1 gave a larger current response than MB-2 (510 nA compared with 480 nA).

The purchased methylene blue modified DNA probes behaved well in comparison with the synthesised probes. However, the current response of porphyrin modified DNA can be changed by the addition of a metal, which is advantageous going forward to design a multiplex system.

From the three tags investigated so far it is noted that the porphyrin tag gave the largest change in current response with a high concentration of complementary target DNA with the anthraquinone tag giving the lowest LOD. Other tags, as introduced in 1.6, could be used but this work was focused on anthraquinone, methylene blue and porphyrin.

5.3 Detection of DNA mutations

DNA mutations can be used as biomarkers for many diseases. Once mutations specific to a disease have been identified, probes can be designed to detect the changes. A variation in only a single base is known as single-nucleotide polymorphism (SNP). It was shown earlier that the electrochemical sensor with chemically tagged probes has a greatly enhanced sensitivity over unlabelled DNA probes. Therefore in addition to detecting DNA methylation the system can be potentially used for detecting DNA mutations. The advantage of detecting a mutation in the DNA is that it has the potential of being directly detected from a patient sample (for example, urine). To demonstrate feasibility, bladder cancer mutations will be used, that can be detected in urine and have been found specific to the disease [89]. The sequences used in this section are shown in Table 5-2. MB-1 and the DNA targets with one and two mutations were purchased from IBA Life Sciences.

	Sequence 5'-3'
MB-1 (Probe)	ZAAGGCGC**GGAGGATAGTCGGATCGAGTTAACGTC**GCGCCXT
DAPK (Probe)	ZAAGGCGC**GGAGGATAGTCGGATCGAGTTAACGTC**GCGCCYT
Complementary target (DAPK)	GAC**G**TTAACTCGATCC**G**ACTATCCTCC
1 mutation target	GAC**A**TTAACTCGATCC**G**ACTATCCTCC
2 mutation target	GAC**A**TTAACTCGATCC**T**ACTATCCTCC
Completely mismatched target (E. Cad)	ATTAAAATCCAATCTCCCAATAGCGC

Table 5-2: Sequences used in the mutation experiments where X is methylene blue, Y is porphyrin and Z is 5'-thiol (C6) modification. Underlined bases form the stem of the hairpin design in the probe while the bases in bold represent the recognition section of the sequence.

In this study, the focus was on direct signal detection from a physiological sample. To mimic the physiological conditions, Surine (urine negative control, Sigma Aldrich) was used as a test medium. Synthesised porphyrin modified DNA and purchased methylene blue modified DNA probes were tested for this study. Representative DPV data for porphyrin modified DNA probes can be seen in Figure 5-14(A). Upon probe hybridisation with a fully complementary target DNA a large reduction in peak current was observed (0.23 μA), whereas hybridisation with completely mismatched DNA gave a significantly lower peak current reduction (0.05 μA). In addition, Figure 5-14(B) clearly shows the difference between fully complementary target DNA (230 nA) and target DNA containing one mutation (110 nA). This demonstrates that the system can easily distinguish a single mutation (SNP). The sequence containing two mutations had a change in the current response of 65 nA, which was similar to the completely mismatched sequence (50 nA). The methylene blue modified DNA probe gave similar results.

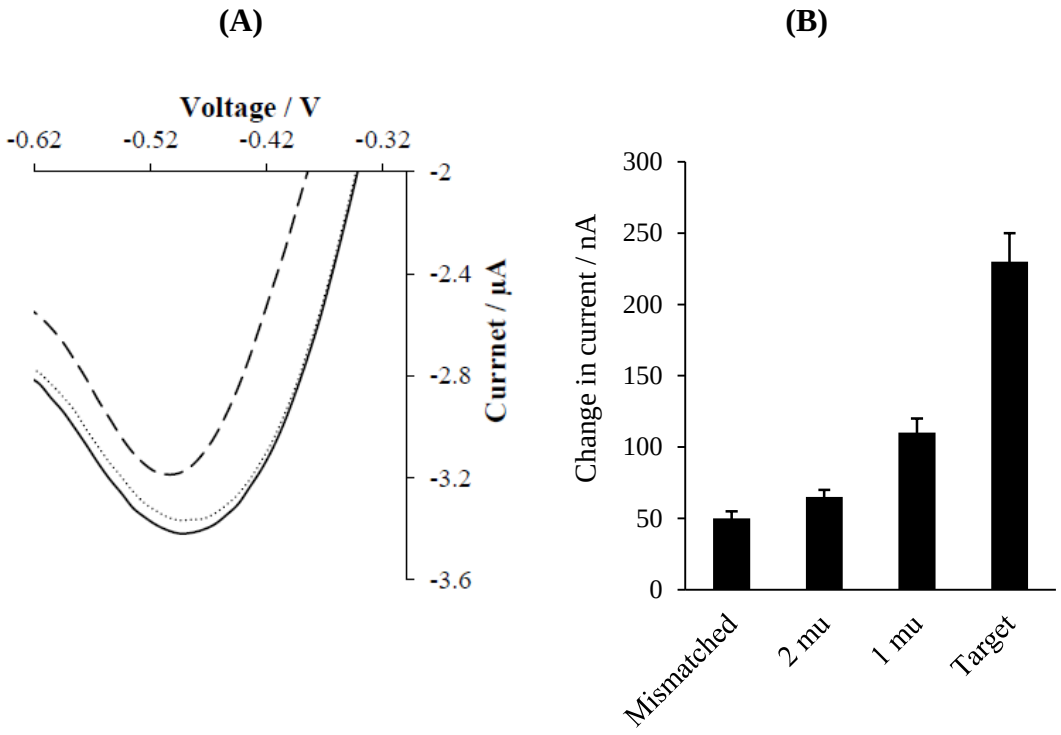

Figure 5-14: (A) Representative DPV of porphyrin modified DNA probe (DAPK, 5'-thiol modification) (solid line), completely mismatched DNA (dotted line) and complementary target DNA (dashed line) in Surine. (B) Comparison of target DNA containing mismatched, two mutations (2 mu), one mutation (1 mu) and fully complementary (Target).

In addition it was noted from the experiment run in Surine that the change in current response when fully complementary target DNA (of same concentration of 100 nM)) is added is reduced from 810 nA to 230 nA. Despite the lower change in current response in the Surine, the complementary DNA can still be detected making the system feasible for detection in bodily fluids such as urine.

5.4 Additional DNA Probes

As observed in 5.1 and 5.2 the negative voltage (-0.8 – -0.6 V) required for the porphyrin, anthraquinone and methylene blue tags caused the DNA probe to detach from the gold surface. This leads to repeated scans being unusable. To avoid the thiol DNA detaching from the gold surface additional probes were synthesised which have a positive redox potential, for example cobalt metallated porphyrin. Repeated scans could then be carried out giving the option for the device to be used multiple times and not solely as a single use device. Due to not having the facilities available for DNA synthesis while in Singapore, the DNA probes in this section were synthesised and purified by Dr Iwona Mames and Christina Xyrafaki. The thiol linker to the gold surface used in these strands was 5'-Thiol-Modifier-C6-CE Phosphoramidite purchased from Link Technologies (item number 2125), and the structure can be seen in Figure 5-15.

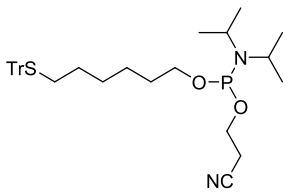

Figure 5-15: Chemical structure of the thiol modification used for the additional DNA probes, 5'-Thiol-Modifier-C6-CE Phosphoramidite. Where Tr is a trityl protecting group.

Protocol using the 5'-Thiol-Modifier-C6-CE phosphoramidite was carried out as recommended by the manufacturer. The final oxidation is carried out using 0.02 M of iodine in order to minimise the oxidative cleavage of the trityl group. Due to this trityl protecting group an additional deprotection step was required, as it is not acid labile and cannot be removed on the DNA synthesiser, before the probes can be used. This was done by cleaving the trityl-sulphur bond using silver nitrate. An aqueous silver nitrate solution (1 M) was added to the oligonucleotide product which was suspended in TEAA (0.1 M)

and left for 30 mintures. The excess silver, from the silver nitrate, was precipitated using tris(2-carboxyethyl)phosphine (TCEP) for five mintues. After washing with TEAA the excess TCEP was desalted before the oligonucleotides were sent to Singapore for testing.

5.4.1 Cobalt Metallated Porphyrin Tagged DNA Probes

Porphyrin DNA modifications have the advantage over methylene blue that the signal readout can be changed by the addition of a metal. Previous work has shown that cobalt metallated porphyrin is an efficient, sensitive electrochemical probe [77]. To help prevent the probe from being cleaved from the gold surface a positive voltage is required, in order to avoid using a negative voltage. Therefore it was decided that cobalt metallated porphyrin, which only requires a positive voltage, would be attempted. A hairpin design with part of the recognition section incorporated into the stem was used, similar to MB-2 and discussed in 5.2. The sequences were based on DAPK, as seen in Table 5-3, with the cobalt being introduced to the porphyrin post synthesis. The introduction of cobalt to the porphyrin DNA was carried out by heating the strand with an excess of cobalt acetate.

	Sequence 5'-3'
DAPK-CoP	YTATGACG**GGAGGATAGTCGGATCGAGTTAACGTC**AXA

Table 5-3: Sequence used where X is the cobalt metallated porphyrin and Y is the 5'-thiol modification.

CV was run using the cobalt porphyrin modified DNA probe using scan rates in the range of 25 mV/s to 800 mV/s. The peak current of the cobalt porphyrin modified DNA probe was found to be directly proportional to the scan rate, as shown in Figure 5-16, indicating that the electrochemical reaction was surface dependant. This was similar to the free base

porphyrin, anthraquinone and methylene blue tagged probes previously discussed (5.1 and 5.2).

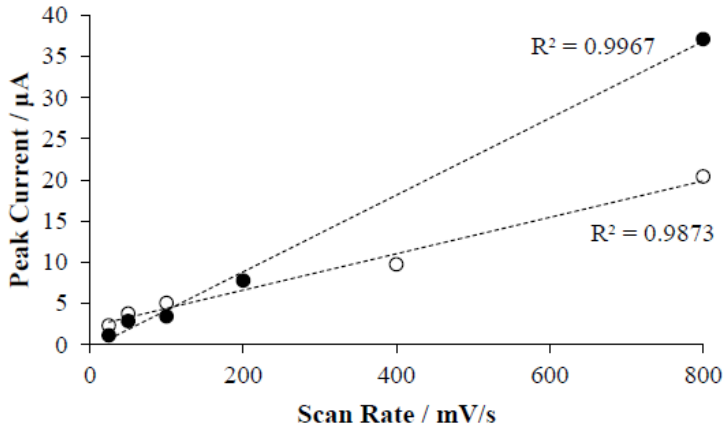

Figure 5-16: Linear relationship between the scan rate and the peak current for Cobalt Porphyrin modified DNA probe (●) and two Cobalt Porphyrin's modified DNA probe (○) both with 5'-thiol modification.

Figure 5-17 shows the CV and DPV of cobalt metallated porphyrin. The DPV shows that the addition of the complementary target reduced the signal response as expected. The current response recorded for the cobalt metallated porphyrin probe is 10x higher than the free base porphyrin probe. As observed in the CV shown in Figure 5-17(A) an oxidation and reduction peak can be seen. This, along with similar repeated scans, show that the probe did not desorb from the gold surface at positive voltages (DPV of repeated scans is shown in Figure 5-18). The voltage measured at the peak current for the CoP probe and target is seen to shift, as seen in Figure 5-17(B), by 0.03 V which is attributed to the Cobalt going from Co^{II} to Co^{III}.

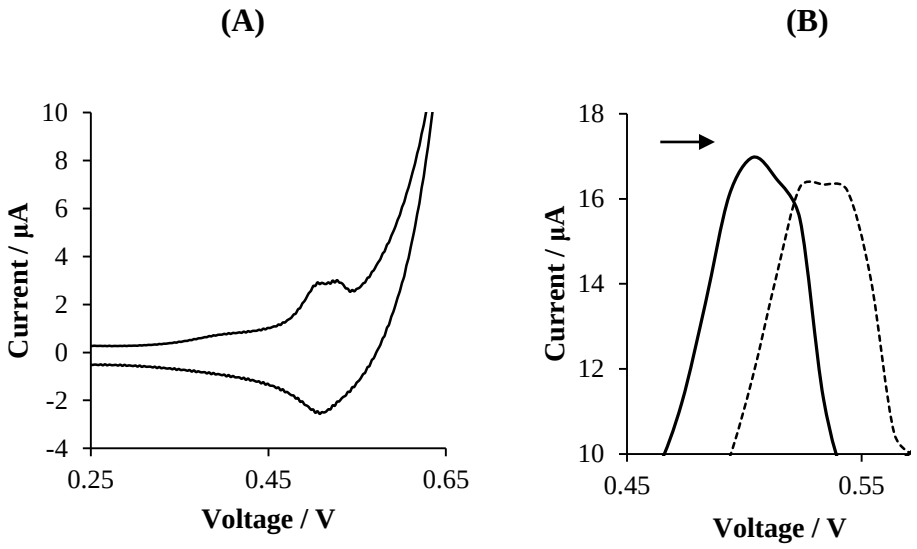

Figure 5-17: (A) CV of CoP modified DNA Probe (with 5'-thiol modification), (B) DPV of CoP modified DNA Probe (with 5'-thiol modification) (solid line) and 100 nM complementary target DNA (dashed line).

To show that the cobalt metallated porphyrin DNA probe does not detach from the surface, repeated DPV was run with 4 repeated scans shown in Figure 5-18. All of the values of the repeat were within the range for the probe without target and shows that the CoP can be used multiple times.

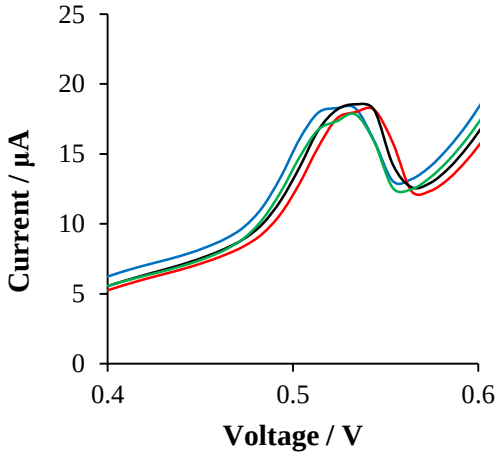

Figure 5-18: Repeated DPV of CoP probe where: scan 1 (black), scan 2 (blue), scan 3 (red) and scan 4 (green).

5.4.2 Multiple Porphyrin Tagged DNA Probes

Strands containing two porphyrin tags were synthesised as an extra comparison to the single porphyrin modified DNA probes. The sequences synthesised with two porphyrin modifiers are shown in Table 5-4. Both free-base and cobalt metallated porphyrin were used. The cobalt was added post synthetically as previously discussed.

	Sequence 5'-3'
DAPK – PP	YTAATGACG**GGAGGATAGTCGGATCGAGTTAACGTC**AXXA

Table 5-4: Sequence synthesised with two porphyrin units where X is either cobalt or free-base porphyrin and Y is 5'-thiol modification. Bases underlined form the stem of the hairpin design while bases in bold show the recognition section of the sequence.

The current responses from probes containing either one or two cobalt porphyrin modifications were proportional with the scan rate (Figure 5-16). It was seen from Figure 5-16 that at higher scan rates the probe containing one cobalt porphyrin modifications had a higher current response (than the DNA probe containing two cobalt porphyrin modifications). Both responses were proportional to the scan rate, indicating that both probes were dependent on surface reactions for the electrochemical reaction of the redox active tag.

CV and DPV of the DNA probe containing two cobalt porphyrin modifications show that the current response obtained from the probe is lower than the DNA probe with only a single cobalt porphyrin modification (Figure 5-19). Interestingly, after the addition of complementary DNA target, the signal output was increased. The increased value was similar to the equivalent signal received for the target DNA solution when a probe with one porphyrin was used. Therefore the signal for the target DNA solution is as expected but the signal for the probe, with two porphyrins, is lower. This could be due to the two porphyrin units stacking together when in the double stranded DNA conformation in the stem of the hairpin probe. After the addition of the target DNA the hairpin opens causing the two porphyrin units to be in single stranded DNA with more flexibility.

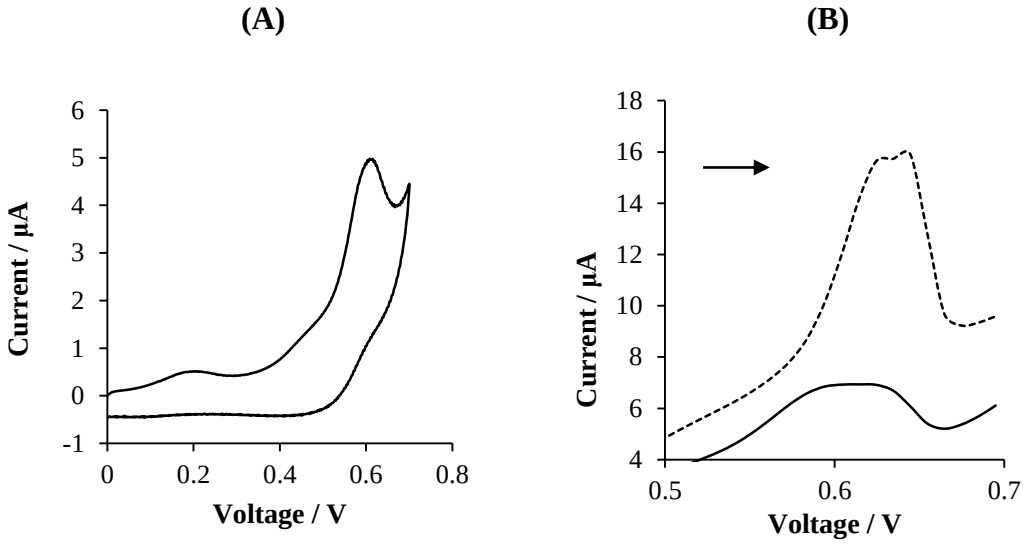

Figure 5-19: (A) CV of DNA probe containing two cobalt porphyrin modifications (with 5'-thiol modification), (B) DPV of DNA probe containing two cobalt porphyrin modifications (with 5'-thiol modification) (solid line) and 100 nM complementary DNA target (dashed line).

The increased current response upon hybridisation with a complementary DNA target, was confirmed with the use of free-base porphyrin as seen in Figure 5-20. The current response of the probe containing two free-base porphyrin modifications increased by the addition of the complementary target DNA, when compared with the same sequence of

free-base porphyrin. This sequence contained part of the recognition section within the stem of the hairpin design.

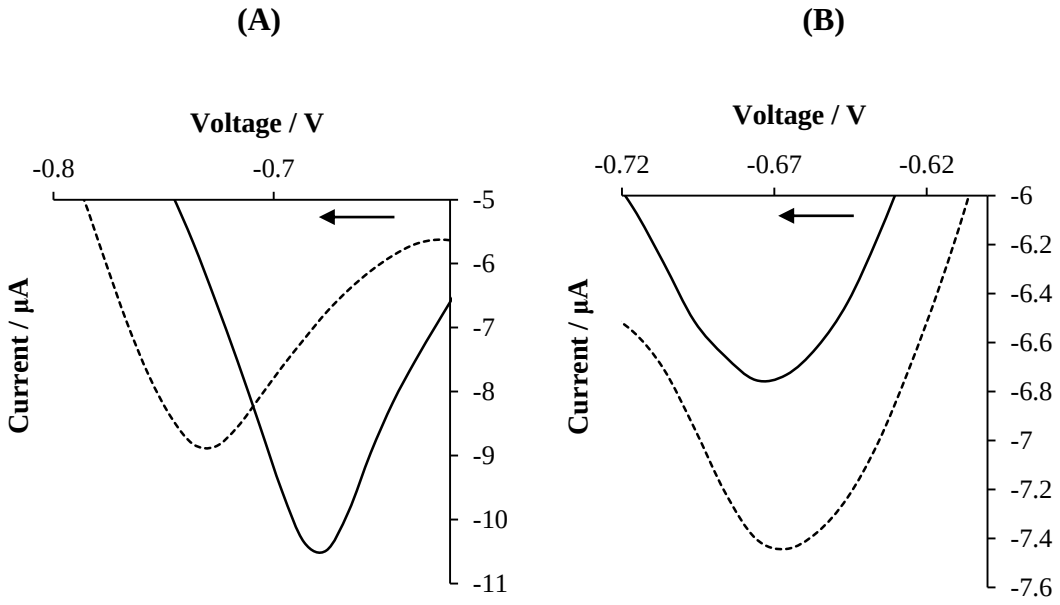

Figure 5-20: (A) DPV of porphyrin modified DNA probe (solid line) and 100 nM complementary target DNA (dashed line), (B) DPV of two porphyrin modified DNA probe (solid line) and 100 nM complementary target DNA (dashed line).

As can be seen in Figure 5-20 the current response recorded from the new free-base porphyrin modified DNA probes were higher than previously tested free-base strands. The peak observed was also shifted -200 mV compared with data shown in 5.1. This could correspond to the strands not being free base as expected. Silver acetate was used during the extra purification stage required to remove the trityl-sulphur bond. The free-base porphyrin could be potentially metallated (during this purification step) to form silver metallated porphyrin.

Two possible scenarios were speculated to underline the changes to the peak seen by the free base porphyrin modified DNA probes. The first being that the porphyrin had been metallated with silver from the silver nitrate used in the deprotection process. This idea is supported by the previous reports which show that silver can form a complex with porphyrin [107-109]. The second idea is that the silver could form a complex with DNA [110].

In order to show that the porphyrin had been metallated with silver from the silver nitrate a small amount (0.1 nmoles) of the original free base porphyrin probe was sent back to Southampton. Here silver nitrate solution was added to the sample and was heated. The water was then removed using reduced pressure. Due to the small sample of DNA purification using a Glen Pak column was not carried out to remove the excess silver nitrate. When the porphyrin probe is immobilised onto the gold surface any excess silver nitrate can be washed away. Unfortunately the large excess of silver nitrate could not be completely removed with the CV and DPV being inconclusive.

A higher number of moles of the original free base porphyrin DNA should be attempted to be metallated with silver in order to have enough material to be able to carry out a Glen Pak which would eliminate excess silver nitrate. Due to time restraints this could not be explored further.

5.5 Conclusions: Electrochemical Sensor with Chemically Tagged Probes

Synthesised porphyrin and anthraquinone chemically tagged probes were found to enhance the sensitivity of detection of bladder cancer biomarkers, while eliminating the need of an external redox solution. The LODs of these probes were 100 fM and 50 fM respectively.

The synthesised probes were compared to a commercially available methylene blue tag. In addition, two different hairpin designs were compared in 5.2. In the first design the recognition section was contained solely in the loop, while the second design contained part of the recognition sequence in the stem of the hairpin. The results were similar with the original design having a lower LOD (70 fM compared to 90 fM).

DNA mutations are an alternative biomarker that can be detected directly in human samples. The system was tested in Surine (urine negative control) which mimics the physiological conditions giving the same reduction in current response as seen previously in this section. It was shown that the system can distinguish between complementary and mismatched DNA with a single base difference (SNP detection).

The negative voltage required for the free base porphyrin, anthraquinone and methylene blue tagged probes desorbed the strands from the gold surface and therefore cobalt metallated porphyrin, which requires a positive voltage, was investigated as an alternative. In addition, strands containing two porphyrin monomers were tested. It was found that the addition of complementary target DNA increased the current response which was the reverse from probes containing a single porphyrin. It was noted that the current response when the target was added was similar for both the one and two porphyrin modified probes.

6. Advanced Sensor Probes

As discussed in Chapter 5, chemically tagged DNA probes can enhance the sensitivity of DNA detection as demonstrated using DNA methylation in bladder cancer biomarkers. This chapter will explore multiplex detection by the design of a microfluidic chamber to detect the three bladder cancer biomarkers (DAPK, E. Cad and RARβ) simultaneously using CV. An additional biomarker that can be detected in bladder cancer is miRNA. Detection of miRNA (with the electrochemical sensor described in section 4.4) and chemically tagged DNA probes will also be investigated. The electrochemical tags used in this section were free-base porphyrin, cobalt metallated porphyrin and methylene blue.

6.1 Multi-Sensor Electrode Array Chip [111]

Building on findings with the single sensor chip previously discussed in section 4.4, a chip with multiple sensors was developed as a potential multiplexing platform. This section was published [111]. The chip was designed and manufactured in A*STAR (Singapore) by Dr. Yu Chen. The gold sensor array chip was designed to have 20 individual sensors and was made based on the process previously reported [100, 112]. Briefly, a SiO_2 layer was deposited on a silicon layer, and Ti/Au was added via PVD. Lithography was used to define the electrodes before wet etching to form the electrodes. The surface was then passivated before the bonding pads were opened. The chips were used as received.

Figure 6-1 shows an image of the chip with a chamber made from double sided adhesive, isolating each individual sensor. The insert shows a magnified image of a sensor. The circular working electrode was 140 μm in diameter, whereas the reference and counter electrodes were horseshoe shaped and engulfed the working electrode.

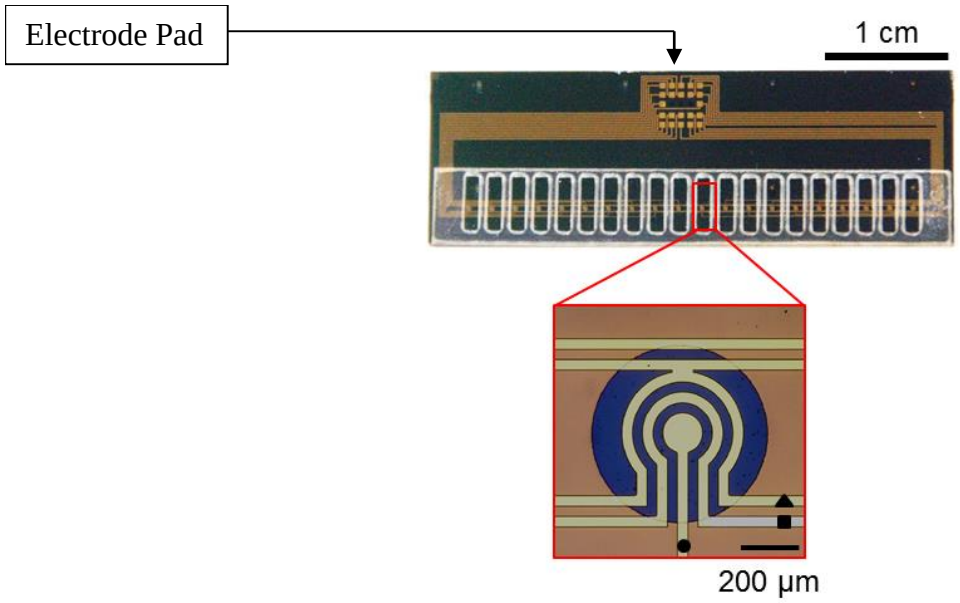

Figure 6-1: Image of the device used with an array of 20 sensors including a magnified image of an individual sensor where ● – working electrode, ■ – reference electrode and ▲ – counter electrode, the scale bar is 200 µm.

Initial work was carried out to determine the position of each sensor on the corresponding electrode pad. This was mapped using a microscope with a schematic diagram showing the positions shown in Figure 6-2.

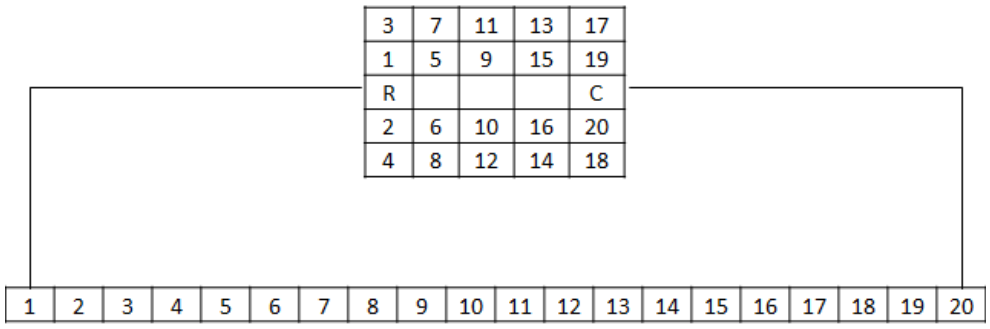

Figure 6-2: Schematic map showing which sensor corresponds to which position on the electrode pad, where R is the reference electrode and C is the counter electrode. Each electrode has diameter of 40 µm with 30 µm spacing between each.

6.1.1 Chip Characterisation and Microfluidic Design

A microfluidic chamber was designed to allow target DNA solution to flow over every sensor pad. In this way the same target solution can be added to the chip and each sensor can be easily compared, as it will record the contents of the target solution individually (see below). The microfluidic channel design consisted of three layers as shown in Figure 6-3. The bottom two layers (45 mm x 7 mm) were made from double sided adhesive while the top layer was a thin sheet of plastic. A laser cutting technique was used to cut the double sided adhesive and the plastic sheet.

The bottom layer was cut into an array of 20 individual sections, where each section was used to form a chamber around each sensor pad (can be seen in Figure 6-1). The physical separation of the chambers allow different probes to be immobilised on different sensors. The middle section of the double sided adhesive was used as a spacer to create a channel that allows fluid to flow through all the sensors. Circular holes (with a diameter of 1.4 mm) were made in the top plastic layer to fit tubing for the fluid inlet and outlet. With this fluidic channel design, every sensor would be exposed to the same environment allowing direct signal comparison between different electrodes without a need for normalisation.

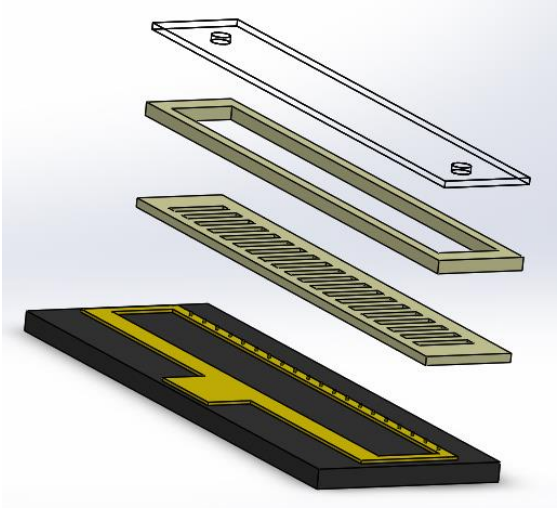

Figure 6-3: Schematic of the multi sensor device and the three layered microfluidic channel design. The bottom layer contains 20 individual sections which are positioned over each sensor. The middle layer is a spacer while the top layer contains two holes to allow solution to enter and leave the channel.

During the surface modification step, only the bottom most layer of the fluidic channel is attached to the chip while the adhesive spacer and the top plastic sheet were left un-assembled so that the sensors could be accessed individually. It was important that the solution from each sensor pad remain separated from other sensors because each sensor needs different surface modifications for multiplexing purpose. Thus, before the designed chamber was used on the chip, it was initially tested using a plastic backing. The optimum volume (5 µL) was determined in order to fill each section and to avoid solutions from each section mixing, as seen in Figure 6-4. Different colour dye solutions (water based) were used to ensure no mixing occurred. The DNA probes will be immobilised onto the chip at this stage before the rest of the chip is assembled.

Figure 6-4: Bottom layer of the microfluidic chamber (45 mm x 7 mm) on a plastic backing demonstrating the individual chambers using different dye containing water solutions (5 µL).

Following the surface modification, the other two parts (middle and top section) of the full chamber design was then tested. The middle layer made from double sided adhesive, was placed on top of the initial chamber. An experiment was carried out to ensure that a solution would flow through the entire chamber. Before the last layer of the fluidic channel was assembled a small drop of a blue water based dye was added to each section to allow the flow to be easily observed. The top layer of the channel was then assembled and water was injected into the system through the inlet hole. The flow was seen to enter each chamber and disturb all of the blue dye indicating that each sensor was reached by the flow solution. Figure 6-5 shows before and after pictures of this process indicating the blue dye was successfully washed out of the channel. Furthermore, this showed that the sample would push away any remaining solution on the sensor surface and make contact with every sensor.

Before

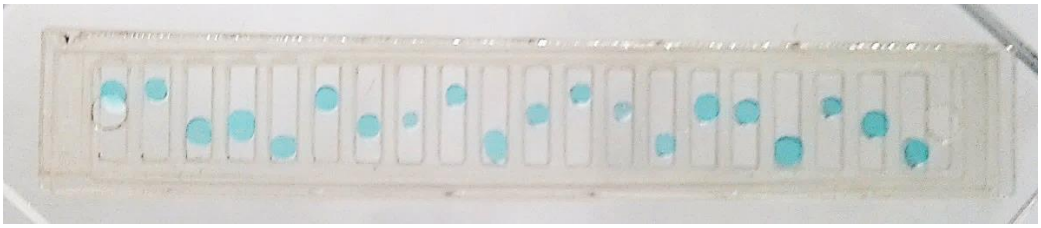

After

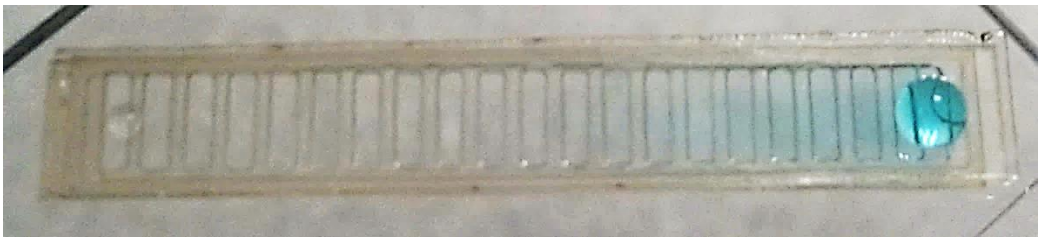

Figure 6-5: Three layers of the microfluidic chamber assembled on a plastic backing showing pictures from before and after a clear solution is injected. The top picture (before) shows blue dye inside the individual chambers, while the bottom picture (after) shows that all of the blue dye has been washed through the chamber. The inlet was on the left while the right side contains the outlet.

Initial testing was carried out to characterise the multi sensor chip in comparison with the single sensor chip as discussed in 4.4. The same redox probe as used previously (5 mM $[Fe(CN)_6]^{3-/4-}$, pH 7.4) was used for the blank sensor readings taken for both EIS and CV. Figure 6-6 compares both blank chips EIS readings. It can be seen that the multi sensor chip has a higher R_{ct} value (increase of x100) showing that there is a higher resistance than the single sensor chip. The design of the multi sensor chip mean that the gold pathways are thinner causing the higher resistance.

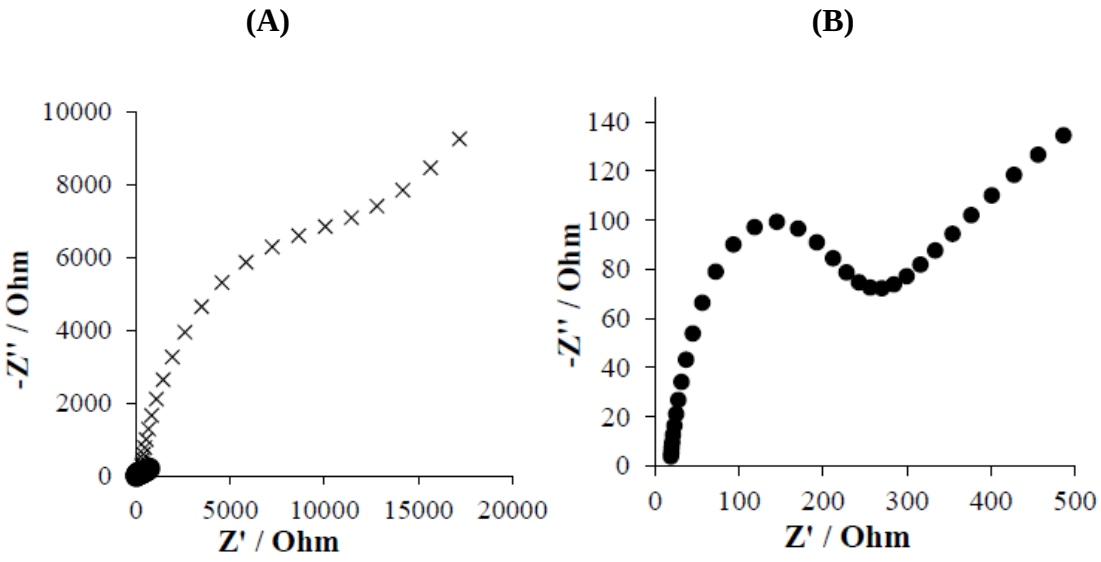

Figure 6-6: (A) EIS spectrum comparing the multi sensor (x) device with a single sensor (●) device. (B) EIS spectra of a blank single sensor device (expansion of A). 5 mM $[Fe(CN)_6]^{3-/4-}$, pH 7.4 was used as an external redox solution.

A blank CV of the multi sensor chip was also carried out (Figure 6-7) which showed that the current in the multi sensor chip gave a lower response than the single sensor chip. As previously determined, the resistance of the multi sensor chip was higher and therefore the current was lower due to the following equation:

$$V = I\ x\ R$$

Where V is voltage (V), I is current (A) and R is resistance (Ω).

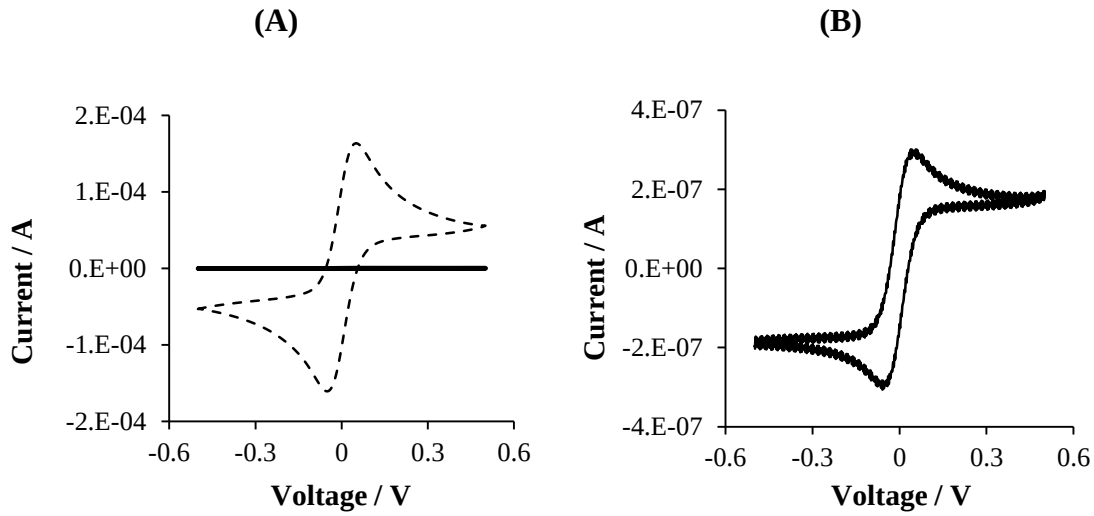

Figure 6-7: (A) CV comparing a blank single sensor device (dashed line) with a blank multi sensor device (solid line). (B) CV of blank multi sensor device (expansion of A). 5 mM $[Fe(CN)_6]^{3-/4-}$, pH 7.4 was used as an external redox solution.

The multi sensor chip is novel and therefore EIS was carried out on every blank sensor to ensure that each sensor is working consistently. Every sensor was found to be in the same region with 6 of these being shown in Figure 6-8. A dashed line is added to show how the Rct value can be calculated from the data. The position where the dashed line crosses the x-axis gives the Rct value.

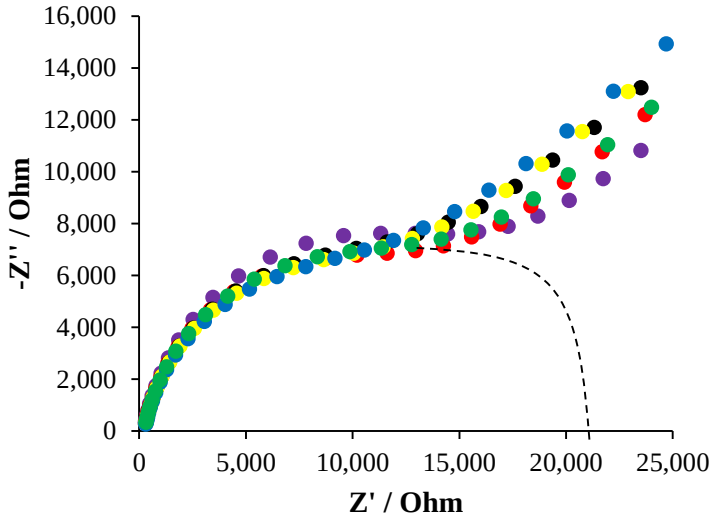

Figure 6-8: Nyquist plot from EIS of multiple blank sensors of the multi sensor chip. Data shows sensors from all areas of the electrode pad. Purple (1), red (17), green (4), black (11), yellow (14) and blue (20). Dashed line added to show Rct value.

In order to show that the chemically tagged probes were attaching to the surface of the multi sensor chip, EIS was carried out and can be seen in Figure 6-9. Porphyrin modified DNA probe (RARβ) was immobilised on the multi sensor device (5 μL, 1 M sodium chloride, 0.1 M sodium citrate) and 100 nM complementary DNA target was used. MCH (1 mM) was added after the DNA probe to limit non-specific binding.

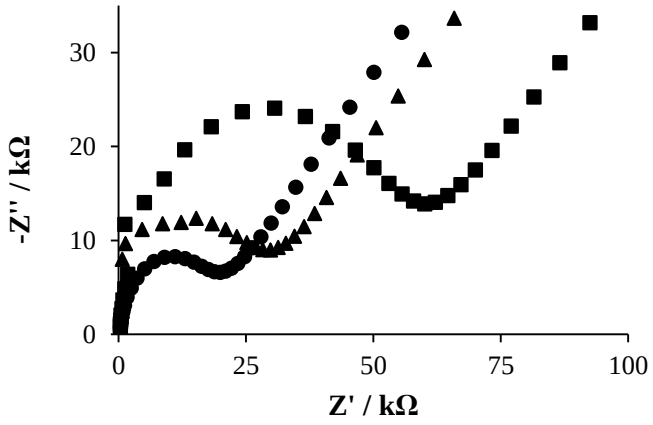

Figure 6-9: Nyquist plot from EIS confirming stable attachment of the porphyrin tagged RARβ probe on the surface of the multi sensor device with the specific response to the target DNA sequence. Where blank ●, probe ▲ and target ■. 1 M sodium chloride, 0.1 M sodium citrate was used as an external redox solution.

The stable attachment of the porphyrin modified RARβ probe onto the multi sensor device surface and its specific response to the target DNA sequence was confirmed by (EIS). Figure 6-9 shows the Nyquist plot of the measurements using 5 mM $[Fe(CN)_6]^{3-/4-}$ (pH 7.4) as the redox probe. The increase in the charge transfer value, shown by the diameter of the semi-circle (R_{ct}) where the values are 21,382 Ω (blank), 35,634 Ω (probe) and 68,721 Ω (target). This increase in R_{ct} value indicated that a change occurred on the surface corresponding to the immobilised probe and the selective formation of the duplex with the target DNA.

6.1.2 Multiplex Detection

Bladder cancer has three biomarkers, DAPK, E. Cad and RARβ, which require simultaneous detection. Therefore the multi sensor chip was used with the microfluidic chamber that separates the individual sensors for multiplex detection. Although the chamber separates the individual sensors the probes were immobilised in sections (DAPK – sensors 2-7, E.Cad – sensors 8-13 and RARβ – sensors 14-19) with the first and last (1 and 20) left blank. A solution was then added onto the chip which contained complementary DNA to one, two or all three probes to investigate whether the three targets could be distinguished from the same target solution.

The porphyrin modified DNA probes were immobilised individually on the electrodes, and the top sections of the microfluidic chamber were assembled. First, a solution containing 300 nM of the RARβ target was added to the microfluidic sensor array and incubated for 20 minutes before CV measurements were carried out; the measurements were repeated at least three times. As porphyrin modified DNA probes were used an external redox solution was not required. Representative results are shown in Figure 6-10 (A), (B) and (C). Figure 6-10 (A) and (B) showed the weak change in current response, of approximately 16 nA to a non-specific target using DAPK and E Cad probes with RARβ target, whereas Figure 6-10 (C) showed the much larger change in the current response, of approximately 50 nA, when the probe and target were matched as with RARβ in this case.

The large increase in current can be used as a clear positive signal that reports on the presence of the target DNA. In principle, the larger distance of the porphyrin to the electrode surface should give a signal decrease. However, we have seen previously [64] that porphyrins in a duplex environment are buried within the hydrophobic major groove of the dsDNA, thus are hardly accessible to the electrolyte and giving low current, even when attached close to the electrode surface. On the other hand, porphyrins on a single stranded DNA gave a much larger current in the same orientation. In this respect, the

hairpin is a “signal-off” state because it is in effect in a duplex environment, whereas when hybridised with the target the porphyrin is attached to a single strand overhang and is therefore in the “signal-on” state. This increase in the current response, after adding the target, was reproducible, thus validating the results.

In a second set of experiments, solutions containing a mixture of two or all three target strands were tested. As can be seen from the representative data in Figure 6-10 (D), (E) and (F) the multi sensor device clearly distinguishes from target DNA which contains complementary target DNA to one, two or all three porphyrin modified DNA probes. The experiments were reproducible and accurately determined which complementary DNA targets were present in the solution injected into the microfluidic chamber in a single run. The data indicated that the developed sensor is highly specific and can be easily applied for multiplexing of the three bladder cancer biomarkers.

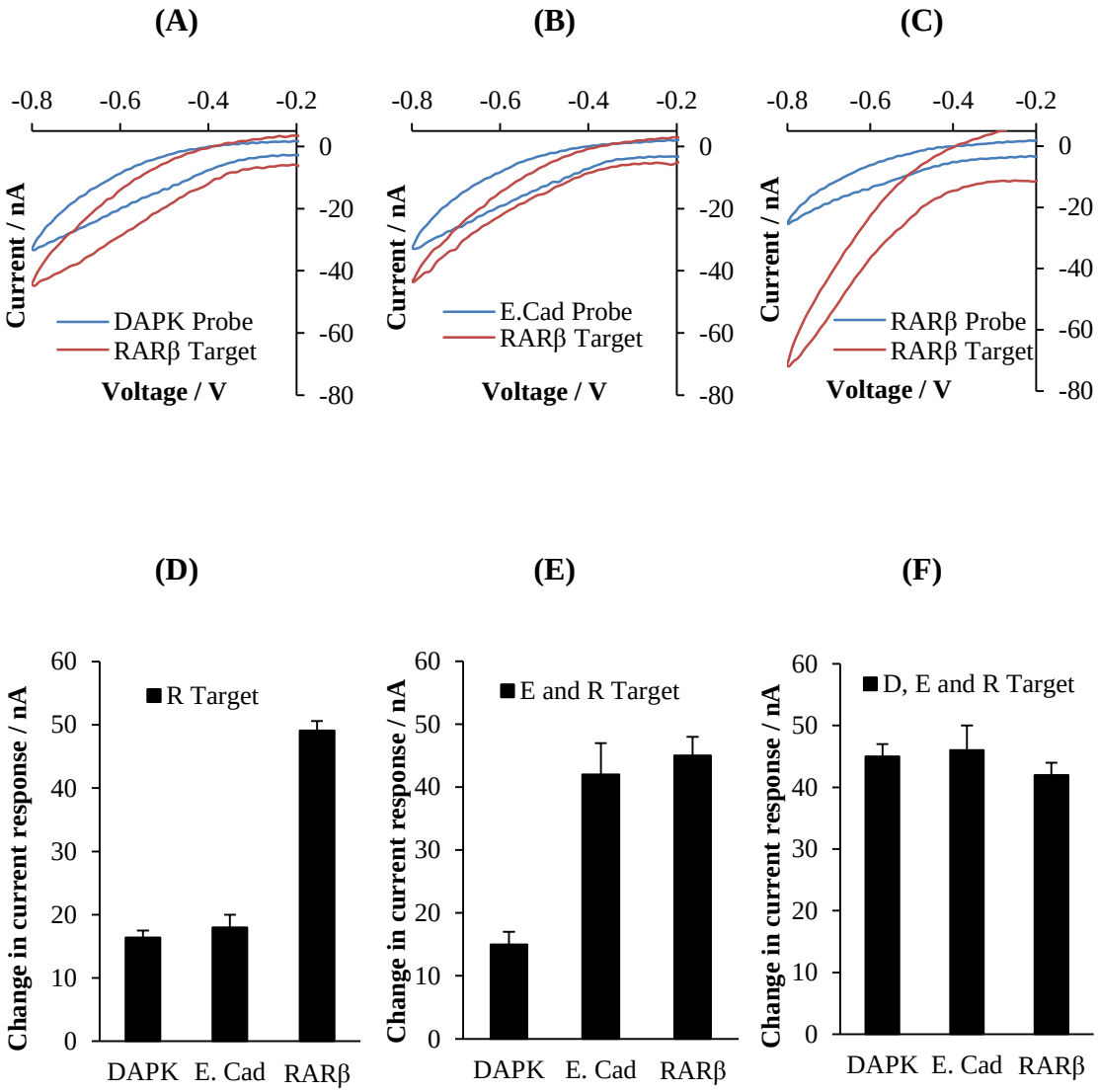

Figure 6-10: Electrochemical analysis of porphyrin modified DNA (with 5'-thiol modification) showing the selectivity of the different probes on the different sensors on the chip: difference in current response between mismatched (A), (B) and complementary (C) target DNA sequences; relative change in current using target solutions with one (D), two (E) and three (F) complementary target strands to the corresponding probes. Average of three measurements.

6.1.3 Limit of Detection

A dynamic range of concentrations were tested (200 fM – 100 nM) using the multi sensor chip to determine the detection limit of the system. Representative results, obtained using the E. Cad probe and target, are shown in Figure 6-11. The data show a linear increase in current difference upon increasing the target concentration over the entire range, which spans five orders of magnitude. The multi sensor chip can therefore be used to determine the concentration of the target DNA over a large dynamic concentration range with good accuracy. Additionally, a high concentration of 100 nM of mismatched DNA was tested, which is well above what is found in samples of bladder cancer patients. The response was within the error range of the matched target at 200 fM, and significantly smaller than for the matched DNA at 250 fM. This value can therefore be regarded as a lower limit for the detection of the target DNA. As reported in previous work using unlabelled DNA probes that were immobilised on a silicon sensor a detection limit in the region of 10 nM was achieved [18]. This was in comparison to the unlabelled DNA probes used in chapter 4, which showed a limit of 5 nM for SPR and the single sensor electrochemical chip. With great improvements in the current design of the sensor, a much higher sensitivity with a detection limit of 250 fM is demonstrated. The distinctively lower detection limit gives a clear advantage of using an electrochemical sensor compared to a silicon sensor that works using optical methods. The sensor therefore allows the detection of marker genes at the relevant biological level.

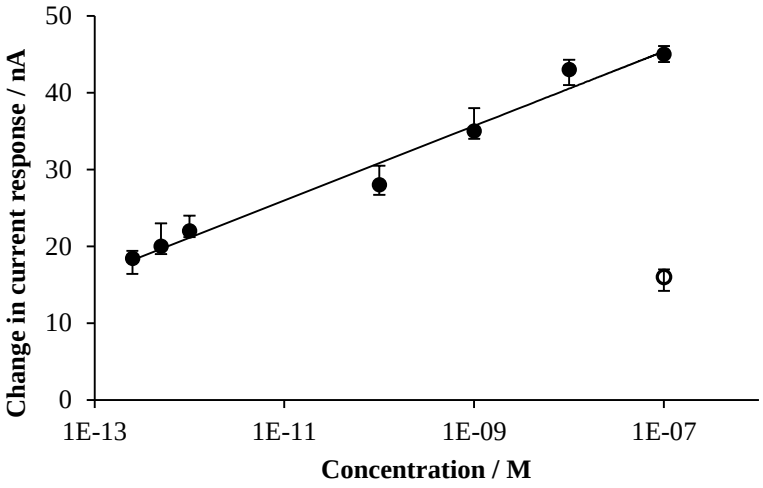

Figure 6-11: Representative data of relative change in current repsonse at variable target concentrations from 250 fM to 100 nM obtained from E. Cad complementary target and porphyrin modified probe. The full circles represent complementary DNA probe, whereas the open circle measurement corresponds to the response of a mismatched sequence, which determines the lower detection limit.

6.2 Electrochemically tagged DNA probes for miRNA detection

Chemically tagged DNA probes also have the potential to be used to detect microRNA (miRNA). As potential biomarkers for cancer detection it is important to detect miRNA with a high sensitivity [6, 113, 114] without over complicating the system. The previously used single sensor device was used to show the capability of the system (see Chapter 5). One sequence of miRNA, miR-21, was used which is known to be detected in bladder cancer patients [115] as a representative miRNA for a proof of concept system.

The chemically tagged DNA probes used for miRNA detection were either synthesised with porphyrin tags (free-base and cobalt metallated) or purchased with commercially available methylene blue. The porphyrin modified DNA probes were synthesised by Dr. Iwona Mames and Christina Xyrafaki in Southampton. In addition to using a hairpin design, as previously used, a linear probe was designed with the electrochemical tag positioned close to the surface as discussed in section 1.7. This should then be similar to previous work in Chapter 5 where the signal decreased upon addition of target, due to the porphyrin modified sequence transitioning from ssDNA to dsDNA [77]. In this way a direct comparison of the two systems (hairpin and linear) can be made. In addition the RNA:DNA duplex that is formed has the A-form compared with the previous DNA:DNA duplex that has the B-form. A-form has bigger major groves, allowing the porphyrin to bind in the major grove. This could reduce the electrochemical current observed and hence a reduction in current response upon hybridisation with the RNA target. The sequences of the synthesised DNA probes and complementary RNA target are shown in Table 6-1. The 5'-thiol modification was the same as discussed in section 5.4 and required a post synthetic deprotection step.

For the sensor to be sensitive enough and to be suitable for clinical use, the limit of detection is require to be less than 1 nM [115].

	Sequence 5'-3'
MiR-21 Linear	YTAX**CAACATCAGTCTGATAAGCTA**
MiR-21 Hairpin	YTATTAGC**TCAACATCAGTCTGATAAGCTA**AXA
RNA target	UAGCUUAUCAGACUGAUGUUGA

Table 6-1: Sequences used for DNA probes with RNA target where X is methylene blue, cobalt porphyrin or free base porphyrin and Y is a 5'-C6 thiol linker. The bases underlined form the stem of the hairpin while the bases in bold show the recognition part of the sequence.

In order to show that the linear probe character behaves in a similar way to the hairpin probes, the relationship between the peak current and the scan rate was tested. A linear relationship was observed between the peak current and scan rate indicating that the process is dependent on the surface chemistry rather than diffusion. This is shown using the cobalt porphyrin probe in Figure 6-12. Therefore the linear and hairpin probes, previously developed in this study, are both surface dependant.

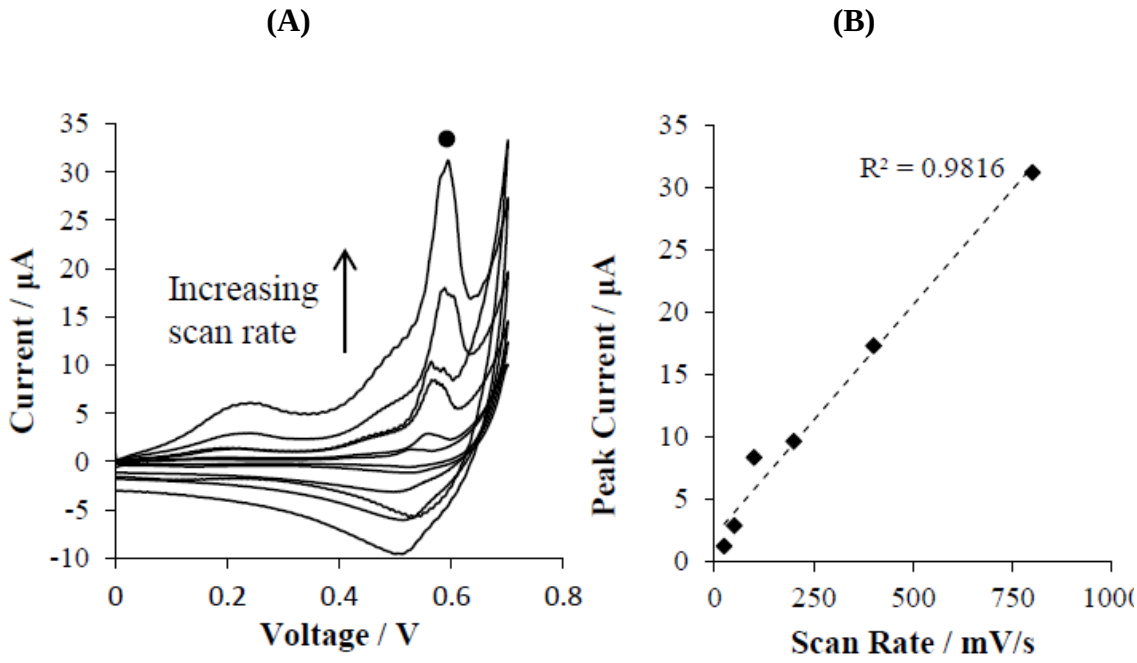

Figure 6-12: (A) CV of linear cobalt metallated porphyrin DNA probe with increasing scan rates. (B) Linear relationship between peak current and scan rate for linear cobalt metallated porphyrin DNA probe, monitoring peak labelled with ● from (A).

6.2.1 Detection of miRNA in Buffer

All three tags, cobalt and free base porphyrin and methylene blue, were tested using the RNA target strand. As previously discussed, the porphyrin modified probes were synthesised while the methylene blue modified probe was purchased. To ensure that the target would not degrade RNase free water was used for the buffer and probe solutions. For these experiments the same buffer as previously described (1 M sodium chloride, 0.1 M sodium citrate) was used.

Methylene blue tagged DNA probe with the hairpin and linear designs were tested and the results can be seen in Figure 6-13. Both of the probes showed a decrease in the current response when the complementary target RNA was added. Representative data for both designs are shown in Figure 6-13(A) and Figure 6-13(B), for hairpin and linear designs respectively. A comparison of both designs over a dynamic range of concentration is shown in Figure 6-13(C) where it can be seen that the hairpin design has a larger change in peak current over the linear design.

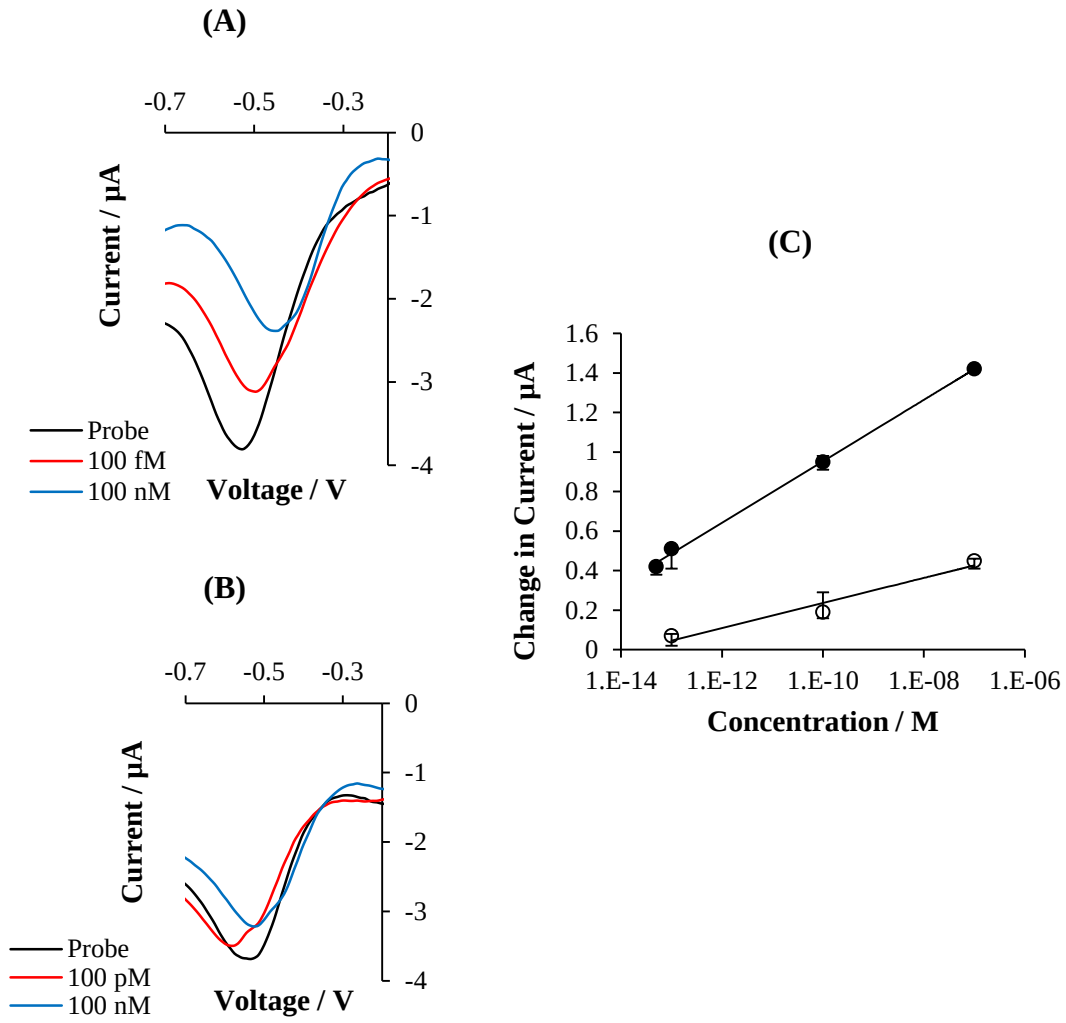

Figure 6-13: Methylene blue modified DNA probe (A) Representative DPV data of the hairpin probe. (B) Representative DPV of the linear probe. (C) Comparison of the hairpin probe (●) against the linear probe (○) at varying concentrations of target RNA.

In addition to the methylene blue tag, porphyrin modified DNA probes were also used with both cobalt metallated and free base porphyrin. Representative data from these tags are shown in Figure 6-14 and Figure 6-15. It can be seen that both of these tags follow the same pattern as observed for the methylene blue tag. The hairpin design consistently gave a larger difference in peak current upon addition of the target. Both designs caused a decrease in the peak current with the more concentrated target causing a larger observable change in the peak current.

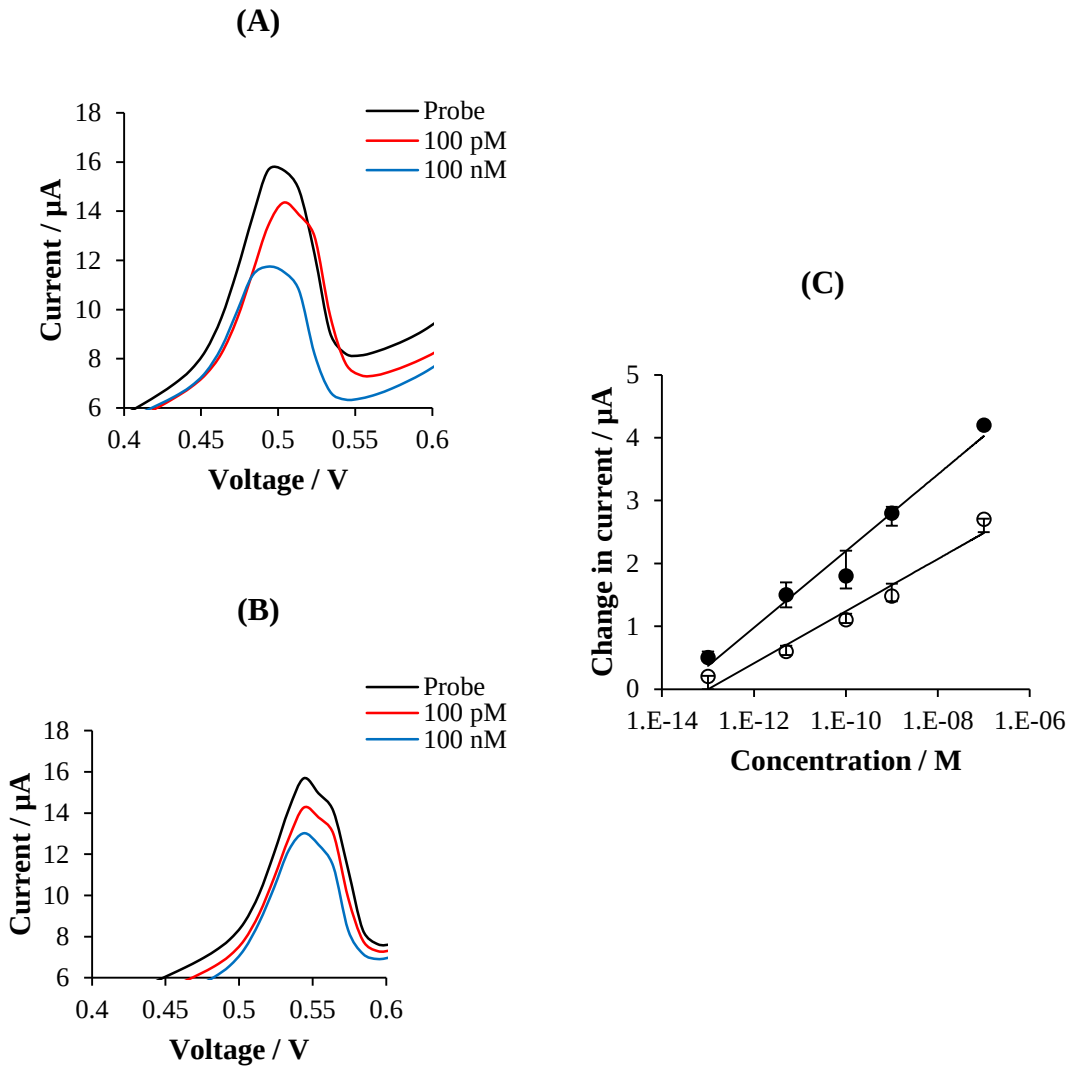

Figure 6-14: Cobalt metallated porphyrin tagged DNA probe, (A) Representative DPV data of the hairpin probe. (B) Representative DPV data of the linear probe. (C) Comparison of hairpin (●) and linear (○) probes using different target RNA concentrations.

Representative data for cobalt porphyrin modified DNA probes is shown in Figure 6-14(A) and Figure 6-14(B) for the hairpin and linear probes respectively. The peak for the cobalt porphyrin in the linear design appeared at 0.55 V compared to the hairpin design in which the peak appeared at 0.5 V. Similar to the methylene blue tagged DNA the hairpin design of the cobalt porphyrin gave a larger change in peak current (compared with the linear probe design) as seen in Figure 6-14(C).

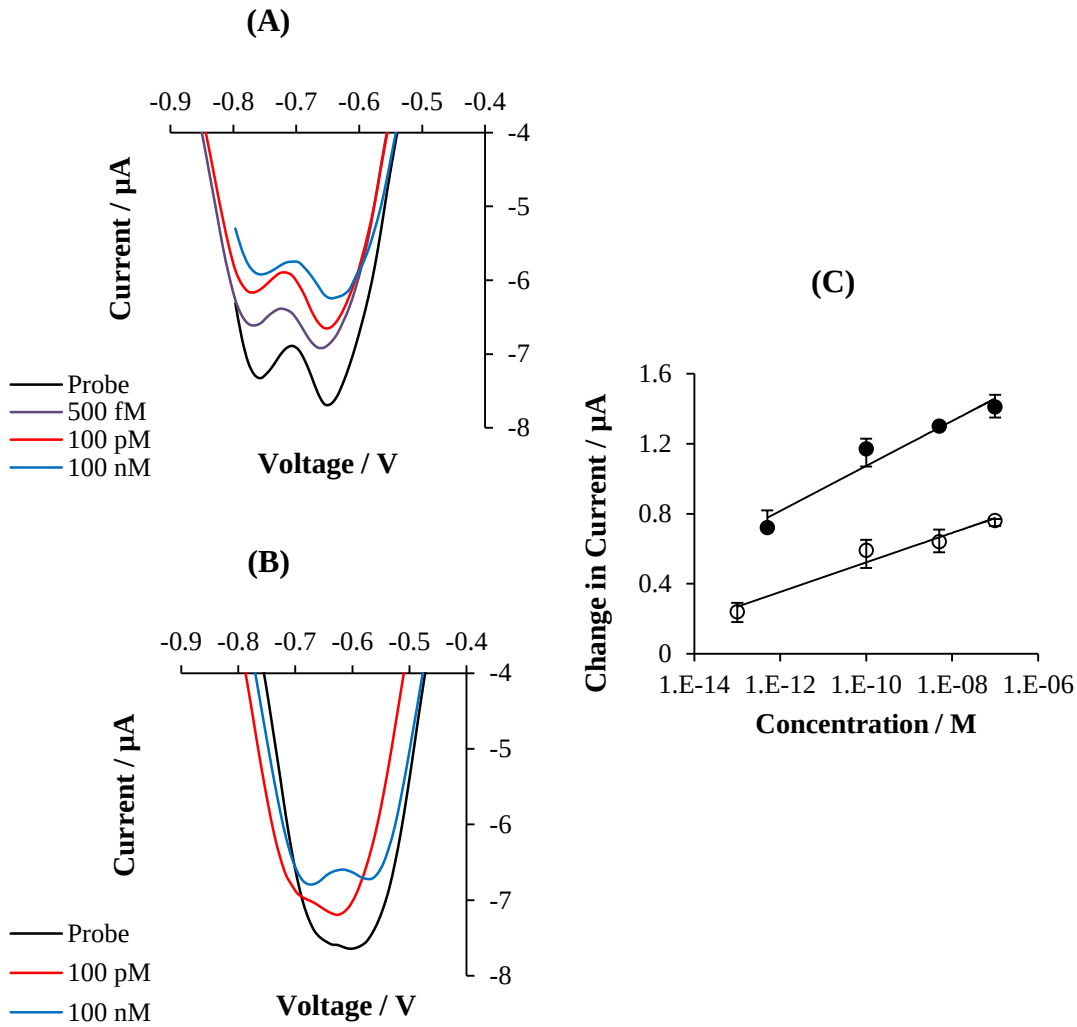

Figure 6-15: Free-base porphyrin tagged DNA probe, (A) Representative DPV data of the hairpin probe. (B) Representative DPV data of the linear probe. (C) Comparison of hairpin (●) and linear (○) probes using different concentrations of complementary target RNA.

Finally, free base porphyrin modified DNA probes were investigated for detecting miRNA. Representative DPV data for the hairpin and linear probes are shown in Figure 6-15(A) and Figure 6-15(B) respectively. The two peaks that appeared along with the previous shift in peak in 'free base' porphyrin could be due to silver being present which was discussed in 5.4.2. The value of the peak current for the free base porphyrin modified probe can be seen as -7.6 µA compared to the methylene blue value of -3.8 µA. The

addition of varying concentrations of target RNA gave the same trend as the previous two tags tested and can be seen in Figure 6-15(C).

In order to compare the different chemical tags of both probe designs (hairpin and linear), the two designs are plotted separately in Figure 6-16. In both designs it was observed that at a higher concentration of target miRNA the cobalt porphyrin gave the greatest change in peak current. However, the free base porphyrin and methylene blue tags have a lower limit at a lower concentration of target RNA.

The change in peak current response for the DNA:RNA hybrid is noted to be higher than for the DNA:DNA duplex for the hairpin design. The methylene blue tagged DNA probe had the change of peak current increased from 510 nA to 1.4 µA. Similarly, the free base porphyrin tagged DNA probe peak current increased from 810 nA to 1.5 µA. This could be partly due to the increased stability of DNA:RNA hybrids [116-118]. The probe concentration remained the same for both experiments (1 µM).

(A)

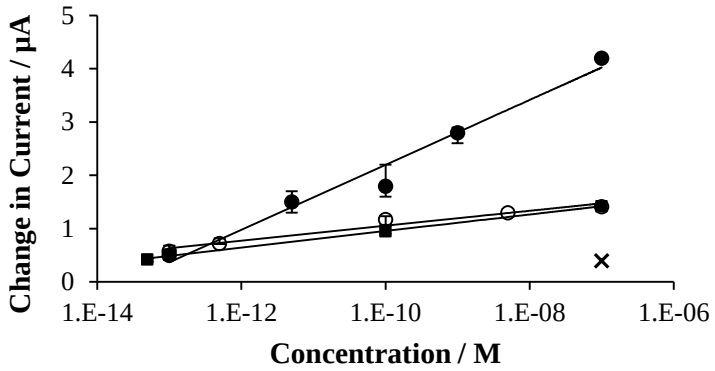

(B)

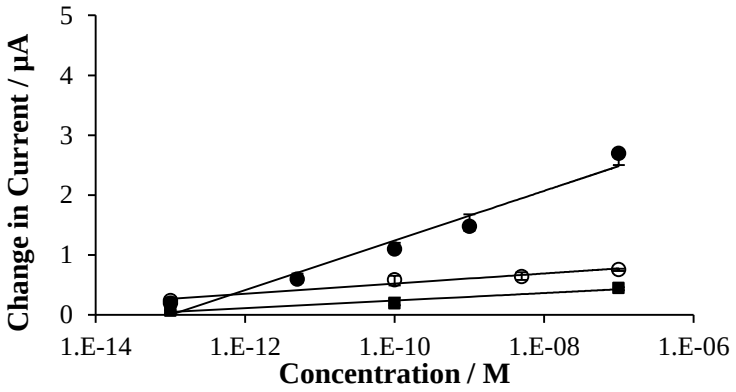

Figure 6-16: Comparison of 3 different modified DNA probes using different concentrations of target RNA with (A) hairpin and (B) linear designs. Where (●) is cobalt porphyrin, (○) is free base porphyrin and (■) is methylene blue tagged DNA probes.

The limit of detection for the different tags was calculated by using mismatched target RNA. As before, the concentration of target RNA which is just above the range of peak current change of the mismatched DNA is the LOD. The LODs are shown in Table 6-2 for the hairpin probe design and Table 6-3 for the linear probe design. The LOD for the DNA:RNA hybrids are very similar to the LOD for DNA:DNA duplexes being between 20 to 30 fM lower that the DNA:DNA duplexes.

Chemical Tag	**Current change for 100 nM complementary RNA target**	**Limit of detection**
Methylene Blue	1.42 μM	50 fM
Free-base porphyrin	1.41 μM	70 fM
Cobalt metallated porphyrin	4.20 μM	100 fM

Table 6-2: Comparison of the change in current response for 100 nM RNA target and the limit of detection for the hairpin probes with each chemical tag.

It was concluded that the linear design of DNA probe were not as sensitive as the hairpin design with the LODs shown in Table 6-3.

Chemical Tag	**Current change for 100 nM complementary RNA target**	**Limit of detection**
Methylene Blue	0.45 μM	1 pM
Free-base porphyrin	0.76 μM	500 fM
Cobalt metallated porphyrin	2.70 μM	700 fM

Table 6-3: Comparison of the change in current response for 100 nM RNA target and the limit of detection for the linear probes with each chemical tag.

This limit of detection of previous work detecting miRNA has shown to be sub femtomolar range [119, 120]. However, the methods required have long incubation steps involving temperature control and complex equipment, with mechanisms for additional signal enhancement (nano-particles). Such complicated approached are unsuitable for POC devices and multiplex detection. One method reported has shown multiplexing ability, however, it only has a limit of detection 1 nM [115]. Therefore this simple system is beneficial as there is multiplexing potential with a LOD in the femtomolar range.

6.2.2 Detection of miRNA in Surine (Urine Negative Control)

To demonstrate that the sensor system is feasible in urine, where the bladder cancer biomarkers are present, Surine (urine negative control) was used as the test buffer. As previously mentioned in 5.3, Surine was obtained from Sigma Aldrich.

Figure 6-17 shows the results for the detection of miRNA for three different chemical tags using the linear DNA probe (Figure 1-30) over a range of concentrations (100 fM to 100 nM) in both buffer (1 M NaCl, 0.1 M sodium citrate) and Surine. It can be seen from Figure 6-17(B) that the same trend is observed for miRNA in Surine. The decrease in signal upon hybridisation with the target indicated that the system is working in Surine. As this is the medium that is required from bladder cancer patients it shows that this system is a feasible method for miRNA detection. It is noted that the decrease in peak current is smaller when Surine is used compared with buffer (sodium chloride/sodium citrate). Nevertheless, the detectable peak current change in Surine suggests that the system has a potential for miRNA detection in a clinical sample.

While the hairpin design showed the same trend, by the peak current response decreasing upon hybridisation with the complementary RNA target, there was not enough material to fully characterise. Further work could involve the synthesis of more of these probes to fully characterise the hairpin design in Surine.

(A)

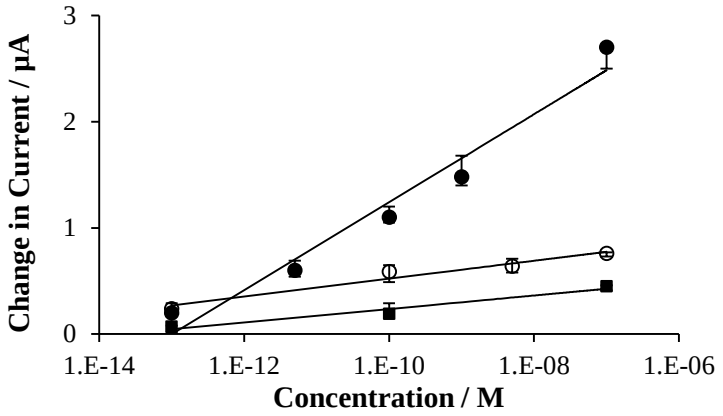

(B)

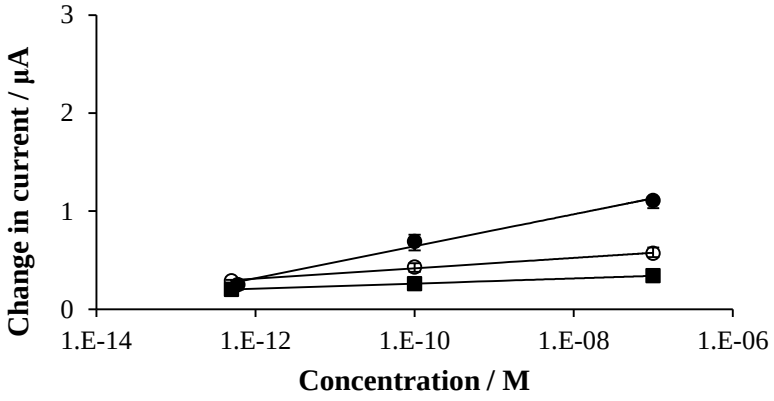

Figure 6-17: Comparison of three chemically tagged DNA probes of linear design in buffer (A) and Surine (B). Where (●) is cobalt porphyrin, (○) is free base porphyrin and (■) is methylene blue tagged DNA probes with complementary RNA target.

6.3 Conclusions: Advanced Sensor Probes

A porphyrin tagged hairpin-DNA probe can be used to create a selective and sensitive multiplex sensor. The attachment of the highly versatile porphyrin tag removes the need of a redox probe solution, allowing a sample to be directly used in analysis. Three different DNA markers, which are selective for bladder cancer, can simultaneously be detected on a single microchip containing up to 20 sensors. This design allows for measuring the target DNA in multiple repeats, thus eliminating false readouts. Furthermore, the low detection limit of 250 fM is in the range of the clinically relevant concentrations where the cancer marker genes generally can be found in a patient's urine sample. Methylation specific PCR will still be required to differentiate between methylated and unmethylated gene markers. However, research has already been done to allow this step to be carried out on-chip [121, 122]. Therefore, combining both selective detection and methylation specific PCR should be the next focus of research. Our microchip design is a further significant step towards a point-of-care device for cancer detection, which otherwise requires costly and invasive methods, and will help to reduce the increasing burden on health care.

Detection of miRNA is also achievable using porphyrin and methylene blue tagged DNA probes. A linear probe design was run alongside the previous hairpin design. Three different chemical tags were used as a comparison (CoP, FB-P and MB). Firstly the experiments were run in buffer to ensure that the probes would successfully detect the miRNA target. It was noted that the change in peak current with a high concentration of target RNA was larger than for the previous experiments run with DNA. It was also observed that the LOD was 20-30 fM lower for the hairpin design while the linear design was not as sensitive. While there are reported devices with sub femtomolar limits they are not suitable for POC and do not have multiplexing capability.

To demonstrate the feasibility of the detection of miRNA directly in bodily fluids the experiments were run in Surine (urine negative control). These showed that the same

trend was observed for both buffer and Surine. The decreased current response seen upon hybridisation with the target was reduced when measured in Surine, however the same trend was observed. Only the linear probes were tested in Surine due to a lack of material. The hairpin probes should also be tested to complete the comparison.

In addition, it was thought that silver porphyrin may have been present. DNA probes which were synthesised by Dr. Iwona Mames and Christina Xyrafaki required a post synthetic deprotection due to the trityl group. This was achieved by the addition of silver nitrate, a source of silver. A peak current peak in 5.4.2 for porphyrin modified DNA was -200 mV in comparison with free base porphyrin. In addition an extra peak was observed in 6.2.1. However, more work is needed in order to confirm this as only a small sample of porphyrin modified DNA could be sent back to Southampton to introduce silver nitrate.

7. Concluding Remarks

Detection of DNA methylation, a cancer biomarker, is an important step in cancer diagnosis. To show feasibility detection of methylated DAPK, E. Cad and RARβ were chosen (methylated genes in bladder cancer patients). This was carried out by designing probes and target to detect the product of MS-PCR. A DNA probe was designed to have a hairpin design in which a redox active tag could be in close proximity to the surface of a device once immobilised, but move away from the surface upon hybridisation with the complementary methylated DNA target. This causes a reduction in the current observed.

During this work chemically tagged DNA probes were synthesised incorporating anthraquinone and porphyrin monomers into a hairpin design. Initial work was done to compare methods for DNA detection by using SPR, nanoplasmonic and electrochemical devices. A gold chip for electrochemical measurements was then further used with the chemically tagged DNA probes. The LOD for unlabelled DNA probes for the different sensors were found to be between 5 nM and 10 nM.

The porphyrin and anthraquinone tagged DNA were compared with the commercially available methylene blue (LOD for anthraquinone was 50 fM, porphyrin was 100 fM and methylene blue was 70 fM). The required negative voltage caused the DNA probes to desorb from the gold surface. Therefore, cobalt metallated porphyrin probes were tested which require a positive voltage. Future work should further analyse the cobalt porphyrin probes to determine the LOD. As well as DNA methylation, the system can also be used to detect DNA mutations. This was shown by using the same probes with Surine (urine negative control) and target DNA with one and two mutations.

In addition to the cobalt porphyrin probes, multiple porphyrin probes were tested. Interestingly, these probes showed the reverse behaviour to the single porphyrin probes.

Further testing into the effect of the number of porphyrin tags on the DNA probe should be conducted to have further understanding of this.

A device containing 20 sensors was obtained to conduct multiplexing experiments. A microfluidic chamber was developed so that all three bladder cancer biomarkers could be tested on the same device. This was successfully carried out with the LOD determined to be 250 fM.

Another biomarker for bladder cancer is miRNA. The sensitivity required to detect direct from urine means that often multiple procedures are carried out to isolate and amplify the miRNA. The system used in this project was used to detect miRNA in Surine. In addition to the previous hairpin DNA, a linear DNA probe was designed and tested. Although the current response was reduced in spiked Surine the miRNA was still detected. Therefore future work should work with the detection of miRNA in human samples.

Silver nitrate was introduced during the deprotection of a trityl protecting group which could form a silver porphyrin complex. An additional peak in DPV approximately -200 mV from the original free base porphyrin peak was observed. Further work to confirm the presence of the silver porphyrin is required.

This project developed a single sensor and multi sensor device to electrochemically detect DNA hybridisation. Developing a microfluidic chamber for multiplex sensing furthered work into the rapid diagnosis of bladder cancer, eliminating the need for an invasive cystoscopy. The approach also has the potential to detect miRNA in spiked Surine. The hairpin design with incorporated chemical tags could be applied to diagnose many different diseases in which the DNA biomarkers have been identified.

8. General Experimental Details

8.1 Suppliers

Chemicals were supplied by Fischer Scientific, Sigma Aldrich, Glen Research, Cambio and Link Technologies. All chemicals were used as instructed by the supplier. Glen-Pak columns (method used as described from manufacturer) were supplied from Glen Research. Spin filters were supplied by Costar. De-ionised water was filtered by a Milli-Q Gradient A10 which was supplied by Millipore. Solvents used for DNA synthesis were obtained from Tides Service Technology (GER). Oligonucleotides were purchased from Integrated DNA Technologies and IBA Life Sciences where mentioned.

8.2 Column Chromatography and TLC

Column chromatography was conducted using silica gel (40 – 60 µm particle size), silica gel type H (10 – 40 µm particle size) supplied from Sigma Aldrich and basic aluminium oxide (50 – 200 µm, Brockmann activity I) supplied from Acros Organics.

TLC plates were supplied my Merck. TLC silica gel 60 F_{254} on aluminium backed sheets. Compounds were visualised on the TLC plates using UV light of wavelengths 254 nm and 365 nm. Anisaldehyde stain was also used.

8.3 NMR Spectroscopy

NMR was conducted at room temperature using a Bruker Advance DPX-300 spectrometer with ^{1}H frequency of 300.130 MHz. Wilmad-LabGlass tubes were used with a diameter of 5 mm. Coupling constants (*J*) are given in Hertz (Hz).

8.4 Mass Spectrometry

Low resolution electrospray mass spectrometry was conducted using a Walters ZMD. HPLC-MS was carried out using a Bruker micrOTOF mass spectrometer with a Dionex UltiMate 300 HPLC system.

8.5 UV-Visible Spectroscopy

Scans were carried out at room temperature using a Varian Cary 300 Bio spectrometer with quartz cells of 1 cm path length (supplied by Hellma and Starna).

8.6 Fluorescence Spectroscopy

Scans were carried out at room temperature using a Varian Cary Eclipse spectrometer using quartz cells supplied by Hellma and Starna. Excitation wavelength for fluorescence spectroscopy were the λ_{max} values as found by UV-Vis.

8.7 DNA Synthesis

DNA synthesis was carried out on an Applied Biosystems Expedite machine using 500 Å pore CPG beads on a 1 µmol scale. Standard coupling times were used for the bases. Extended coupling times up to 7 mintues was used for the modified monomers. Deblocking steps used 3% TCA in DCM. Activation used 'BTT Activator' 0.3 M Benzylthio-1 *H*-tetrazole in acetonitrile. Capping steps used acetic anhydride in THF (Cap A) and 10% methylimidazole in THF / pyridine (8:1) (Cap B). Oxidation used 0.02 M iodine in THF / pyridine / water. Washing steps used acetonitrile.

Cleavage of the oligonucleotides was achieved by passing through concentrated ammonium hydroxide (1 mL) at room temperature for 1 hour. Deprotection of the bases was carried out by either heating to 55 °C for 4 hours or to 40 °C for 24 hours. Both methods were carried out with agitation in an Eppendorf Thermomixer Compact.

8.8 High Performance Liquid Chromatography of Oligonucleotides

HPLC was carried out using a Varian 920-LC and Spectra Physics (Thermo Fisher) instrument with Waters XBridge OST C18 2.5 µm columns (4.8 X 50 mm and 10 X 50 mm). Eluent, gradients and column temperature varied and so are mentioned in the relevant sections. Flow rates were set to 1 mL min^{-1}.

8.9 Drying DNA Samples

DNA samples were dried using an Eppendorf Concentrator 5301 at room temperature with the setting used as appropriate to the solvent used.

8.10 SPR

SPR was carried out using a Biacore® X100. Blank gold chips were purchased from Biacore® and used as received. DAPK, E.Cad or RARβ probes (1 μM), were immobilised onto the chip in buffer (PBS or 1 M NaCl, 0.1 M sodium citrate) over multiple (x4) manual runs of 1080 seconds. 1 mM MCH was added before the target DNA to reduce nonspecific binding. Target DNA was added using the immobilisation buffer (PBS or 1M NaCl, 0.1 M sodium citrate) to the chip on a manual run of 1080 seconds.

8.11 Nanoplasmonic Sensor

Light source used for DNA detection was StockerYale Model 21DC. For fluorescence experiments X-Cite Series 120 was used.

8.12 Electrochemical Tests

All electrochemical tests (EIS, CV, DPV) were carried out using a three electrode system with gold being used as the pseudo reference and counter electrode. The instrument was Reference 600™ (Gamry Instrument, USA) with a Signatone H100 series probe station. CV was carried out with a scan rate of 50 mV/s unless otherwise stated. While EIS measurements were taken using a frequency range of 0.5 Hz – 500 kHz with an amplitude of 25 mV. A redox probe solution (5 mM $[Fe(CN)_6]^{3-/4-}$, pH 7.4) was used for EIS measurements. Chambers for the chips were cut using a universal laser engraving/cutting machine (Scottsdale, Arizona). During the cleaning process the chips were cleaned using a sonicator (Branson 1510) and surface of the chip prepared using UV/Ozone ProCleaner™.

9. Experimental

9.1 Synthesis of 5'-DMT-5-Iodo-deoxyuridine (1)

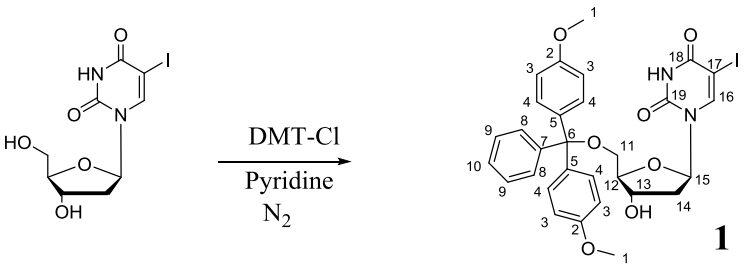

5-Iodo-deoxyuridine (2.5 g, 7.06 mmol, 1.0 equiv) was dried by coevaporation with pyridine (3 x 5 mL), dissolved in anhydrous pyridine (20 mL) and purged with nitrogen (20 minutes). 4, 4' dimethoxytrityl chloride (DMT-Cl, 2.6 g, 7.77 mmol, 1.1 equiv) was added portion wise over 4 hours. The solution turned orange after a portion was added and returned to the original yellow after around 20 minutes. Once all the DMT-Cl was added the reaction was left for a further 30 minutes. MeOH : water (1:1, v:v, 5 mL) was then added to quench the reaction. After a further 15 minutes the solution, now pale yellow, and the solvent was removed *in vacuo* which left a yellow oil.

The oil was dissolved in DCM (50 mL) and then washed with water (2 x 50 mL). The aqueous phase was then extracted with DCM (30 mL) and the organic phases combined. The organic phases were then washed with sat. KCl (3 x 60 mL) before drying (Na_2SO_4) and concentrated *in vacuo*. The crude product was then coevaporated with toluene (3 x 20 mL) and neutralised chloroform (3 x 20 mL) to remove any remaining pyridine. The crude product was purified by column chromatography (silica neutralised with 1 mL TEA, eluent – EA:hexane 6:4 to 6:1). The fractions which contained the product were coevaporated with toluene (3 x 20 mL) and neutralised chloroform (3 x 20 mL) to remove any remaining TEA. The product was obtained as a white solid with a yield of 3.93 g (5.99 mmol, 85%).

^{1}H NMR (300 MHz, CHLOROFORM-*d*) δ ppm : 2.31 (dd, *J* = 14.6, 7.7 Hz, 1 H, **H14**) 2.58 (dd, *J* = 12.5, 4.7 Hz, 1 H, **H14**) 3.35 - 3.48 (m, 2 H, **H11**) 3.79 (s, 6 H, **H1**) 4.18 (d, *J* = 1.9 Hz, 1 H, **H12**) 4.59 (d, *J* = 2.2 Hz, 1 H, **H13**) 6.36 (t, *J* = 6.7 Hz, 1 H, **H15**) 6.88 (d, *J* = 8.9 Hz, 4 H, **H3**) 7.22 (t, *J* = 6.9 Hz, 1 H, **H10**) 7.29 (dd, *J* = 13.3, 6.0 Hz, 2 H, **H9**) 7.34 - 7.40 (m, 4 H, **H4**) 7.46 (d, *J* = 7.5 Hz, 2 H, **H8**) 8.18 (s, 1 H, **H16**).

^{13}C NMR (75 MHz, CHLOROFORM-*d*) δ ppm : 41.4 (CH_2, **14**), 55.3 (CH_3, **1**), 63.7 (CH_2, **11**), 68.9 (C, **17**), 72.5 (CH, **13**), 85.8 (CH, **15**), 86.7 (CH, **12**), 87.0 (C, **6**), 113.4 (CH, **3**), 127.1 (CH, **9**), 128.1 (CH, **10**), 129.1 (CH, **8**), 130.1 (CH, **4**), 135.6 (C, **5**), 144.4 (C, **7**), 144.5 (CH, **16**), 150.4 (C, **19**), 158.7 (C, **2**), 160.5 (C, **18**).

ESI+ ($C_{30}H_{29}IN_2O_7$): Monoisotopic mass = 656.10, observed m/z = 679.0 $[M + Na]^+$

UV-Vis (MeCN, 49.5 µM): λ_{max} (log ε) 233 (4.34), 276 (3.98)

Emission (MeCN, 49.5 µM): No fluorescence observed

R_f (10% MeOH in DCM): 0.57

9.2 Synthesis of 5'DMT-5-propargylamino-deoxyuridine (2)

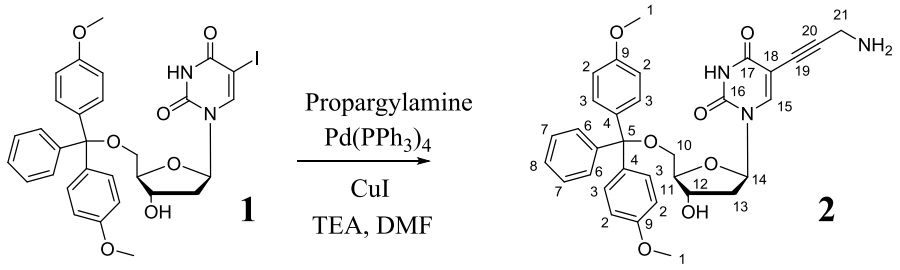

In oven dried glassware, 5'DMT-5-Iodo-deoxyuridine (**1**) (500 mg, 0.76 mmol, 1.0 equiv) was dissolved in anhydrous DMF (5 mL). 3 Å molecular sieves were added to the flask and placed under nitrogen in the dark for 30 minutes. Propargylamine (0.1 mL, 1.5 mmol, 2.0 equiv) and copper iodide (36 mg, 0.19 mmol, 0.25 equiv) were added to the solution which was then left under nitrogen for a further 20 minutes. Tetrakis(triphenylphosphine)palladium(0) (88 mg, 0.076 mmol, 0.1 equiv) and triethylamine (0.75 mL, 5.3 mmol, 7.0 equiv) were added and the reaction was left to stir under nitrogen and in the dark for 2 hours and 30 minutes. During this time the reaction mixture turned dark brown.

The reaction mixture was extracted into ethyl acetate (50 mL) and washed with EDTA (5%, w:v, pH 9) (3 x 50 mL) and sat. KCl (2 x 50 mL). The aqueous phases were back extracted and the organic phases were combined, dried (Na_2SO_4) and concentrated *in vacuo*. This left an orange oil which was coevaporated with toluene (3 x 20 mL) and neutralised chloroform (3 x 20 mL) to remove any DMF and TEA which remained. The crude product was purified by column chromatography (silica neutralised with 1 mL TEA, eluent – 5% MeOH in DCM). Fractions containing product were combined and coevaporated with toluene (3 x 20 mL) and chloroform (3 x 20 mL) to remove the TEA. The product was obtained as a yellow oil with a yield of 240 mg (0.41 mmol, 54%).

^{1}H NMR (300 MHz, CHLOROFORM-*d*) δ ppm : 2.30 (dd, *J* = 14.2, 7.0 Hz, 1 H, **H13**), 2.51 (dd, *J* = 8.1, 2.6 Hz, 1 H, **H13**), 3.19 (s, 2 H, **H21**), 3.29 (dd, *J* = 10.6, 3.1 Hz, 1 H, **H10**), 3.44 (dd, *J* = 10.6, 1.8 Hz, 1 H, **H10**), 3.78 (s, 6 H, **H1**), 4.10 (d, *J* = 2.4 Hz, 1 H, **H11**), 4.54 (d, *J* = 2.7 Hz, 1 H, **H12**), 6.34 (t, *J* = 6.5 Hz, 1 H, **H14**), 6.85 (d, *J* = 8.2 Hz, 4 H, **H2**), 7.19 (t, *J* = 7.4 Hz, 1 H, **H8**), 7.23 - 7.31 (m, 2 H, **H7**), 7.35 (dd, *J* = 8.7, 1.7 Hz, 4 H, **H3**), 7.44 (d, *J* = 7.5 Hz, 2 H, **H6**), 8.18 (s, 1 H, **H15**).

^{13}C NMR (101 MHz, CHLOROFORM-*d*) δ ppm : 31.6 (CH_2, **C22**), 42.3 (CH_2, **C14**), 55.1 (CH_3, **C1**), 63.2 (CH_2, **C11**), 71.9 (CH, **C13**), 85.3 (CH, **C15**), 86.4 (CH, **C12**), 86.9 (C, **C6**), 113.8 (CH, **C3**), 127.1 (CH, **C10**), 127.8 (CH, **C9**), 128.3 (CH, **C8**), 129.8 (CH, **C4**), 135.7 (C, **C5**), 158.9 (C, **C2**).

ESI+ ($C_{33}H_{33}N_3O_7$): Monoisotopic mass = 583.23, observed m/z = 606.2 $[M + Na]^+$, 584.2 $[M + H]^+$

UV-Vis (MeCN, 13.0 µM): λ_{max} (log ε) 230 (4.43), 282 (4.03)

Emission (MeCN, 13.0 µM): No fluorescence observed

R_f (10% MeOH in DCM): 0.18

9.3 Synthesis of 5‘-DMT-5-propargyl-(anthraquinone-2“-carboxamidyl)-deoxyuridine (3)

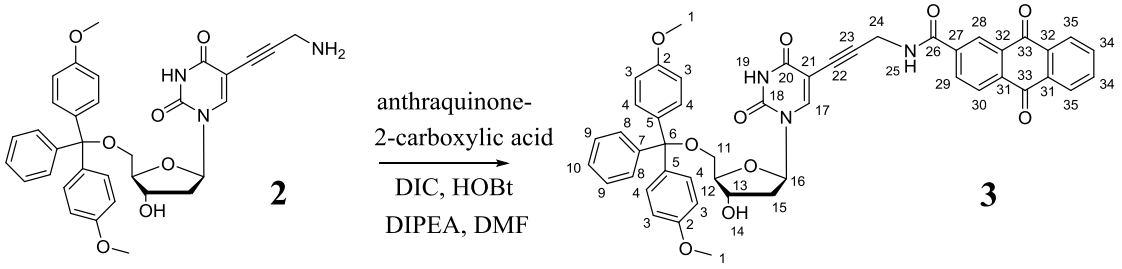

2 **3**

5’DMT-5-propargyl-deoxyuridine (**2**) (110 mg, 0.20 mmol, 1.0 equiv), anthraquinone-2-carboxylic acid (52 mg, 0.20 mmol, 1.0 equiv), HOBt (27 mg, 0.20 mmol, 1.0 equiv) and DIPEA (47 µL, 0.27 mmol, 1.3 equiv) were dissolved in DMF (6 mL) and purged with nitrogen. DIC (39 µL, 0.25 mmol, 1.1 equiv) was dissolved in DMF (2 mL) and added portion wise over 30 minutes. The reaction was left overnight.

The reaction mixture was diluted with DCM (20 mL) and washed with sat. KCl (4 x 40 mL). The organic phases were dried (Na_2SO_4), filtered and concentrated *in vacuo*.

The crude product was purified by column chromatography (silica neutralised with 1 mL TEA, eluent – 3% MeOH in DCM). Fractions containing product were combined and coevaporated with toluene (3 x 20 mL) and chloroform (3 x 20 mL) to remove the TEA. This obtained a yellow solid with a yield of 0.13 g (0.16 mmol, 80%).

^{1}H NMR (300 MHz, CHLOROFORM-*d*) δ ppm : 2.21 (dd, *J* = 13.2, 6.2 Hz, 1 H, **H15**), 2.52 (dd, *J* = 13.2, 3.3 Hz, 1 H, **H15**), 3.19 - 3.30 (m, 2 H, **H11**), 3.64 (s, 6 H, **H1**), 3.69 (dd, *J* = 10.6, 2.2 Hz, 1 H, **H12**), 4.07 (br. s., 2 H, **H24**), 4.53 (t, *J* = 2.6 Hz, 1 H, **H13**), 6.23 (t, *J* = 6.6 Hz, 1 H, **H16**), 6.71 (d, *J* = 8.8 Hz, 4 H, **H3**), 7.07 (s, 1 H, **H10**), 7.14 - 7.17 (m, 2 H, **H9**), 7.21 - 7.27 (m, 4 H, **H4**), 7.35 (d, *J* = 7.3 Hz, 2 H, **H8**), 7.68 - 7.73 (m, 2 H, **H34**), 8.02 (dd, *J* = 8.24, 1.65 Hz, 1 H, **H29**), 8.11 (s, 1 H, **H17**), 8.14 - 8.17 (m, 1 H, **H28** or **H30**), 8.17 - 8.22 (m, 2 H, **H35**), 8.51 (d, *J* = 1.5 Hz, 1 H, **H28** or **H30**).

^{13}C NMR (101 MHz, CD_3CN) δ ppm : 30.9 (CH2, **C24**), 41.3 (CH2, **C15**), 54.8 (CH3, **C1**), 63.3 (CH2, **C11**), 71.9 (CH, **C13**), 75.3 (C, **C21**), 86.4 (CH, **C16**), 86.9 (CH, **C12**), 87.2 (C, **C6**), 88.7 (C, **C23**), 99.4 (C, **C22**), 113.9 (CH, **C4**), 125.3 (CH, **C26**), 127.0 (CH, **C10**), 127.1 (CH, **C35**), 127.4 (CH, **C30**), 127.7 (CH, **C33**), 128.1 (CH, **C8**), 128.8 (CH, **C9**), 130.5 (CH, **C3**), 133.2 (C, **C27**), 133.5 (CH, **C33**), 134.9 (CH, **C34**), 135.2 (C, **C32**), 135.4 (C, **C5**), 138.5 (C, **C31**), 143.5 (CH, **C17**), 150.1 (C, **C18**), 158.1 (C, **C2**), 162.7 (C, **C20**), 165.5 (C, **C26**), 182.9 (C, **C33**).

ESI+ ($C_{48}H_{39}N_3O_{10}$): Monoisotopic mass 817.26, observed *m/z* 840.1 $[M + Na]^+$

UV-Vis (MeCN, 9.8 μM): λ_{max} (log ε) 237 (4.53), 255 (4.60)

Emission (MeCN, 9.8 μM): No fluorescence observed

R_f (10% MeOH in DCM): 0.57

9.4 Synthesis of 5'-DMT-5-propargyl-(anthraquinone-2"-carboxamidyl)- deoxyuridine-3'-amidite (4)

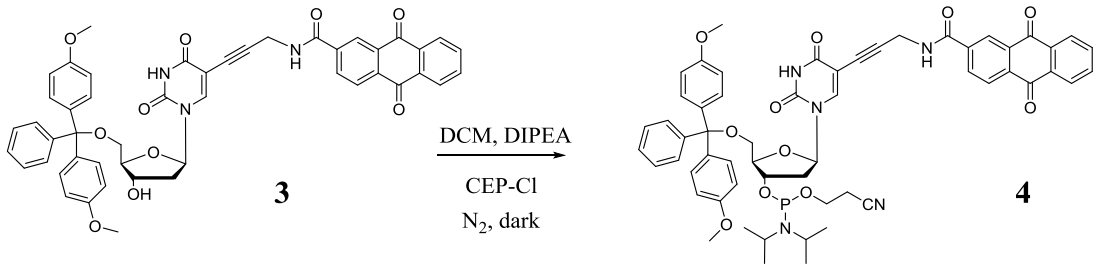

Dry 5'-DMT-5-propargyl-(anthraquinone-2''-carboxamidyl)-deoxyuridine (**3**) (100 mg, 0.12 mM, 1.0 equiv) was added to a 2-necked flask and purged with nitrogen. Anhydrous DCM (5 mL), DIPEA (85 µL, 0.49 mM, 4.0 equiv) and CEP-Cl (87 µL, 0.37 mM, 3.0 equiv) were added and left in the dark under nitrogen for 1 hour.

The reaction mixture was passed through a cannula filter system, due to product instability, and was precipitated out using hexane (10 mL). After being in ice for 15 minutes the cannula filter system was used again to remove the solvent and leave the product behind.

The product was then dissolved in acetonitrile (3 mL) and used immediately for DNA synthesis. Due to its instability full characterisation was not possible.

R_f (10% MeOH in DCM): 0.67

9.5 Synthesis of 5-(ρ-methyl benzoate)-10,15,20-triphenyl porphyrin (5)

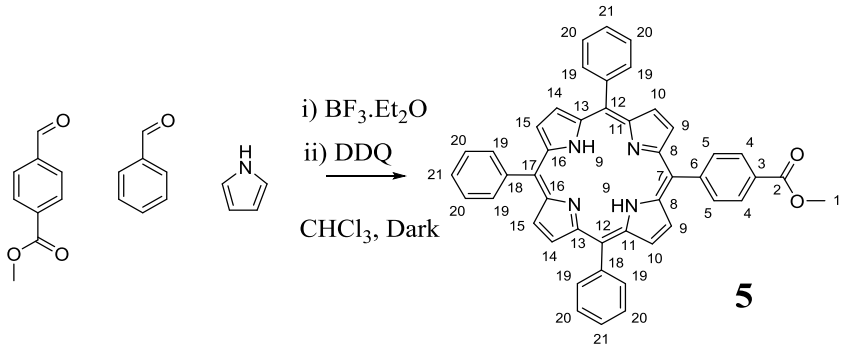

Pyrrole (2.52 mL, 36 mmol, 6.0 equiv), benzaldehyde (3.64 mL, 36 mmol, 6.0 equiv) and methyl ρ-formylbenzoate (0.99 g, 6.0 mmol, 1.0 equiv) were dissolved in chloroform (500 mL) and purged with nitrogen for 1 hour in the dark. Boron trifluoride etherate (0.69 mL, 5.4 mmol, 0.9 equiv) was added and the reaction left for a further hour. 2,3-Dichloro-5,6-dicyano-1,4-benzoquinone (8.14 g, 36 mmol, 6.0 equiv) was added and the reaction left overnight.

Column chromatography was carried out twice to purify the product (first column - silica/alumina, eluent DCM; second column - silica, eluent toluene). The product was obtained as a dark purple solid with a yield of 0.59 g (0.88 mmol, 15%).

^{1}H NMR (300 MHz, CHLOROFORM-*d*) δ ppm : -2.85 (s, 2 H, **H22**), 4.03 (s, 3 H, **H1**), 7.63 - 7.71 (m, 9 H, **H20, H21**), 8.10 - 8.16 (m, 6 H, **H19**), 8.23 (d, *J* = 8.3 Hz, 2 H, **H5**), 8.36 (d, *J* = 8.7 Hz, 1 H, **H4**), 8.71 (d, *J* = 4.9 Hz, 2 H, **H9**), 8.78 (d, *J* = 6.8 Hz, 6 H, **H10, H14, H15**).

^{13}C NMR (75 MHz, CHLOROFORM-*d*) δ ppm : 53.1 (CH_3, **C1**), 117.3 (C, **C6**), 121.7 (C, **C18**), 125.9 (CH, **C20** and **C21**), 127.3 (CH, **C4** or **C5**), 127.4 (CH, **C4** or **C5**), 128.6 (CH, **C10**), 129.3 (C, **C8**), 129.5 (CH, **C9**), 133.8 (CH, **C19**), 142.6 (C, **C7**), 147.8 (C, **C3**), 166.9 (C, **C2**).

ESI+ ($C_{46}H_{32}N_4O_2$): Monoisotopic mass 672.3, observed *m/z* 673.3 $[M + H]^+$

UV-Vis (DCM, 3.5 µM): λ_{max} (log ε) 417 (5.28), 514 (4.21), 549 (3.85), 589 (3.71), 645 (3.58)

Emission (DCM, 3.5 µM): λ_{ex} 417 nm, λ_{em} (rel int) 650 (1), 716 (0.34)

R_f (DCM): 0.69

9.6 Synthesis of 5-(ρ-benzoic acid)-10,15,20-triphenyl porphyrin (6)

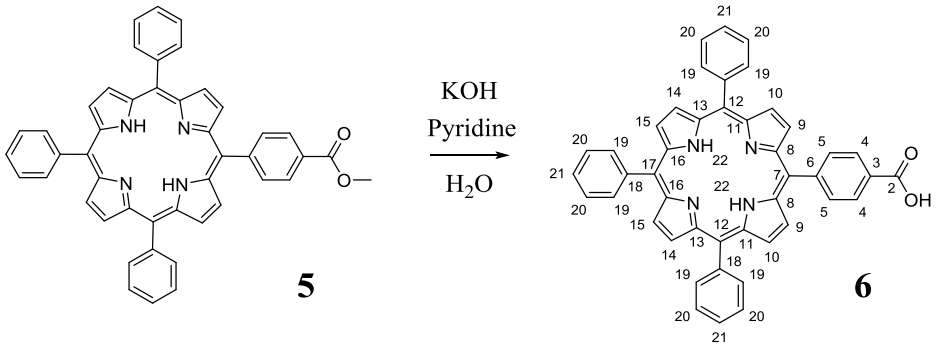

5 **6**

5-(ρ-methyl benzoate)-10,15,20-triphenyl porphyrin (**5**) (0.59 g, 0.88 mmol, 1.0 equiv) was dissolved in pyridine (15 mL). Potassium hydroxide (2.46 g, 44 mmol, 50 equiv) was dissolved in de-ionised water (2 mL) and added to the reaction mixture forming a colourless aqueous layer under the dark purple organic layer. The reaction mixture was heated to 40 °C and left overnight.

Pyridine was removed *in vacuo* and the crude product was washed with water (3 x 100 mL) and DCM (100 mL). 1 M hydrochloric acid (5 mL) was added to aid the separation. The aqueous phases were re-extracted and the organic layers combined, dried (Na_2SO_4) and concentrated *in vacuo*. This was then coevaporated with toluene (3 x 20 mL) and chloroform (3 x 20 mL) to remove any remaining pyridine.

The crude product was purified by column chromatography (2% MeOH in DCM). This gave a dark purple solid with a yield of 0.41 g (0.61 mmol, 70%).

^{1}H NMR (300 MHz, CHLOROFORM-*d*) δ ppm : -2.84 (br. s., 2 H, **H22**), 7.65 - 7.74 (m, 9 H, **H20, H21**), 8.15 (d, *J* = 7.5 Hz, 6 H, **H19**), 8.29 (d, *J* = 8.2 Hz, 2 H, **H5**), 8.45 (d, *J* = 8.1 Hz, 2 H, **H4**), 8.74 (d, *J* = 4.8 Hz, 2 H, **H9**), 8.77 - 8.84 (m, 6 H, **H10, H14, H15**).

^{13}C NMR (101 MHz, DMSO-d_6) δ ppm : 127.3 (CH, **C20**), 127.5 (CH, **C21**), 128.3 (CH, **C4**), 131.3 (CH, **C9**, **C10**, **C14** and **C15**), 135.1 (CH, **C19**), 135.2 (CH, **C5**), 141.9 (C, **C7**), 147.2 (C, **C3**).

ESI+ ($C_{45}H_{30}N_4O_2$): Monoisotopic mass 658.2, observed *m/z* 659.1 $[M + H]^+$

UV-Vis (DCM, 2.3 µM): λ_{max} (log ε) 417 (5.46), 517 (4.14), 552 (3.87), 593 (3.79), 649 (3.72)

Emission (DCM, 2.3 µM): λ_{ex} 417 nm, λ_{em} (rel int) 650 (1), 716 (0.34)

R_f (10% MeOH in DCM): 0.52

9.7 Synthesis of 5'-DMT-5-propargyl-dU-5, 10, 15-triphenyl-20-(*P*-benzamide)-porphyrin (7)

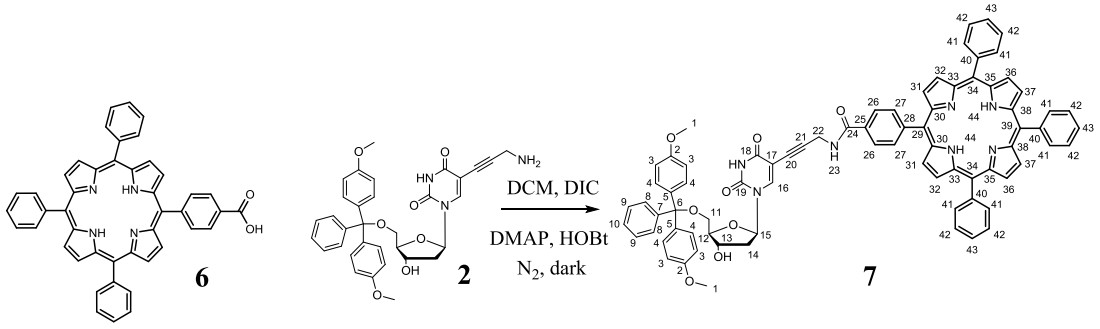

5-(ρ-benzoic acid)-10,15,20-triphenyl porphyrin (**6**) (100 mg, 0.15 mM, 1.0 equiv) was added to an oven dried flask containing 3 Å molecular sieves. Anhydrous DCM (15 mL) was added with DMAP (37 mg, 0.30 mM, 2.0 equiv), HOBt (23 mg, 0.16 mM, 1.05 equiv) and DIC (45 µL, 0.30 mM, 2.0 equiv). The flask was placed under nitrogen in the dark for 15 minutes. 5'DMT-5-propargyl-deoxyuridine (**2**) (115 mg, 0.20 mmol, 1.3 equiv) was then added and the reaction left for 2 hours.

The reaction mixture was then diluted in DCM (60 mL) and washed with water (3 x 60 mL). The aqueous phase was re-extracted and the organic layers were combined. This was dried with Na_2SO_4 and concentrate *in vacuo* and stored at 4 °C.

The crude product was purified by column chromatography (silica neutralised with 1 mL TEA, eluent – 1-5% MeOH in DCM). Fractions containing product were combined and coevaporated with toluene (3 x 20 mL) and chloroform (3 x 20 mL) to remove the TEA. This gave a metallic purple solid with a yield of 144 mg (0.12 mmol, 78%).

^{1}H NMR (300 MHz, CHLOROFORM-*d*) δ ppm : -2.76 (br. s., 2 H, **H44**), 2.31 (dd, *J* = 6.9, 5.9 Hz, 1 H, **H14**), 2.54 (dd, *J* = 7.5, 2.4 Hz, 1 H, **H14**), 3.37 (dd, *J* = 8.8, 2.9 Hz, 2 H, **H11**), 3.71 (s, 6 H, **H1**), 4.10 (d, *J* = 2.2 Hz, 1 H, **H12**), 4.28 (br. s., 1 H, **H22**), 4.52 - 4.58 (m, 1 H, **H13**), 6.35 (t, *J* = 6.8 Hz, 1 H, **H15**), 6.84 (d, *J* = 7.3 Hz, 4 H, **H3**), 7.20 (t, *J* = 6.8 Hz, 1 H, **H10**), 7.29 - 7.33 (m, 2 H, **H9**), 7.37 (d, *J* = 8.8 Hz, 4 H, **H4**), 7.48 (d, *J* = 7.7 Hz, 2 H, **H8**), 7.75 (t, *J* = 7.1 Hz, 9 H, **H42 H43**), 7.97 (d, *J* = 8.1 Hz, 2 H, **H26**), 8.16 - 8.24 (m, 8 H, **H27 H41**), 8.29 (s, 1 H, **H16**), 8.78 (d, *J* = 5.1 Hz, 2 H, **H31**), 8.82 - 8.91 (m, 6 H, **H32**, **H36**, **H37**).

^{13}C NMR (101 MHz, DMSO-d_6) δ ppm : 30.5 (CH_2, **C22**), 41.4 (CH_2, **C14**), 55.6 (CH_3, **C1**), 62.9 (CH_2, **C11**), 71.8 (CH, **C13**), 86.2 (CH, **C15**), 86.9 (CH, **C12**), 87.4 (C, **C6**), 89.1 (C, **C21**), 99.1 (C, **C20**), 113.9 (CH, **C3**), 118.7 (C, **C25**), 121.1 (C, **C40**), 125.8 (CH, **C27**), 126.9 (CH, **C42**), 127.4 (CH, **C10**), 127.9 (CH, **C43**), 128.0 (CH, **C8**), 128.4 (CH, **C9**), 130.3 (CH, **C4**), 131.9 (CH, **C31**, **C36** and **C37**), 134.3 (CH, **C41**), 134.8 (CH, **C26**), 135.4 (C, **C5**), 135.5 (C, **C5**), 143.6 (CH, **C16**), 146.1 (C, **C28**), 159.3 (C, **C2**), 166.7 (C, **C-24**).

UV-Vis (DCM, 1.2 µM): λ_{max} (log ε) 417 (5.54), 517 (4.12), 551 (3.79), 593 (3.64), 647 (3.48)

Emission (DCM, 1.2 µM): λ_{ex} 417 nm, λ_{em} (rel int) 650 (1), 716 (0.33)

R_f (10% MeOH in DCM): 0.49

9.8 Synthesis of 5'-DMT-5-propargyl-dU-5, 10, 15-triphenyl-20-(*P*-benzamide)-porphyrin-3'amidite (8)

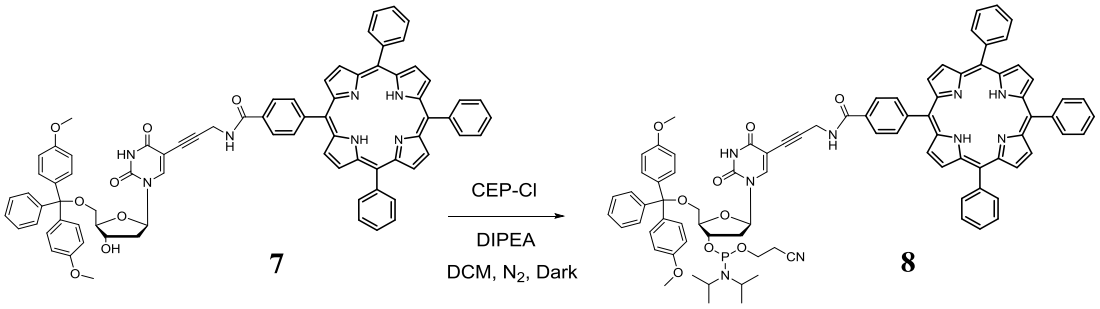

7 **8**

Dry 5'-DMT-5-propargyl-dU-5, 10, 15-triphenyl-20-(*P*-benzamide)-porphyrin (**7**) (150 mg, 0.12 mM, 1.0 equiv) was added to a 2-necked flask and purged with nitrogen. Anhydrous DCM (5 mL), DIPEA (85 µL, 0.49 mM, 4.0 equiv) and CEP-Cl (87 µL, 0.37 mM, 3.0 equiv) were added and left in the dark under nitrogen for 1 hour.

The reaction mixture was then passed through a cannula filter system, due to product instability, and precipitated out into a purple solid using hexane (10 mL). After being in ice for 15 minutes the cannula filter system was used again to remove the solvent and leave the product behind.

The product was dissolved in acetonitrile (1.5 mL) and DCM (1.5 mL) and used immediately for DNA synthesis. Due to its instability full characterisation was not possible.

^{31}P NMR (121 MHz, CHLOROFORM-*d*) δ ppm : 149.71, 149.35

R_f (10% MeOH in DCM): 0.67

9.9 PAGE

A resolving and a stacking gel were made using the following amounts shown in Table 9-1.

	Resolving Gel	Stacking Gel
Deionised water	2.3 mL	2.7 mL
30% Acrylamide mix	5 mL	0.67 mL
Tris (1.5 M, pH 8.8)	2.5 mL	-
Tris (1 M, pH 6.8)	-	0.5 mL
10% SDS	0.1 mL	0.04 mL
Ammonium persulphate	0.1 mL	0.04 mL
TEMED	0.01 mL	0.005 mL

Table 9-1: Required volumes of reagents for resolving and stacking gels for PAGE.

The resolving gel was added to the frame with IPA added after to ensure no bubbles were present. After 45 minutes the gel was set and the IPA was removed. The stacking gel was made and a comb was inserted to form the wells to load in the DNA. After 20 minutes the comb was removed. A loading buffer to load the DNA onto the gel was used. The loadind buffer was a 100 mL stock made up into deionised water containing: Tris (1 M, pH 6.8) 10 mL, SDS 4 g, bromophenol blue 200 mg and glycerol 20 g. Before use 15.4 mg of DTT was added to 1 mL of the loading buffer. DNA was loaded onto the gel using 5 µL of loading buffer and 5 µL of DNA solution. The gel was run at 200 mV for 1 hour. The running buffer made into 1 L of deionised water contained glycine (18.8 g), SDS (1 g) and tris base (3.02 g).

The gel was then imaged and the main band was cut out of the band and the DNA was removed using a ‘crush and soak’ method. The band of gel used was cut into small pieces and an eluting solution added. The solution made up to 5 mL of deionised water contained MeOH (0.5 mL) and NaCl (5 M, 0.25 mL). The gel and eluting solution were added to a thermomixer and heated to 36 °C and left overnight. The tubes were then centrifuged at 8000 rpm for 15 mintues and the supernatant was carefully removed using a filter tube. The pieces of gel were then washed with water. The DNA was then desalted using a Glen-pak and solvent removed.

9.10 SPR Measurements

The Biacore® X100 SPR machine was loaded with a DNA probe of concentration 1 µM in PBS. To immobilise the DNA probe onto a blank gold chip, the sample was injected by using a manual run of 1080 seconds six consecutive times. PBS was used as the running buffer. A solution of 1 mM MCH was injected, for 600 seconds, to block the surface of the chip for non-specific binding. Target DNA was then added to the machine in a range of concentrations, 10 nM to 500 nM in PBS, and a manual injection of 1080 seconds was carried out separately. 50 mM NaOH was used to regenerate the surface. The response unit would then return to the background value and target DNA can be re-injected into the machine.

9.11 Nanoplasmonic Device

9.11.1 Surface sensitivity testing

The chip was cleaned in a Piranha solution (H_2O_2:$3H_2SO_4$) for 15 minutes and then washed with water (3 x 5 minutes). The chip was immersed in a 2 mM solution of 3-mercaptopropoionic acid in denatured ethanol for 6 hours. The functionised chip was then rinsed alternatively with ethanol and de-ionised water. The chip was dried under a nitrogen flow. A measurement was then taken of the chip to have a blank reading. The bilayers were then added on in cycles.

First the chip was immersed in a solution of PAH (Polyallyamine hydrochloride, 1 mg/mL) in 50 mmol NaCl for 15 minutes then washed (3 x 5 minutes). The chip was dried under nitrogen flow. The chip was then immersed in a solution of PSS (Polysodium styrene sulfonate, 1 mg/mL) in 50 mmol NaCl for 15 minutes then washed (3 x 5 minutes). The chip was dried under nitrogen flow. The chip was measured and the cycle repeated until the desired number of bilayers is achieved.

9.11.2 Bulk sensitivity testing

The chip was cleaned in a Piranha solution for 15 minutes and then washed with water (3 x 5 minutes). The chip was then placed in a petri dish with different concentrations of NaCl solution ranging from 0% to 10%. The chip was fully immersed in the solution before measurement.

9.11.3 Immobilisation of DNA probe

The chip was cleaned in a Piranha solution for 15 minutes and then washed with water (3 x 5 minutes). A solution of 1 μM in PBS of thiol modified DNA probe was added onto the gold chip. After 1 hour the chip was washed to remove unbound DNA. The chip was then measured. 1 mM MCH was then added to the chip to reduce non-specific binding.

9.11.4 Measuring target DNA hybridisation

To obtain a baseline measurement the chip was measured in PBS (100 μL) every 3 minutes up to 30 minutes (0 min, 3 min, 6 min, 9 min, 12 min, 15 min, 18 min, 21 min, 24 min, 27 min, 30 min). It was observed that the measurements in PBS remain at a constant level throughout the whole 30 minutes.

The target DNA, of concentrations ranging from 10 nM to 500 nM in PBS, was added to the chip and measured at regular intervals up to 1 hour.

The surface of the chip was regenerated by using 50 mM NaOH to remove the target DNA. The chip was then washed before use again. The chip was used three times before the PBS baseline measurements did not remain constant and so the chip was then cleaned using Piranha and fresh probe DNA was immobilised.

9.12 Single Sensor Device for Electrochemical Experiments with Unlabelled Probe

To ensure that the sensor surface is not damaged the chip is first checked under the microscope for scratches. In order to confirm that there is not a short circuit within the chip it was checked using a voltmeter. The chip was then cleaned by immersing in acetone and sonicating for 10 minutes. It was then rinsed with IPA and a copious amount of de-ionised water. The chip was then treated under UV/ozone for 20 minutes before measurement. 40 µL of redox probe (5 mM $[Fe(CN)_6]^{3-/4-}$, pH 7.4) was added and incubated for 1 minute before a blank measurement was taken (CV or EIS).

9.12.1 Immobilisation of DNA

A chamber was put onto the chip before the probe was added (40 µL, 1 µM in PBS) and left to immobilise for two hours. The unbound probe was washed off using PBS before 1 mM MCH was used to minimise non-specific binding. 40 µL of redox probe (5 mM $[Fe(CN)_6]^{3-/4-}$, pH 7.4) was added and incubated for 1 minute before a measurement was taken (CV or EIS).

9.12.2 Hybridisation of target DNA

The chip was rinsed in PBS buffer and target DNA was added (40 µL). After 1 hour the chip was rinsed with PBS before 40 µL of redox probe (5 mM $[Fe(CN)_6]^{3-/4-}$, pH 7.4) was added and incubated for 1 minute before a measurement (CV or EIS) was taken. The chip was rinsed in PBS and the chamber removed before the cleaning process was started again to reuse the chip. This could be done 3 times before the baseline measurements significantly changed.

9.12.3 TNF–α Detection [100]

The first step was to prepare the magnetic beads. Carboxylated magnetic beads (200 µL, 0.31 µm, 2.5% w/v) were washed with PBS (3 x 800 µL). They were activated using EDC (15.3 mg, 0.4 M) and NHS (2.3 mg, 0.1 M) in PBS (200 µL). The tubes were sealed with parafilm and left on the rotator for 30 minutes at room temperature. The EDC/NHS solution was removed from the magnetic beads before the beads were incubated with one of the following: anti-human albumin antibody (250 µg/mL), anti-human IgG antibody (250 µg/mL) or anti human TNF-α antibody (50 µg/mL) in a 200 µL solution. After one hour at room temperature on the rotator the solution was removed and replaced with fresh PBS and placed at 4 °C until use.

The chips were cleaned before the first experiment was run in PBS. Samples of concentrations 0, 1, 10, 100 and 1000 pg/mL of TNF-α were made and 3 µL of the pre-prepared magnetic beads with the TNF-α antibody attached was added. This was incubated for 1 hour. The solution was removed and the beads washed with PBS (3 x 200 µL). TNF-α was eluted (40 µL, 10 minutes, 63 °C) from the magnetic beads using 2% SDS in 0.5 M Tris (pH 7.0). The eluted sample (40 µL) was then incubated on the electrode (chip) for 15 minutes. 40 µL of redox probe (5 mM $[Fe(CN)_6]^{3-/4-}$, pH 7.4) was added and incubated for 1 minute before an EIS measurement was taken. Before the measurements are taken blank chips are measured to test for the baseline R_{ct} value (diameter of the Nyquist plots).

The experiments were then repeated in human serum (carried out by Hui Hwee Ng) adding the beads with IgG and albumin antibodies coupled to remove the most abundant background. The experiment then continued as with PBS.

9.13 Single electrode chip with chemically tagged DNA probes

The same chip was used as for the unlabelled probes therefore the same cleaning process was used. The probe was immobilised onto the chip (40 µL, 1 µM in 1 M NaCl, 0.1 M sodium citrate) for 5 hours. 1 mM MCH was added to reduce non-specific binding. The measurement (CV or DPV) was taken without the need of an external redox solution (except EIS which still requires external redox solution). Target DNA (buffer 1 M NaCl, 0.1 M sodium citrate) was added to the chamber for one hour before measurement. For more details on the experimental procedure see 9.12.

9.14 Multi-Sensor electrode array chip

Prior to assembly of the microfluidic channel onto the sensor electrode, the chips were cleaned by immersing in acetone and sonicating for 10 minutes, followed by rinsing with IPA and thorough washing with de-ionised water. The chip was then treated with UV/Ozone for 20 minutes. The bottom layer of the fluidic channel made from double sided adhesive, was pasted onto the chip to form separate chambers surrounding each sensor pad. The DNA probe (5 μL, 1 μM in 1 M NaCl, 0.1 M Sodium citrate) was then immobilised on the chip for 5 hours. The 20 sensors allow for measuring three repeats simultaneously; with three probes and measuring both target and mismatch sequence, 18 sensor pads were used, leaving the first and last sensors blank for background measurement. The unbound probe was then washed off the chip using the buffer solution (1 M NaCl, 0.1 M Sodium citrate). To reduce nonspecific binding, the chip was incubated with 1 mM 6-mercaptohexanol solution for 30 minutes. The adhesive spacer and top plastic sheet layers were then assembled to finish the chip. Target DNA solutions of various concentrations were injected into the microfluidic channel and left to hybridise for 20 minutes before measuring.

9.15 Detection of miRNA

For details on cleaning and use of the chips see previous sections (9.12). Care was taken to only use RNase free water for preparation of the buffer (1 M NaCl, 0.1 M sodium citrate). Probes were chemically tagged so no external redox marker was used. For experimental procedure see 9.12 and 9.13.

9.16 Summary of Oligonucleotides

9.16.1 Purchased Oligonucleotides

Oligonucleotides purchased from Integrated DNA Technologies are shown in Table 9-2.

	Sequence 5'-3'
DAPK un	XAAGGCGC**GGAGGATAGTCGGATCGAGTTAACGTC**GCGCCTT
E. Cad un	XAAGGCGC**TAATTTTAGGTTAGAGGGTTATCGCG**GCGCCTT
RARβ un	XAAGGCGC**GGTTAGTAGTTCGGGTAGGGTTTATC**GCGCCTT
DAPK-ATTO 594	XAAGGCGC**GGAGGATAGTCGGATCGAGTTAACGTC** GCGCCTT ATTO 594
DAPK-ATTO 633	XAAGGCGC**GGAGGATAGTCGGATCGAGTTAACGTC** GCGCCTT ATTO 633
DAPK-ATTO 647	XAAGGCGC**GGAGGATAGTCGGATCGAGTTAACGTC** GCGCCTT ATTO 647

Table 9-2: List of sequences purchased from Integrated DNA Technologies. Where X was 5'-thiol (C6) modification and ATTO dye was attached via an amine linker. Bases underlined form stem of hairpin design while bases in bold are the recognition section of the sequence.

Oligonucleotides purchased from IBA Life Sciences (Germany) are shown in

	Sequences 5'-3'
MB-1	Y<u>AAGGCGC</u>**GGAGGATAGTCGGATCGAGTTAACGTC**<u>GCGCCX T</u>
MB-2	Y<u>TATGACG</u>**GGAGGATAGTCGGATCGAGTTAA<u>CGTC</u>**<u>AXA</u>
MiR-21 Linear	YTAX**CAACATCAGTCTGATAAGCTA**
MiR-21 Hairpin	Y<u>TATTAGC</u>**TCAACATCAGTCTGATAA<u>GCTA</u>**<u>AXA</u>
RNA target	UAGCUUAUCAGACUGAUGUUGA
1 mutation target	GACATTAACTCGATCCGACTATCCTCC
2 mutation target	GACATTAACTCGATCCTACTATCCTCC

Table 9-3: List of sequences purchased from IBA Life Sciences (Germany). Where X was methylene blue and Y was a 5'-thiol (C6) linker. Bases underlined form stem of hairpin design while bases in bold are the recognition section of the sequence.

9.16.2 Synthesised Oligonucleotides

Oligonucleotides synthesised in Chapter 3 are shown in Table 9-4.

Probe	Sequences 5'-3'
DAPK	YAAGGCGC**GGAGGATAGTCGGATCGAGTTAACGTC**GCGCCXT
E. Cad	YAAGGCGC**TAATTTTAGGTTAGAGGGTTATCGCG**GCGCCXT
RARβ	YAAGGCGC**GGTTAGTAGTTCGGGTAGGGTTTATC**GCGCCXT
Target	Sequences 3'-5'
DAPK unmethylated	CCTCCTATCAACCTAACTCAATTGCAG
DAPK methylated	CCTCCTATCAGCCTAGCTCAATTGCAG
E. Cad unmethylated	ATTAAAATCCAATCTCCCAATAACAC
E. Cad methylated	ATTAAAATCCAATCTCCCAATAGCGC
RARβ unmethylated	CCAATCATCAAACCCATCCCAAATAA
RARβ methylated	CCAATCATCAAGCCCATCCCAAATAG

Table 9-4: List of sequences where X is free-base porphyrin or anthraquinone and Y is 5'-thiol (C6) or 5'amine (C6) modification. Bases underlined form stem of hairpin design while bases in bold are the recognition section of the sequence. Methylated sequences are used as the mismatched throughout.

Oligonucleotides synthesised by Dr Iwona Mames and Christina Xyrafaki are shown in Table 9-5.

	Sequence 5'-3'
DAPK-CoP	YTATGACG**GGAGGATAGTCGGATCGAGTTAACGTC**AXA
DAPK – PP	YTAATGACG**GGAGGATAGTCGGATCGAGTTAACGTC**AXXA
MiR-21 Linear	YTAX**CAACATCAGTCTGATAAGCTA**
MiR-21 Hairpin	YTATTAGC**TCAACATCAGTCTGATAAGCTA**AXA

Table 9-5: List of sequences synthesised by Dr Iwona Mames and Christina Xyrafaki. Where X is either free-base porphyrin or cobalt metallated porphyrin and Y is 5'-thiol (C6) modification (except in DAPK-CoP where X is only cobalt metallated porphyrin). Bases underlined form stem of hairpin design while bases in bold are the recognition section of the sequence.

Bibliography

1. J. D. Watson and F. H. C. Crick, *Nature*, 1953, **171**, 737-738.
2. M. H. F. Wilkins, A. R. Stokes and H. R. Wilson, *Nature*, 1953, **171**, 738-740.
3. R. E. Franklin and R. G. Gosling, *Nature*, 1953, **171**, 740-741.
4. K. T. Kool, *Chem. Rev.*, 1997, **97**, 1473-1487.
5. S. Carr, *http://www.mun.ca/biology/scarr/A_B_Z_DNA.html*, Accessed 02/12/2014, 2014.
6. H. Lan, H. Lu, X. Wang and H. Jin, *BioMed Res. Int.*, 2015, **2015**, 17.
7. C. Yang, B. Dou, K. Shi, Y. Chai, Y. Xiang and R. Yuan, *Anal. Chem.*, 2014, **86**, 11913-11918.
8. S. George, V. Chaudhery, M. Lu, M. Takagi, N. Amro, A. Pokhriyal, Y. Tan, P. Ferreira and B. T. Cunningham, *Lab Chip*, 2013, **13**, 4053-4064.
9. E. M. Harcourt and E. T. Kool, *Nucleic Acids Res.*, 2012, **40**, e65-e65.
10. T. Tian, J. Wang and X. Zhou, *Org. Biomol. Chem.*, 2015, **13**, 2226-2238.
11. X. Zheng, L. Niu, D. Wei, X. Li and S. Zhang, *Sci. Rep.*, 2016, **6**, 35982.
12. L. J. McBride and M. H. Caruthers, *Tetrahedron Lett.*, 1983, **24**, 245-248.
13. L. T. Vassilev, B. T. Vu, B. Graves, D. Carvajal, F. Podlaski, Z. Filipovic, N. Kong, U. Kammlott, C. Lukacs, C. Klein, N. Fotouhi and E. A. Liu, *Science*, 2004, **303**, 844-848.
14. P. Cairns, M. Esteller, J. G. Herman, M. Schoenberg, C. Jeronimo, M. Sanchez-Cespedes, N.-H. Chow, M. Grasso, L. Wu, W. B. Westra and D. Sidransky, *Clin. Cancer Res.*, 2001, **7**, 2727-2730.
15. P. Anglim, T. Alonzo and I. Laird-Offringa, *Mol Cancer*, 2008, **7**, 81.
16. M. W. Y. Chan, L. W. Chan, N. L. S. Tang, J. H. M. Tong, K. W. Lo, T. L. Lee, H. Y. Cheung, W. S. Wong, P. S. F. Chan, F. M. M. Lai and K. F. To, *Clin. Cancer Res.*, 2002, **8**, 464-470.
17. P. Negraes, F. Favaro, J. Camargo, M. Oliveira, J. Goldberg, C. Rainho and D. Salvadori, *BMC Cancer*, 2008, **8**, 238.
18. Y. Shin, A. P. Perera, J. S. Kee, J. Song, Q. Fang, G.-Q. Lo and M. K. Park, *Sensor Actuat B-Chem*, 2013, **177**, 404-411.
19. A. M. Deaton and A. Bird, *Genes Dev.*, 2011, **25**, 1010-1022.

20. C. Yeung, T. Dinh and J. Lee, *PharmacoEconomics*, 2014, **32**, 1093-1104.
21. K. D. Sievert, B. Amend, U. Nagele, D. Schilling, J. Bedke, M. Horstmann, J. Hennenlotter, S. Kruck and A. Stenzl, 2009, **27**, 295-300.
22. P.-C. Chen, M.-H. Tsai, S. K. Yip, Y.-C. Jou, C.-F. Ng, Y. Chen, X. Wang, W. Huang, C.-L. Tung, G. C. Chen, M. M. Huang, J. H. Tong, E.-J. Song, D.-C. Chang, C.-D. Hsu, K.-F. To, C.-H. Shen and M. W. Chan, *BMC Med Genomics*, 2011, **4**, 1-11.
23. W. M. Rideout, P. Eversole-Cire, C. H. Spruck, C. M. Hustad, G. A. Coetzee, F. A. Gonzales and P. A. Jones, *Mol. Cell. Biol* 1994, **14**, 6143-6152.
24. M. M. Suzuki and A. Bird, *Nat. Rev. Genet.*, 2008, **9**, 465-476.
25. M. Esteller, P. G. Corn, S. B. Baylin and J. G. Herman, *Cancer Res.*, 2001, **61**, 3225-3229.
26. J. G. Herman, J. R. Graff, S. Myöhänen, B. D. Nelkin and S. B. Baylin, *Proc. Natl. Acad. Sci.*, 1996, **93**, 9821-9826.
27. Y. Zhang, V. Bailey, C. M. Puleo, H. Easwaran, E. Griffiths, J. G. Herman, S. B. Baylin and T.-H. Wang, *Lab Chip*, 2009, **9**, 1059-1064.
28. R. Mao and L.-S. Chou, *Clin. Chem.*, 2010, **56**, 1050-1052.
29. S. Kurdyukov and M. Bullock, *Biology*, 2016, **5**, 3.
30. X. Ma, Y.-W. Wang, M. Q. Zhang and A. F. Gazdar, *Epigenomics*, 2013, **5**, 301-316.
31. K. N. Rand, G. P. Young, T. Ho and P. L. Molloy, *Nucleic Acids Res.*, 2013, **41**, e15-e15.
32. J. Yoon, M. K. Park, T. Y. Lee, Y.-J. Yoon and Y. Shin, *Lab Chip*, 2015, **15**, 3530-3539.
33. T. Y. Lee, Y. Shin and M. K. Park, *Lab Chip*, 2014, **14**, 4220-4229.
34. M. A. Cooper, *Nat. Rev. Drug Discov.*, 2002, **1**, 515-528.
35. L. Yobas, J. Hongmiao, H. Wing-Cheong, C. Yu, L. Tit-Meng, H. Chew-Kiat and K. Dim-Lee, *IEEE J Solid-St Circ*, 2007, **42**, 1803-1813.
36. F. B. Myers and L. P. Lee, *Lab Chip*, 2008, **8**, 2015-2031.
37. A. Bayan and B. Christian, *IJIAR*, 2014, **6**, 187-191.
38. R. Gambari and G. Feriotto, *J. AOAC Int.*, 2006, **89**, 893-897.
39. I. Palchetti and M. Mascini, *Analyst*, 2008, **133**, 846-854.

40. M. J. LaGier, J. W. Fell and K. D. Goodwin, *Mar. Pollut. Bull.*, 2007, **54**, 757-770.
41. M. Minunni, S. Tombelli, M. Mascini, A. Bilia, M. C. Bergonzi and F. F. Vincieri, *Talanta*, 2005, **65**, 578-585.
42. H. Shi, T. Xia, A. E. Nel and J. I. Yeh, *Nanomed.*, 2007, **2**, 599-614.
43. H. Radecka and J. Radecki, *Development of Electrochemical Sensors for DNA Analysis, in "DNA in Supramolecular Chemistry and Nanotechnology", Ed. Eugen Stulz and Guido Clever*, Wiley Blackwell, p. 139-157, 2015.
44. D. Kang, X. Zuo, R. Yang, F. Xia, K. W. Plaxco and R. J. White, *Anal Chem*, 2009, **81**, 9109-9113.
45. J. Pollet, F. Delport, K. P. F. Janssen, K. Jans, G. Maes, H. Pfeiffer, M. Wevers and J. Lammertyn, *Biosens. Bioelectron.*, 2009, **25**, 864-869.
46. J. Wang, Z. Zhu and H. Ma, *Anal. Chem.*, 2013, **85**, 2096-2101.
47. P. Wang, H. Wu, Z. Dai and X. Zou, *Chem. Commun.*, 2012, **48**, 10754-10756.
48. Y. Wang, E. J. H. Wee and M. Trau, *Chem. Comm.*, 2015, **51**, 10953-10956.
49. H. Yin, B. Sun, Y. Zhou, M. Wang, Z. Xu, Z. Fu and S. Ai, *Biosens. Bioelectron.*, 2014, **51**, 103-108.
50. M. Daneshpour, L. S. moradi, P. Izadi and K. Omidfar, *Biosens. Bioelectron.*, 2016, **77**, 1095-1103.
51. Y. Tang, X. Zeng and J. Liang, *J. Chem. Educ.*, 2010, **87**, 742-746.
52. J. Homola, S. S. Yee and G. Gauglitz, *Sensor Actuat B-Chem*, 1999, **54**, 3-15.
53. S. Kumamoto, M. Watanabe, N. Kawakami, M. Nakamura and K. Yamana, *J. Am. Chem. Soc.*, 2008, **19**, 65-69.
54. N. Ben Gaied, Z. Zhao, S. R. Gerrard, K. R. Fox and T. Brown, *ChemBioChem*, 2009, **10**, 1839-1851.
55. S. Mahajan, J. Richardson, N. B. Gaied, Z. Zhao, T. Brown and P. N. Bartlett, *Electroanalysis*, 2009, **21**, 2190-2197.
56. K. Yamana, S. Kumamoto, H. Nakano and Y. Sugie, *Nucleic Acids Symp. Ser.*, 2001, **1**, 35-36.
57. M. Ma, J. M. Zhang, Z. Dai, X. Q. Wang and Q. Y. Zhang, *Adv. Mat. Res.*, 2011, **298**, 56-62.
58. M. T. Tierney and M. W. Grinstaff, *Org. Lett.*, 2000, **2**, 3413-3416.
59. P. Rothemund, *J. Am. Chem. Soc.*, 1935, **57**, 2010-2011.

60. P. Rothemund, *J. Am. Chem. Soc.*, 1936, **58**, 625-627.
61. A. D. Adler, F. R. Longo, J. D. Finarelli, J. Goldmacher, J. Assour and L. Korsakoff, *J Org*, 1967, **32**, 476-476.
62. J. S. Lindsey, I. C. Schreiman, H. C. Hsu, P. C. Kearney and A. M. Marguerettaz, *J Org*, 1987, **52**, 827-836.
63. A. Brewer, G. Siligardi, C. Neylon and E. Stulz, *Org. Biomol. Chem.*, 2011, **9**, 777-782.
64. I. Grabowska, D. G. Singleton, A. Stachyra, A. Gora-Sochacka, A. Sirko, W. Zagorski-Ostoja, H. Radecka, E. Stulz and J. Radecki, *Chem. Commun* 2014, **50**, 4196-4199.
65. R. García-González, A. Costa-García and M. T. Fernández-Abedul, *Sensor Actuat. B-Chem.*, 2014, **191**, 784-790.
66. D. Pan, X. Zuo, Y. Wan, L. Wang, J. Zhang, S. Song and C. Fan, *Sensors*, 2007, **7**, 2671-2680.
67. M. Tichoniuk, M. Ligaj and M. Filipiak, *Sensors*, 2008, **8**, 2118.
68. C. G. Pheeney and J. K. Barton, *Langmuir*, 2012, **28**, 7063-7070.
69. A. Erdem, K. Kerman, B. Meric, U. S. Akarca and M. Ozsoz, *Anal. Chim. Acta.*, 2000, **422**, 139-149.
70. M. Nakayama, T. Ihara, K. Nakano and M. Maeda, *Talanta*, 2002, **56**, 857-866.
71. T. Ihara, Y. Maruo, S. Takenaka and M. Takagi, *Nucleic Acids Res*, 1996, **24**, 4273-4280.
72. H. Weizman and Y. Tor, *J. Am. Chem. Soc.*, 2002, **124**, 1568-1569.
73. K. Aslan and V. H. Pérez-Luna, *J. Fluoresc.*, 2004, **14**, 401-405.
74. U. Rant, K. Arinaga, S. Fujita, N. Yokoyama, G. Abstreiter and M. Tornow, *Langmuir*, 2004, **20**, 10086-10092.
75. C. Huang, T. Stakenborg, Y. Cheng, F. Colle, T. Steylaerts, K. Jans, P. Van Dorpe and L. Lagae, *Biosens Bioelectron*, 2011, **26**, 3121-3126.
76. Z.-S. Wu, J.-H. Jiang, L. Fu, G.-L. Shen and R.-Q. Yu, *Anal. Biochem.*, 2006, **353**, 22-29.
77. I. Grabowska, D. G. Singleton, A. Stachyra, A. Gora-Sochacka, A. Sirko, W. Zagorski-Ostoja, H. Radecka, E. Stulz and J. Radecki, *Chem. Comm.*, 2014, **50**, 4196-4199.

78. J. Balintová, R. Pohl, P. Horáková, P. Vidláková, L. Havran, M. Fojta and M. Hocek, *Chem. Eur. J.*, 2011, **17**, 14063-14073.
79. S. Matile, N. Berova, K. Nakanishi, S. Novkova, I. Philipova and B. Blagoev, *J. Am. Chem. Soc.*, 1995, **117**, 7021-7022.
80. N. Nombona, W. Chidawanyika and T. Nyokong, *J. Mol. Struct.*, 2012, **1012**, 31-36.
81. J. Chen, N. Chen, J. Huang, J. Wang and M. Huang, *Inorg. Chem. Commun.*, 2006, **9**, 313-315.
82. H. Uchida, P. Y. Reddy, S. Nakamura and T. Toru, *J. Org. Chem.*, 2003, **68**, 8736-8738.
83. B. I. Kharisov, U. Ortiz Mendez, J. L. Almaraz Garza and J. R. Almaguer Rodriguez, *New J. Chem.*, 2005, **29**, 686-692.
84. U. Hitoshi, Y. Hideyuki, R. P. Yella, N. Shuichi and T. Takeshi, *Bull. Chem. Soc. Jpn*, 2004, **77**, 1401-1404.
85. A. Shaabani, R. Maleki-Moghaddam, A. Maleki and A. H. Rezayan, *Dyes Pigm.*, 2007, **74**, 279-282.
86. D. Villemin, M. Hammadi, M. Hachemi and N. Bar, *Molecules*, 2001, **6**, 831.
87. T. Nguyen, A. Brewer and E. Stulz, *Angew. Chem. Int. Ed.*, 2009, **48**, 1974-1977.
88. L.-A. Fendt, I. Bouamaied, S. Thöni, N. Amiot and E. Stulz, *J. Am. Chem. Soc.*, 2007, **129**, 15319-15329.
89. Y. Shin, A. P. Perera and M. K. Park, *Sens. Actuat. B-Chem.*, 2013, **178**, 200-206.
90. J. S. Kee, S. Y. Lim, A. P. Perera, Y. Zhang and M. K. Park, *Sensor Actuat B-Chem*, 2013, **182**, 576-583.
91. T. W. Ebbesen, H. J. Lezec, H. F. Ghaemi, T. Thio and P. A. Wolff, *Nature*, 1998, **391**, 667-669.
92. S. G. Rodrigo, F. J. García-Vidal and L. Martín-Moreno, *Phys. Rev. B*, 2008, **77**, 075401.
93. I. V. Bykov, A. V. Dorofeenko, A. S. Ilyin, I. A. Ryzhikov, M. V. Sedova and A. P. Vinogradov, *Phys. Rev. B*, 2008, **78**, 054201.
94. L. Martín-Moreno, F. J. García-Vidal, H. J. Lezec, K. M. Pellerin, T. Thio, J. B. Pendry and T. W. Ebbesen, *Phys. Rev. Lett.*, 2001, **86**, 1114-1117.

95. A. Mary, S. G. Rodrigo, L. Martín-Moreno and F. J. García-Vidal, *Phys. Rev. B*, 2007, **76**, 195414.
96. P. Bertrand, Jonas, A., Laschewsky, A. and Legras, R., *Macromol. Rapid Commun.*, 2000, **21**, 319-348.
97. Y. Guo, W. Geng and J. Sun, *Langmuir*, 2009, **25**, 1004-1010.
98. M. Michel, V. Toniazzo, D. Ruch and V. Ball, *ISRN Mater. Sci.*, 2012, **2012**, 13.
99. Sigma-Aldrich, *https://www.sigmaaldrich.com/life-science/cell-biology/detection/learning-center/atto.html* Accessed 05/09/2016, 2016.
100. P. Kongsuphol, H. H. Ng, J. P. Pursey, S. K. Arya, C. C. Wong, E. Stulz and M. K. Park, *Biosens Bioelectron*, 2014, **61**, 274-279.
101. S. K. Arya, T. S. Pui, C. C. Wong, S. Kumar and A. R. A. Rahman, *Langmuir*, 2013, **29**, 6770-6777.
102. S. K. Arya, K. Y. Wang, C. C. Wong and A. R. A. Rahman, *Biosens. Bioelectron.*, 2013, **41**, 446-451.
103. P. Kongsuphol, S. K. Arya, C. Chung Wong, L. J. Polla and M. K. Park, *Biosens. Bioelectron.*, 2014, **55**, 26-31.
104. T. S. Pui, P. Kongsuphol, S. K. Arya and T. Bansal, *Sens. Actuat. B-Chem.*, 2013, **181**, 494-500.
105. K. Arinaga, U. Rant, J. Knežević, E. Pringsheim, M. Tornow, S. Fujita, G. Abstreiter and N. Yokoyama, *Biosens. Bioelectron.*, 2007, **23**, 326-331.
106. J. Wang, G. Rivas, M. Jiang and X. Zhang, *Langmuir*, 1999, **15**, 6541-6545.
107. C. Brückner, *J. Chem. Educ.*, 2004, **81**, 1665.
108. T. D. Lash, D. A. Colby and L. F. Szczepura, *Inorg. Chem.*, 2004, **43**, 5258-5267.
109. T. D. Lash, J. M. Rasmussen, K. M. Bergman and D. A. Colby, *Org. Lett.*, 2004, **6**, 549-552.
110. H. Arakawa, J. F. Neault and H. A. Tajmir-Riahi, *Biophys. J.*, 2001, **81**, 1580-1587.
111. J. P. Pursey, Y. Chen, E. Stulz, M. K. Park and P. Kongsuphol, *Sens. Actuators B-Chem.*, 2017, **251**, 34-39.
112. T. S. Pui, P. Kongsuphol, S. K. Arya and T. Bansal, *Sensor Actuat B-Chem*, 2013, **181**, 494-500.
113. P. Qi and X. Du, *Modern Pathol.*, 2013, **26**, 155-165.

114. M. D. Jansson and A. H. Lund, *Mol. Oncol.*, 2012, **6**, 590-610.
115. Q. Liu, Y. Shin, J. S. Kee, K. W. Kim, S. R. Mohamed Rafei, A. P. Perera, X. Tu, G.-Q. Lo, E. Ricci, M. Colombel, E. Chiong, J. P. Thiery and M. K. Park, *Biosens. Bioelectron.*, 2015, **71**, 365-372.
116. J. I. Gyi, A. N. Lane, G. L. Conn and T. Brown, *Nucleic Acids Res.*, 1998, **26**, 3104-3110.
117. E. A. Lesnik and S. M. Freier, *Biochemistry*, 1995, **34**, 10807-10815.
118. Y.-H. Chein and N. Davidson, *Nucleic Acids Res.*, 1978, **5**, 1627-1637.
119. P. Ramnani, Y. Gao, M. Ozsoz and A. Mulchandani, *Anal. Chem.*, 2013, **85**, 8061-8064.
120. F. Degliangeli, P. Kshirsagar, V. Brunetti, P. P. Pompa and R. Fiammengo, *J. Am. Chem. Soc.*, 2014, **136**, 2264-2267.
121. J. Yoon, M. K. Park, T. Y. Lee, Y.-J. Yoon and Y. Shin, *Lab Chip*, 2015, **15**, 3530-3539.
122. T. Y. Lee, Y. Shin and M. K. Park, *Lab Chip*, 2014, **14**, 4220-4229.